International Agreement Report

Validation of RELAP5 Model of Ringhals 4 against a Load Step Test at Uprated Power

Prepared by:
J. Bánáti and A. Stathis

Chalmers University of Technology
Department of Applied Physics
Division of Nuclear Engineering
SE – 41 296 Gothenburg, Sweden

K. Tien, NRC Project Manager

Division of Systems Analysis
Office of Nuclear Regulatory Research
U.S. Nuclear Regulatory Commission
Washington, DC 20555-0001

International Agreement Report

Validation of RELAP5 Model of Ringhals 4 against a Load Step Test at Uprated Power

Prepared by:
J. Bánáti and A. Stathis

Chalmers University of Technology
Department of Applied Physics
Division of Nuclear Engineering
SE – 41 296 Gothenburg, Sweden

K. Tien, NRC Project Manager

Division of Systems Analysis
Office of Nuclear Regulatory Research
U.S. Nuclear Regulatory Commission
Washington, DC 20555-0001

ABSTRACT

After finishing the large component replacement project of the steam generators and the pressurizer, the Unit 4 of the Ringhals Nuclear Power Plant was operated in test mode between 2011 and 2014. In order to reach the ultimate goal of power uprate, and obtain a license for operation at the new nominal conditions, a series of tests had to be accomplished.

The R4-QP-101 maneuverability test was performed on March 3, 2015. The test was focusing on evaluation of the system responses for ± 10 % perturbances in the load. The data collected during test provided a good opportunity for verification of the full plant model, which is being developed for the RELAP5/Mod3.3 Patch04 computer code, with incorporation of the new component models.

The present International Agreement Report introduces the test procedure and shows an overview on the key parameters that are utilized. There is a brief summary given on the applicability field of the computer code. Preparation of the input deck and the nodalization of the primary and secondary sides are touched upon.

Strategies applied for achievement of steady-state conditions are addressed in the document. The steady-state results are presented in plotted format, demonstrating how the control system brought the entire unit to stable conditions. The calculated steady-state parameters were very close to the measured plant data, before the transient initiation.

A chapter summarizes the results of the validation study using the transient data to simulate the startup test. Quantification of simulation accuracy has proven that the stand-alone RELAP5 thermal-hydraulic model is capable of reproduction of the key features and events of the test. Sufficiently good agreement between the measured and simulated data resulted in a successful verification of the plant model. The Ringhals 4 model is suitable for analysis of other types of transients already in its current state of development. Nevertheless, further refinement in the input is planned as soon as new test data will be available.

Keywords: *Ringhals 4, Load Step, RELAP5, code validation*

FOREWORD

The present International Agreement Report was prepared with the intention to provide feedback to the developers and the user community of the NRC computer codes in order to demonstrate the capabilities of RELAP5/Mod3.3 Patch 4. The authors made intensive efforts to build an up-to-date model of the recently uprated Ringhals 4 unit for analyses of transients using best estimate methods. As the results reveal in the current document, the code has successfully been validated against a start-up and maneuverability test conducted at relevant NPP.

I am convinced that the modeling strategies and main conclusions in this study will contribute to better understanding of a number of key thermal-hydraulic phenomena and will broaden the knowledge-base of safety authorities, as well as that of the code users worldwide.

Prof. Imre Pázsit
Division of Nuclear Engineering
Chalmers University of Technology
Gothenburg, Sweden

CONTENTS

FIGURES

TABLES

ACKNOWLEDGMENTS

ABBREVIATIONS

AA	Average Amplitude
BC	Boundary Condition
BWR	Boiling Water Reactor
CAMP	Code Applications and Maintenance Program
CL	Cold Leg
CVCS	Chemical and Volume Control System
DC	Downcomer
DFT	Discrete Fourier Transformation
ECCS	Emergency Core Cooling System
FA	Fuel Assembly
FCV	Feed Control Valve
FFT	Fast Fourier Transform
FFTBM	Fast Fourier Transform Based Method
FSAR	Final Safety Analysis Report
FW	Feed Water
HL	Hot Leg
HS	Heat Structure
INEL	Idaho National Engineering Laboratory
JSI	Jožef Stefan Institute
LB-LOCA	Large Break Loss of Coolant Accident
LOCA	Loss of Coolant Accident
LP	Lower Plenum
MCP	Main Circulation Pump
MSIV	Main Steam Isolation Valve
NPP	Nuclear Power Plant
NRC	Nuclear Regulatory Commission
NSSS	Nuclear Steam Supply System
PARCS	Purdue Advanced Reactor Core Simulator
PI	Proportional Integral
PLS	Precautions, Limitations, and Setpoints
PRZ	Pressurizer
PWR	Pressurized Water Reactor
RCP	Reactor Coolant Pump
RCS	Reactor Coolant System
RAB	Ringhals AB
RPV	Reactor Pressure Vessel
RELAP	Reactor Excursion and Leakage Analysis Program
RTA	Relevant Thermal-hydraulic Aspects
R3	Ringhals Unit 3
R4	Ringhals Unit 4
SB-LOCA	Small Break Loss of Coolant Accident
SG	Steam Generator
SL	Steam Line
SNAP	Symbolic Nuclear Analysis Package
SSM	Swedish Radiation Safety Authority
TCV	Turbine Control Valve
WH	Westinghouse Electric Company

1 INTRODUCTION

1.1 Power Uprates

During the last decades, power utilities made enormous efforts into modernization of their plants in order to increase the amount of produced electricity in a more cost-effective and competitive way. The process of increasing the licensed power level of a commercial nuclear power plant is called a *power uprate* [1]. Power uprates are generally categorized based on the magnitude and the methods used to achieve the power increase. Power uprates have been implemented at a number of nuclear power plants (NPPs) in many countries. Currently, there are also a significant number of NPPs that have plans for larger or smaller power uprates. The increase in the electricity produced at an NPP can be achieved in several ways:

- Increase the thermal power in the reactor;
- Improve the thermal conversion efficiency in the secondary side of the power plant by refurbishing or replacing the steam generators (SGs), the high pressure or low pressure turbine units, or by a combination of these actions.

1.2 Plant Modernizations at Ringhals

The Ringhals NPP (Figure 1) is situated at the Swedish West Coast and it comprises four units: one boiling water reactor (BWR) and three Westinghouse-type (Figure 2) pressurized water reactors (PWRs). The latest-built Unit 4 was commissioned for commercial operation in 1983. It went through a number of extensive modifications and modernizations in 2011. Within the project of "QUATTRO/R4", the SGs, the pressurizer (PRZ), and large parts of the turbine plant have been replaced. Refurbishment of these components affected also the relevant control and protection systems. The new nominal (100 %) thermal power of the unit is 3300 MW$_{th}$ in the current upgraded state. However, the permitted maximal power was still limited to 2773 MW$_{th}$ after the component replacement and a test operational mode was maintained between 2011 and 2014. Finally, the Swedish Radiation Safety Authority (SSM) permitted to increase the power and issued the license for the upgrade during the spring of 2015. Figure 3 shows a timeline of the power uprate process.

Figure 1   Aerial View of the Four Units at Ringhals

STEAM
GENERATOR

PRESSURIZER

MAIN
COOLANT
PUMP
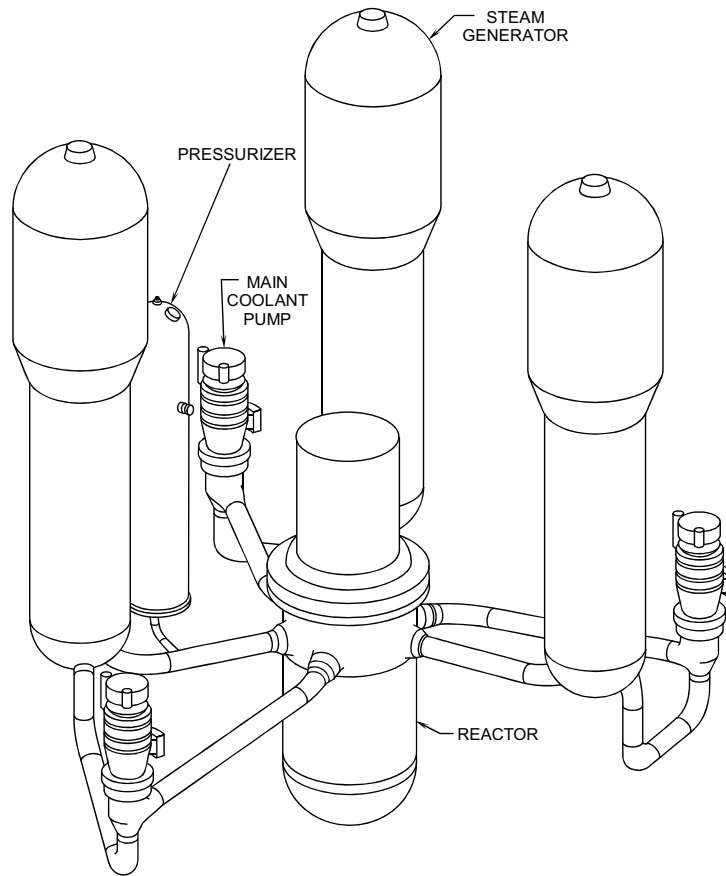
REACTOR

Figure 2   Ringhals 2, 3, and 4 – Similar Type of 3-Loop Westinghouse-Design Reactor

PRZ and SG Replacement   Turbine Refurbishment

| 1983 | 2011 | Dec. 2011 | Mar. 2015 |

Test operation

Start of commercial operation. Licensed for 2773 MWth

First startup tests. The new nominal power is 3300 MWth but still licensed for 2773 MWth.

New tests at ~3300 MWth. Licensing for 3300 MWth.
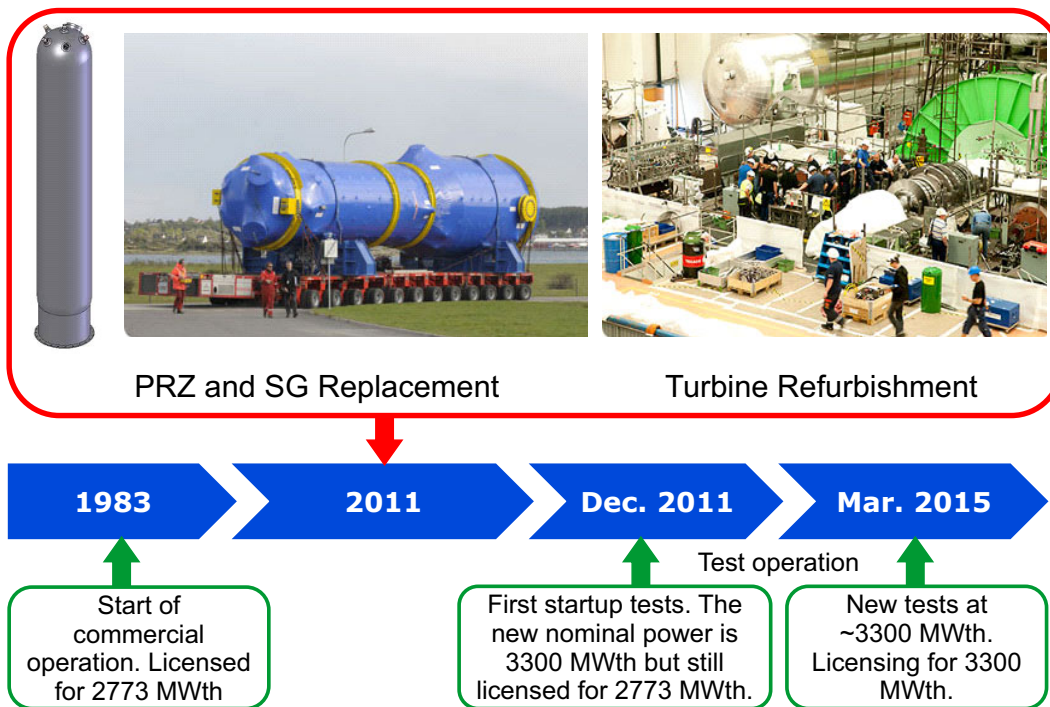
Figure 3   Timeline of the Ringhals 4 Power Uprate

1.3 Objectives of the Test

To ensure the continued safe operation of the plant, several tests, such as a load step, a full scram, and a load rejection test have successfully been conducted after installation of the new components but still operating at the ordinary power (2773 MW$_{th}$). When the license was obtained for operation at the uprated power (~3000 MW$_{th}$), a new series of tests were repeated. One of them was a ± 10 % load step test (R4 – QP-101-b), which is the object of the present study. The main purpose of the current maneuverability test was to verify that the unit, including the recently installed components with the automations and control systems, are able to handle a perturbation of the power in a satisfactory manner.

Specifically, two key issues were highlighted in the investigations:

- Checking the ability of the rod control system to adapt the reactor power according to the turbine power needs, without activation of the steam dump.
- Collecting data on the PRZ level changes due to the temperature variations in the reactor coolant system (RCS).

The magnitude of the power step was carefully set to remain within a ±10 % margin because this change is large enough to generate a challenge for the control systems, but still it remains under the level, which would trigger safety of protection systems, such as a reactor scram or opening a safety valve.

1.4 Motivations for the Model Verification

A new stand-alone RELAP5 computer code model has been built in order to simulate the entire unit 4 at Ringhals by utilizing the experience gained with unit 3 modeling. Comprehensive descriptions of the full-plant models of R3 and R4 are published in [2] and [3], respectively. The new code input includes the replaced component models of the SGs and the PRZ models, which were prepared on the basis of technical details provided by manufacturer. The engineering database specified by the designer reflects the nominal parameters for 100 %, i.e. 3300 MW thermal power, and the model is built accordingly. However, the operation at a lower power needed some modifications and adaptations in the input.

The present validation study on a new load step test is a follow-up to the work, formerly published in a scientific report [4], which discussed a similar subject. Also, a conference paper [5] summarized the results of a startup test performed at a lower power. This test gave the very first opportunity for verification of the model performance against a real plant transient. Within this progression, the current activity is a part of the process in which the ultimate goal is to provide a thoroughly verified, "multi-purpose" R4 model that is suitable for a wide scope of transient analyses. Quantification of simulation accuracy is investigated in Chapter 6, which has been prepared by the co-author of this Report, Athanasios Stathis. The topic is a part of his Master of Sciences Thesis [6].

Last but not least, sharing the knowledge and experiences with verification of the RELAP5 code can be an important feedback for the code developers, as well as essential information for the entire code user community. The work presented in the current study is a Swedish in-kind contribution in a form of an International Agreement Report for the US Nuclear Regulatory Commission (US NRC).

2 PROCEDURE OF THE TEST

2.1 Test Phases

The R4 Load Step Test was performed on March 3, 2015. Preparation for the test began earlier but the data acquisition started at 09 h 25 m 43 s (0 s) and finished at 10 h 40 m 43 s (4500 s). This means that the length of the recorded data is one and a half hours. The test consist of 5 distinct phases, as described in the followings.

2.1.1 Part A: Steady-State

The plant was operated in a steady-state. Obviously, this does not mean that the parameters are "mathematically" stable. Beyond the stochastic noise, most of the measured quantities reflect a continuously oscillating nature, partly due to the control systems. Between 0 s and 333 s, the electric generators T41 and T42 produced a steady value of 533.5 MW (Figure 4).

2.1.2 Part B: Power Decrease

The transient was initiated with an instant decrease of steam demand at 334 s. As a consequence, the generated electric power and the pressure of the turbine impulse chamber started to fall (Figure 5). In a short period of time, the control rod drive mechanism inserted the rods to the core with maximal speed (Figure 6). This is reflected also in decrease of the neutronic power, from 90.5 % to approx. 82 % (Figure 7). During this transition period, as it can be observed on the plots, many parameters show large "undershoots" or "overshoots", represented by huge peaks.

2.1.3 Part C: Operation at Reduced Power

It is difficult to determine the exact starting point when the plant reached a quasi-steady condition. Some kind of stabilization began at approx. 450 s. However, the rod control system continued moving the rods until 2100 s and the position was finally kept constant after that.

2.1.4 Part D: Power Increase

Up-step of the power started with a sudden increase of steam demand at ~3918 s. The control rods were pulled up, while the electric power was increasing to its original level. This transition period lasted until approx. 4000 s.

2.1.5 Part E: Restored Power Level

Despite the fact that the power was restored by 4000 s of transient time, most of the other parameters did not completely stabilize before the end of the data recording.

2.2 Test Results

2.2.1 Database of Measured Quantities

The test database was provided by Ringhals in a set of 533 ASCII files (1 file per measured channel). Frequency of the data sampling was 1 Hz. Due to different interpretation of the engineering units at the plant and in the code simulation, a MATLAB script was prepared for conversion between, for instance overpressure and absolute pressure (Pa), or deg. C and Kelvin.

2.2.2   Plots of the Measured Parameters

R4 Load Step Test 2015 - Generated Electric Power
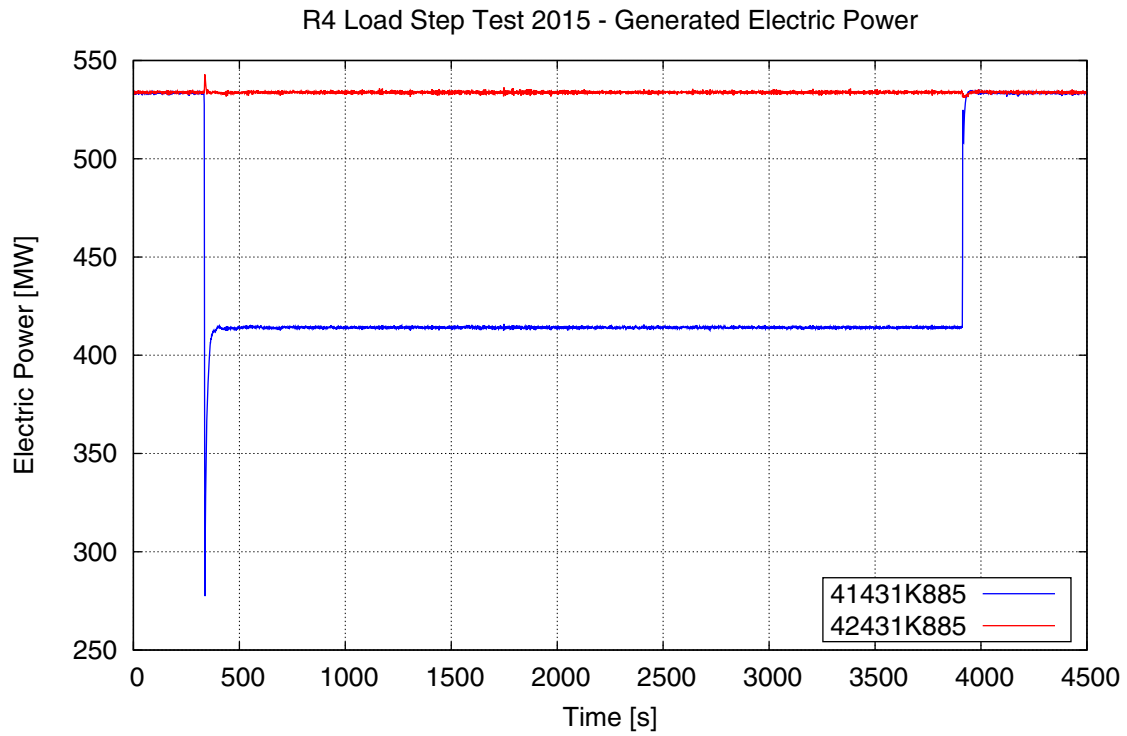
Figure 4   Electric Power from the 2 Generators

R4 Load Step Test 2015 - Pressure in Impulse Chamber
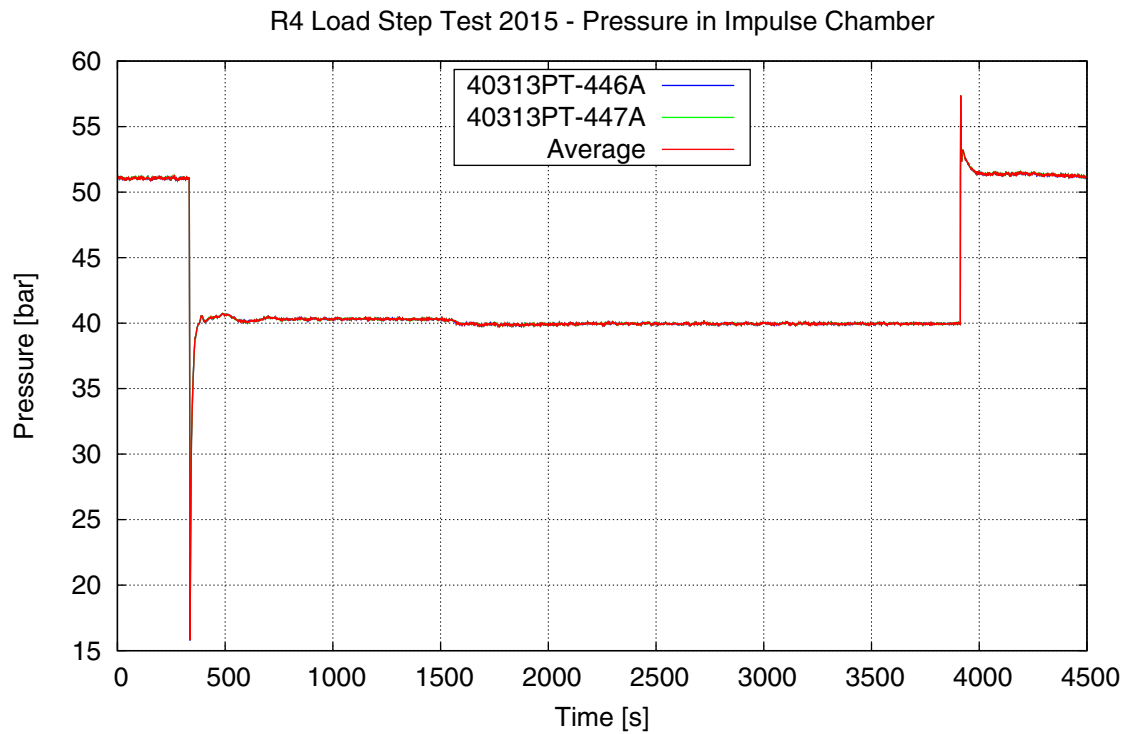
Figure 5   Pressure in the Impulse Chamber

R4 Load Step Test - 2015-03-03 - Control Rod Position
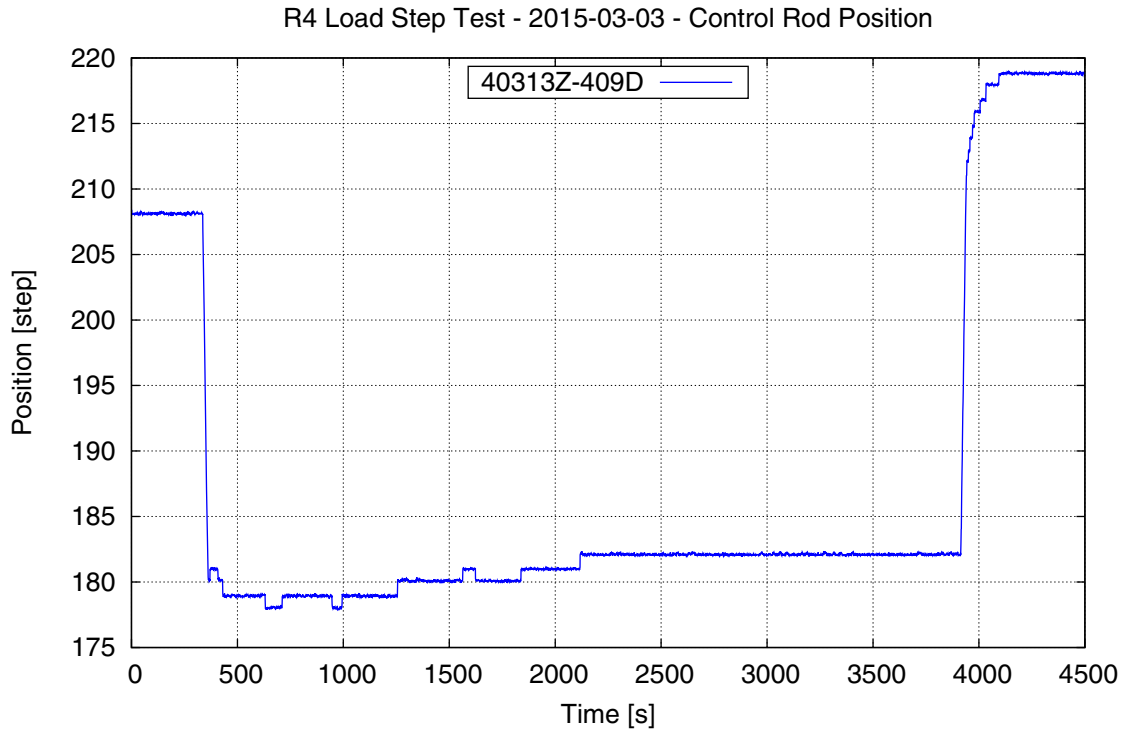
Figure 6   Position of Control Rod Bank D

R4 Load Step Test - 2015-03-03 - Neutronic Power
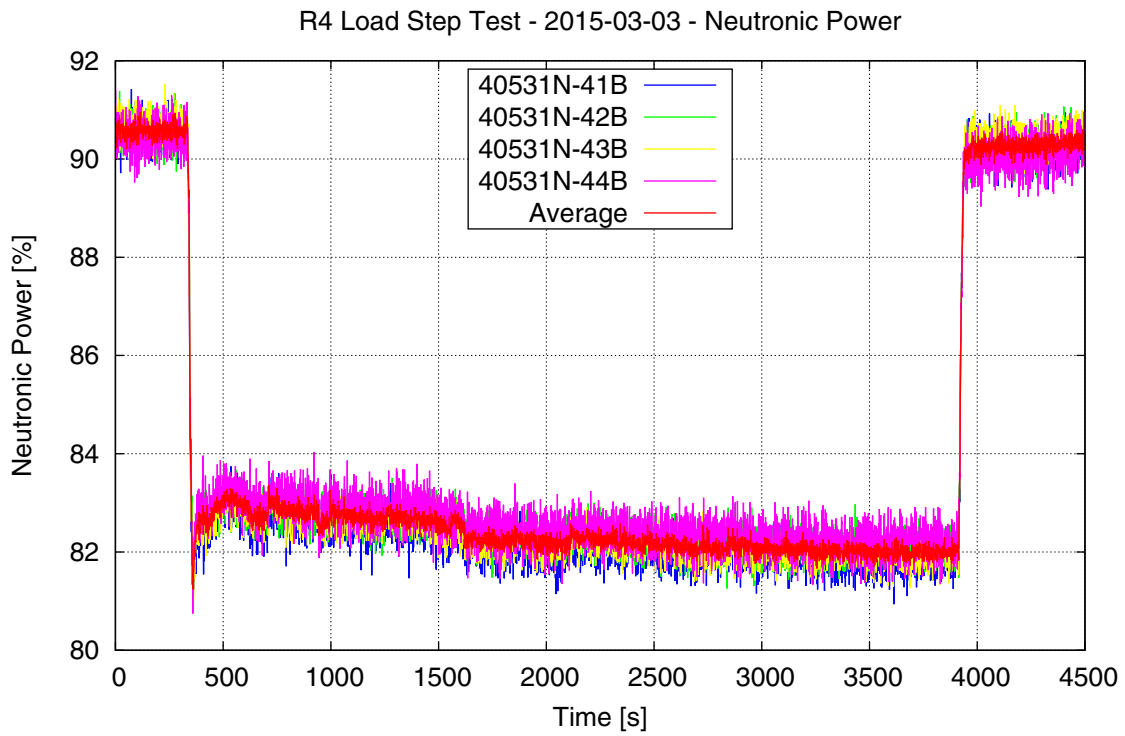
Figure 7   Neutronic Power
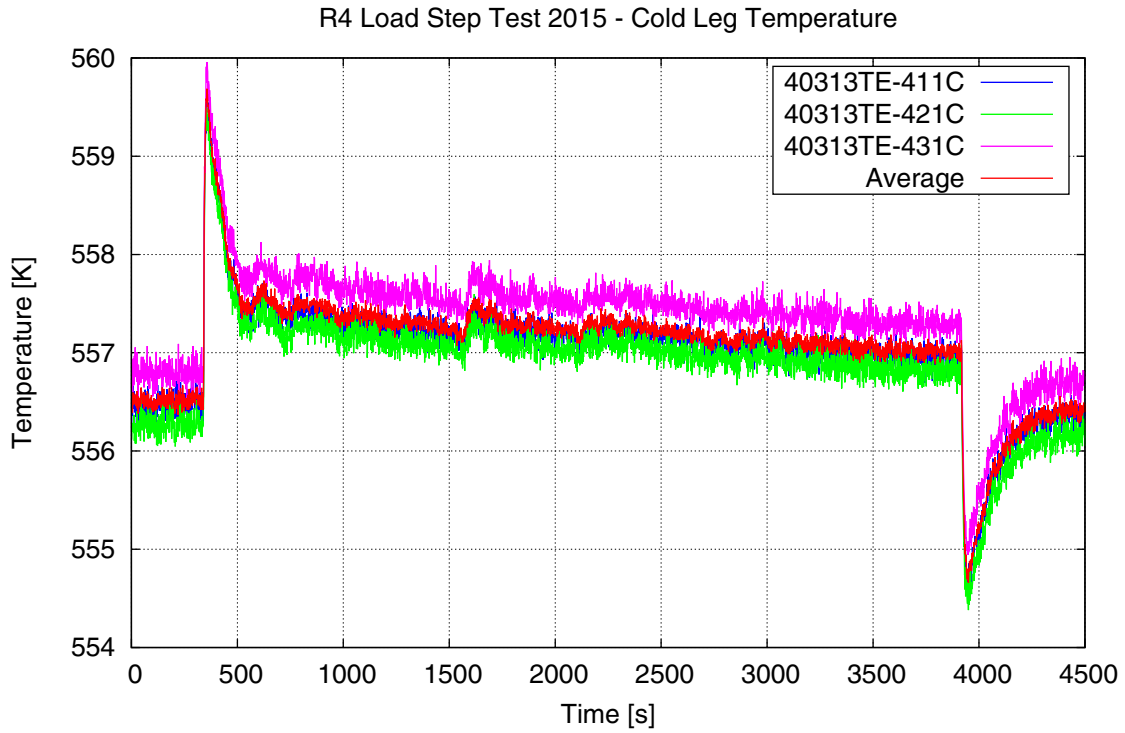
Figure 8   Cold Leg Temperature
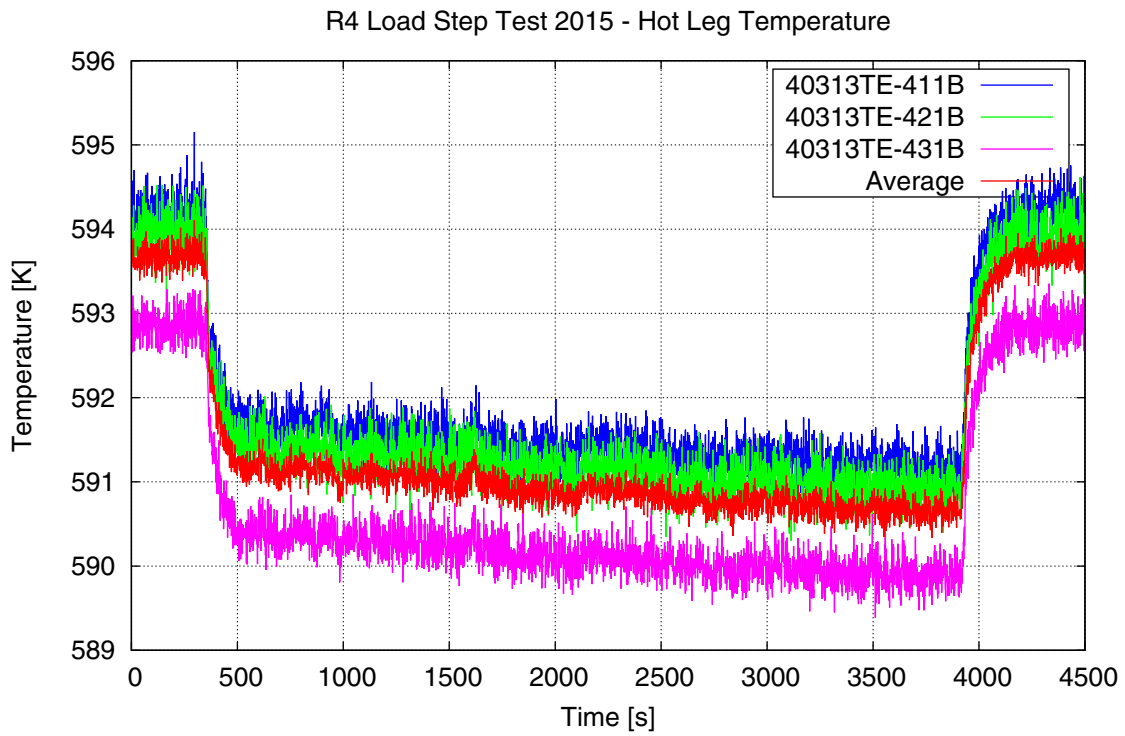
Figure 9   Hot Leg Temperature
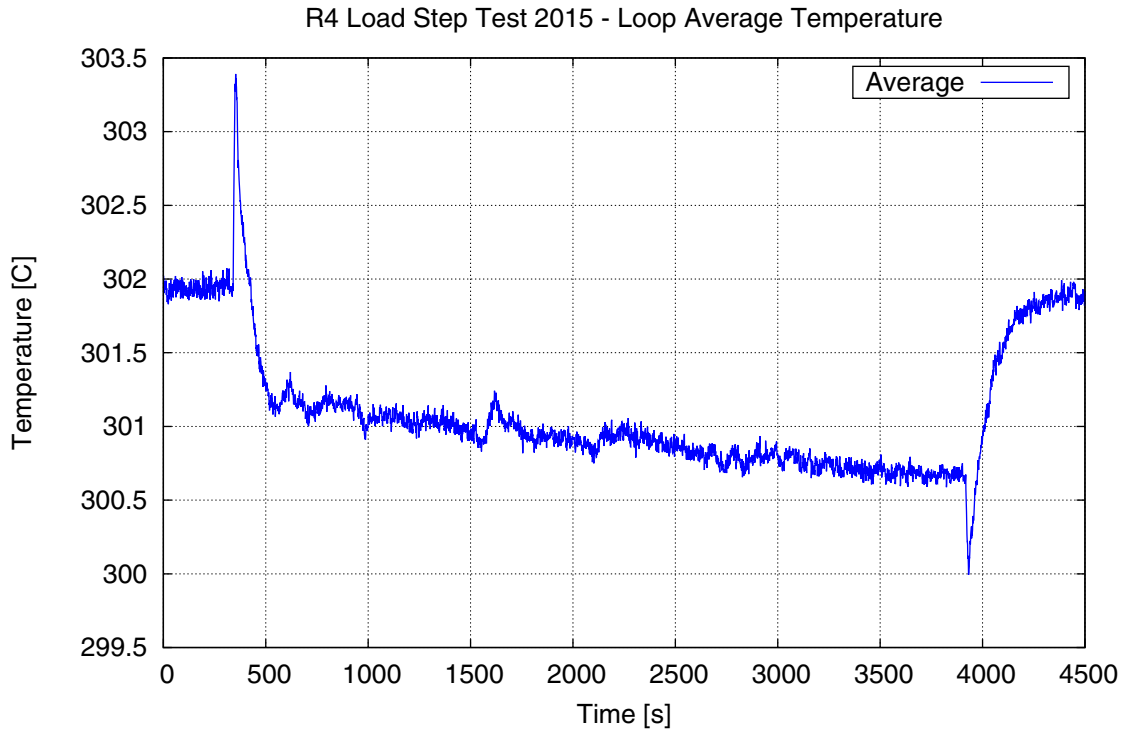
Figure 10   Loop Average Temperature
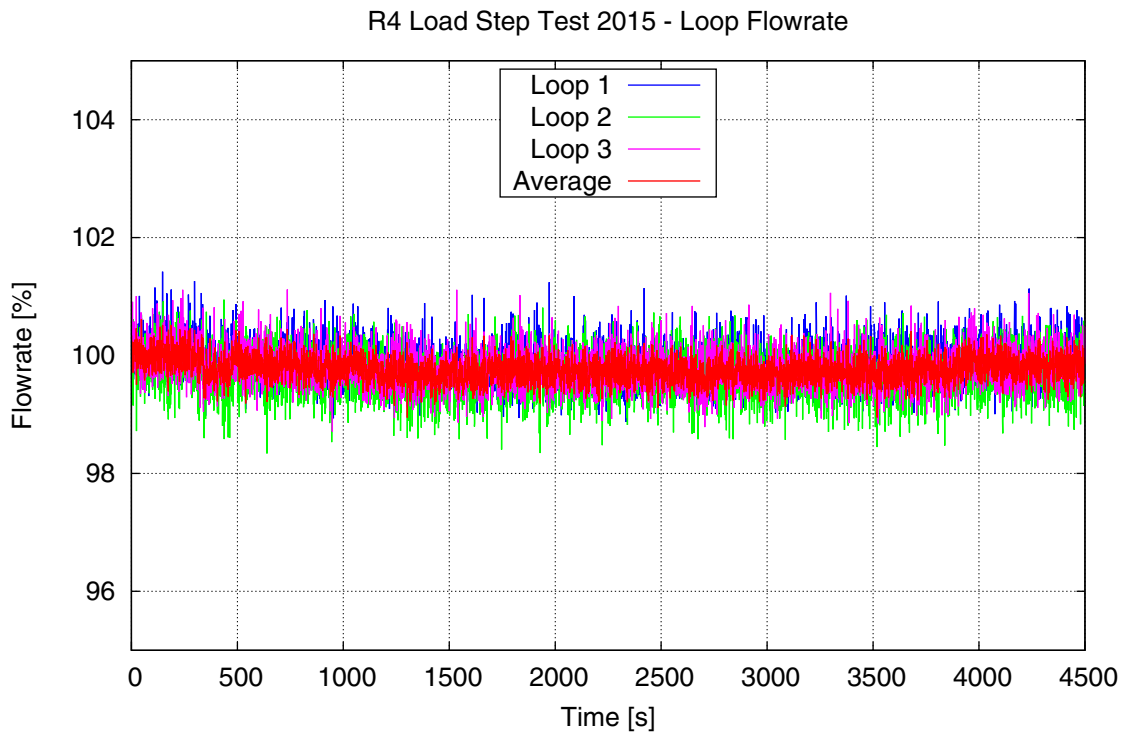
Figure 11   Loop Flowrate

2-5
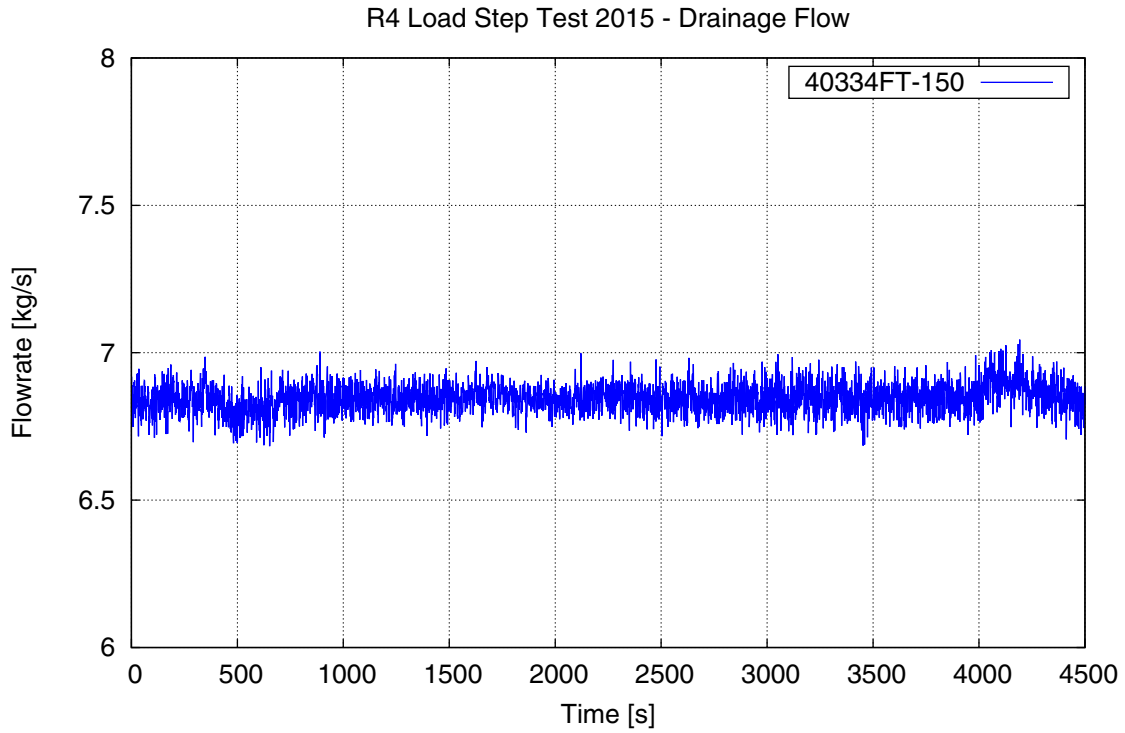
Figure 12   Drainage Flowrate
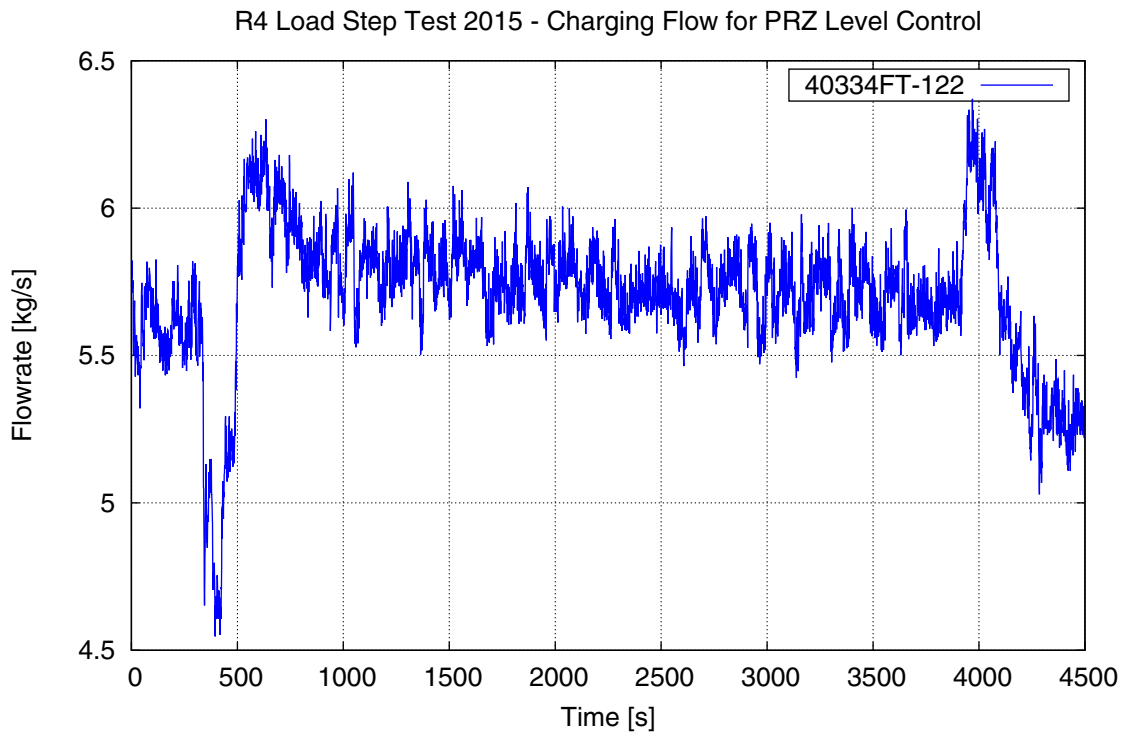
Figure 13   Charging Flowrate for PRZ Level Control
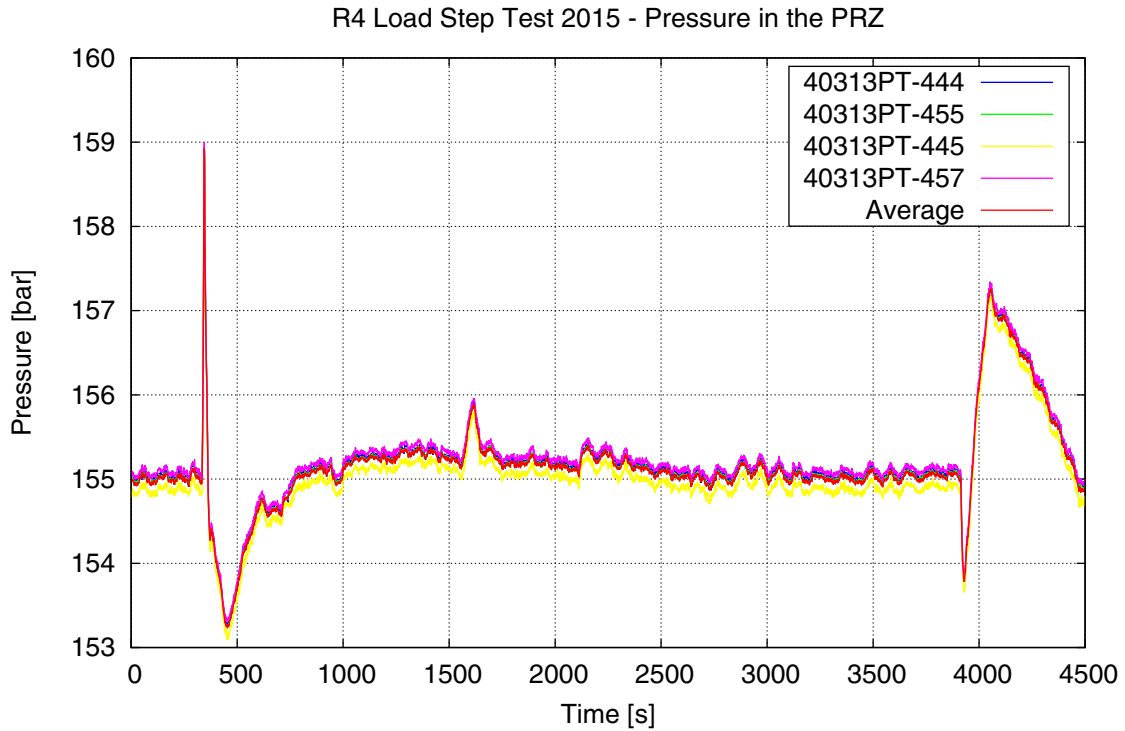
Figure 14   Pressure in the Pressurizer
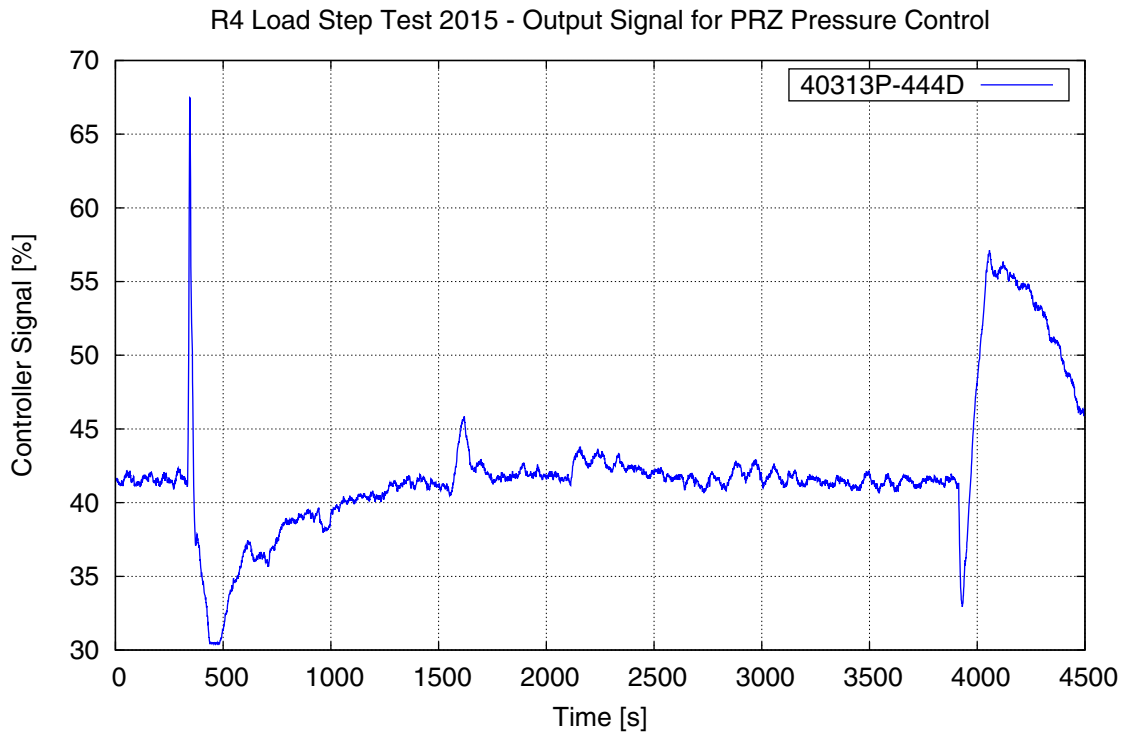
Figure 15   Output Signal for PRZ Pressure Control

R4 Load Step Test 2015 - PRZ Proportional Heater Control
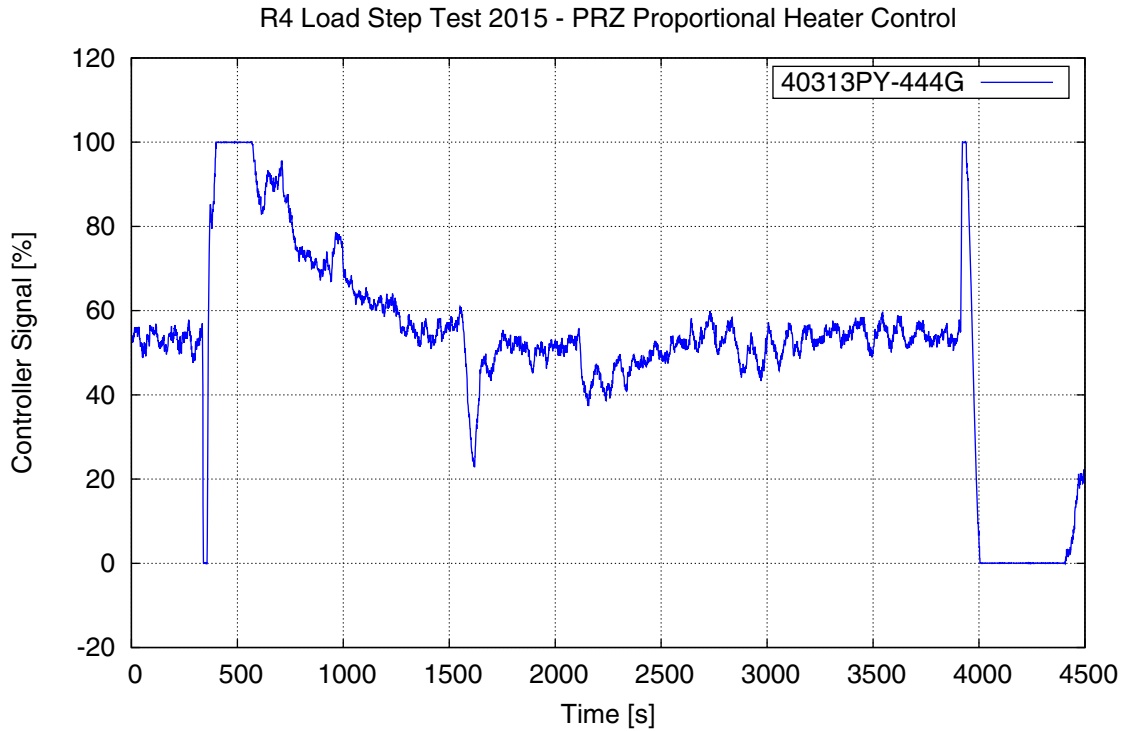
Figure 16   PRZ Proportional Heater Control Signal

R4 Load Step Test 2015 - Control Signal for PRZ Spray Valve
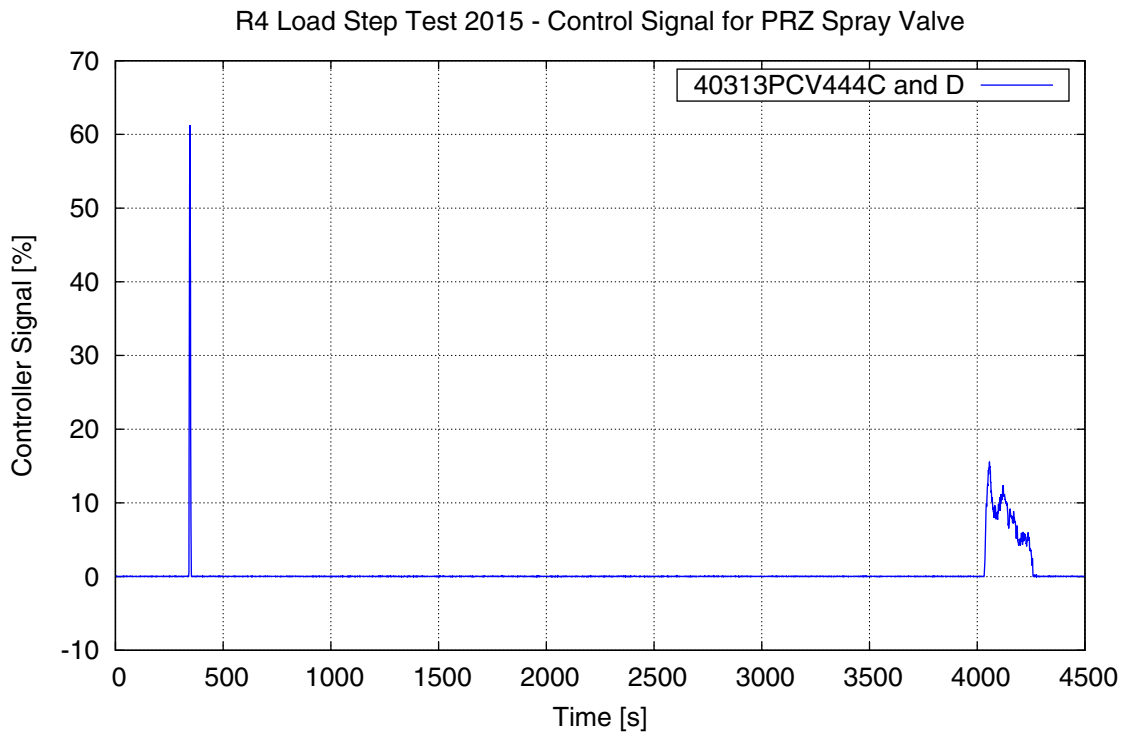
Figure 17   Control Signal for PRZ Spray Valve
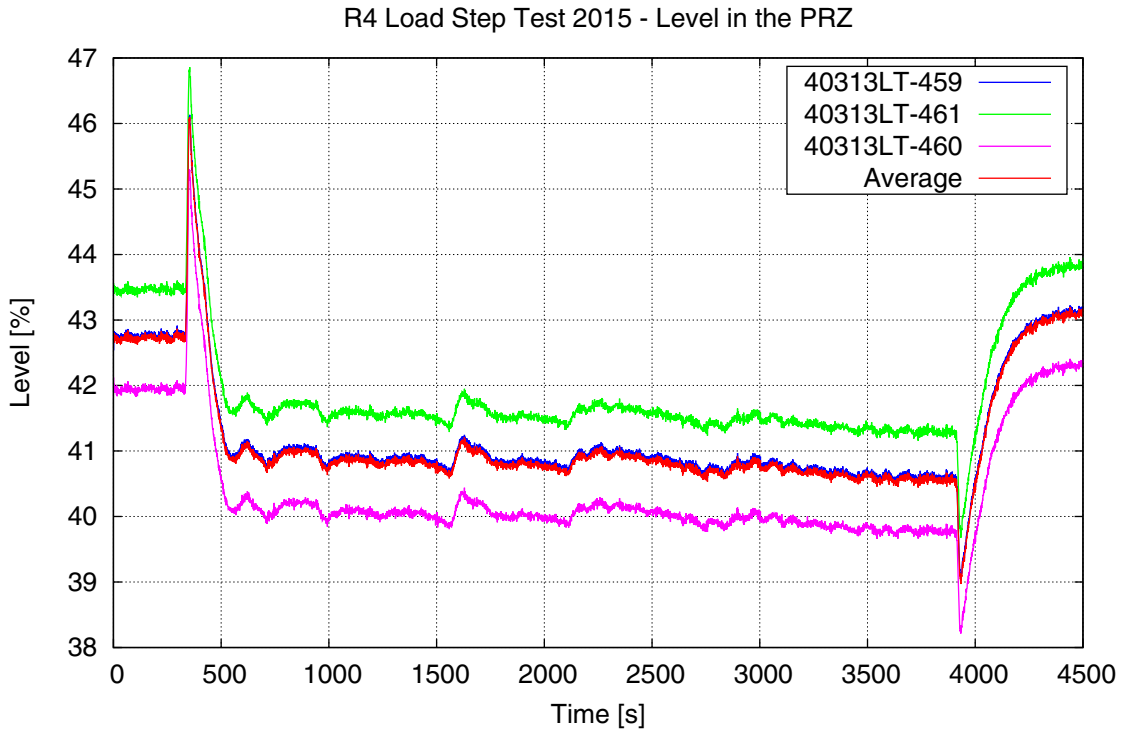
Figure 18   Level in the PRZ
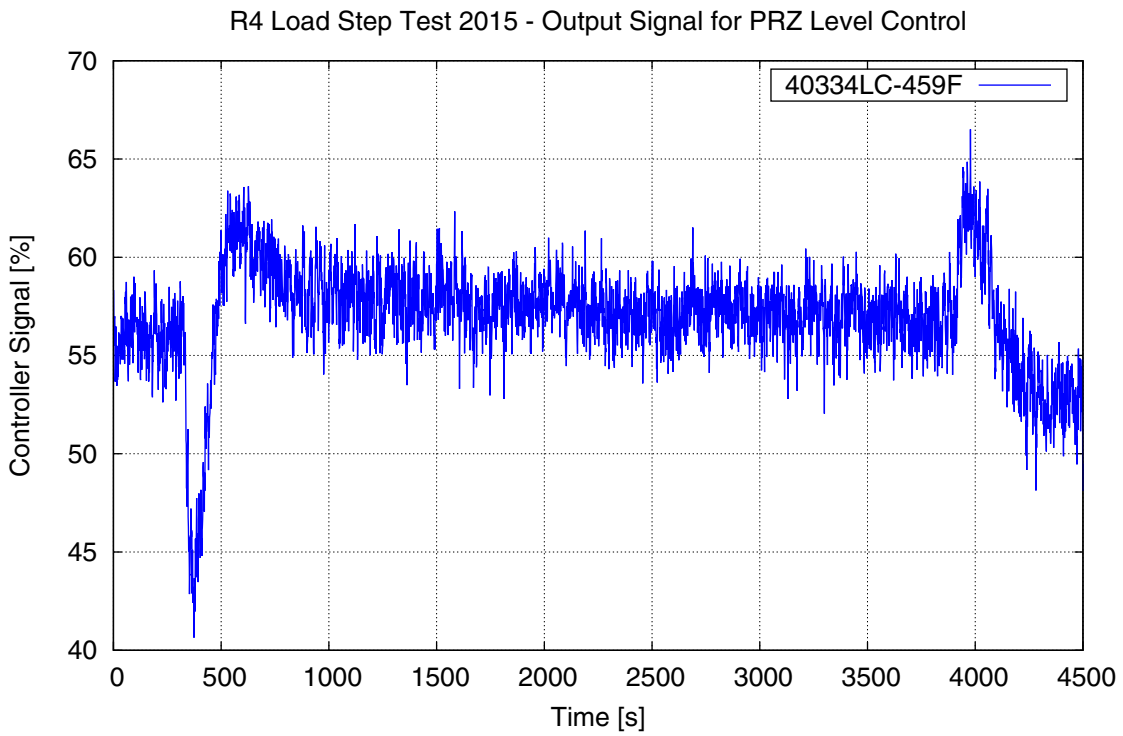
Figure 19   Output Signal for PRZ Level Control

R4 Load Step Test 2015 - Pressure in SGs
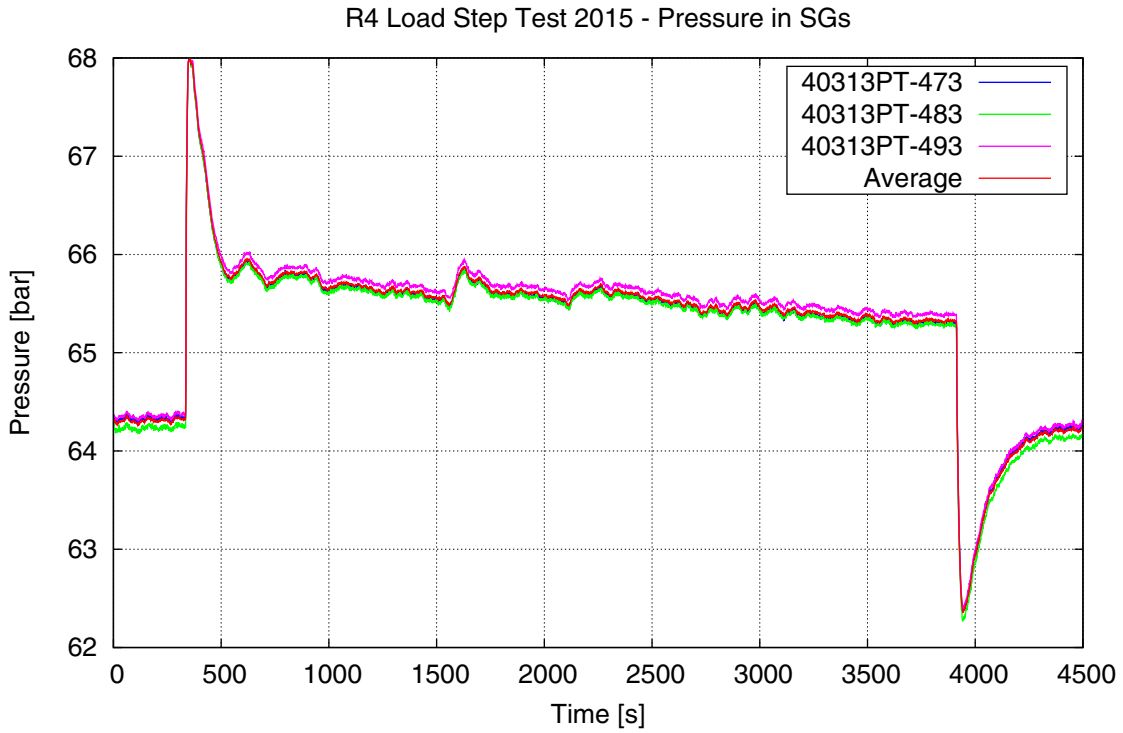
Figure 20   Pressure in the SG Steam Dome

R4 Load Step Test 2015 - Temperature of Feedwater
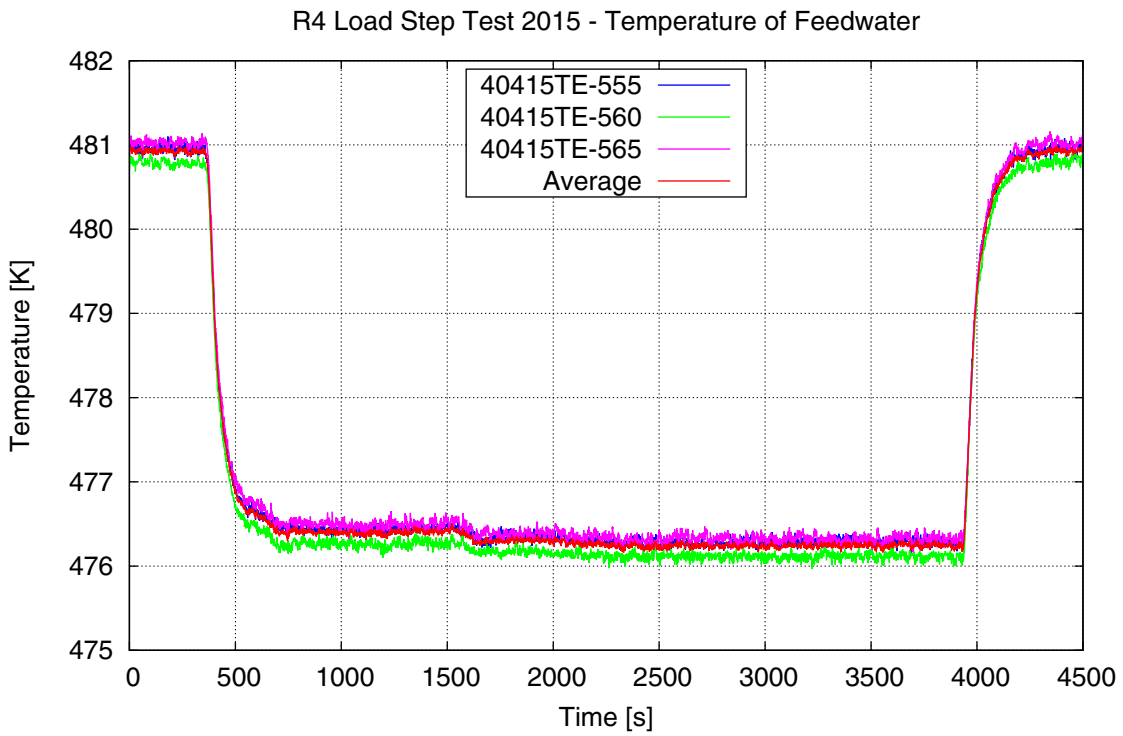
Figure 21   Temperature of Feedwater

R4 Load Step Test 2015 - Turbine Control Valve Position
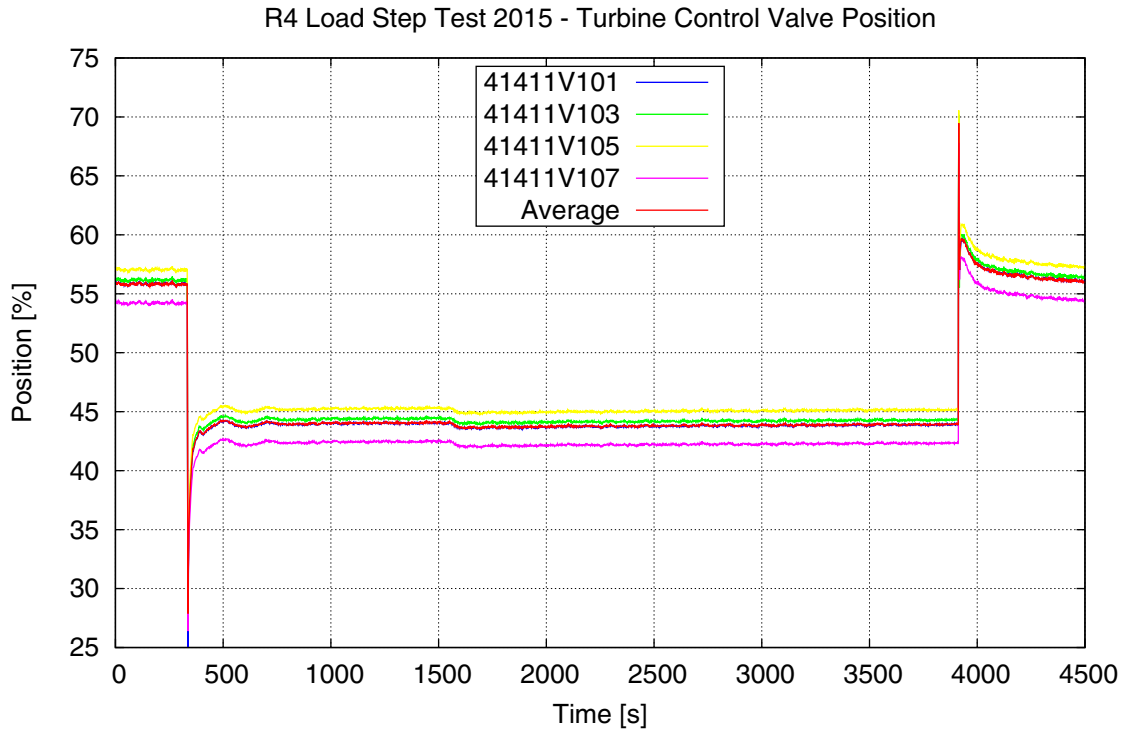
Figure 22   Turbine Control Valve Position

R4 Load Step Test 2015 - Feedwater Flowrate
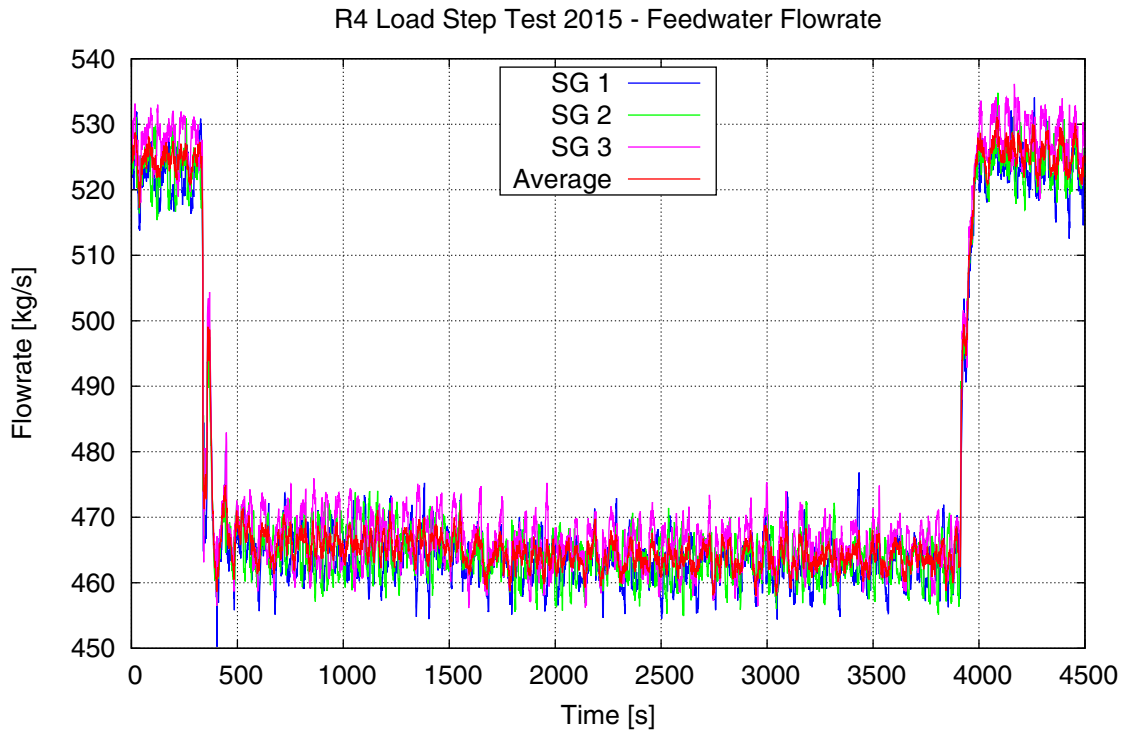
Figure 23   Feedwater Flowrate
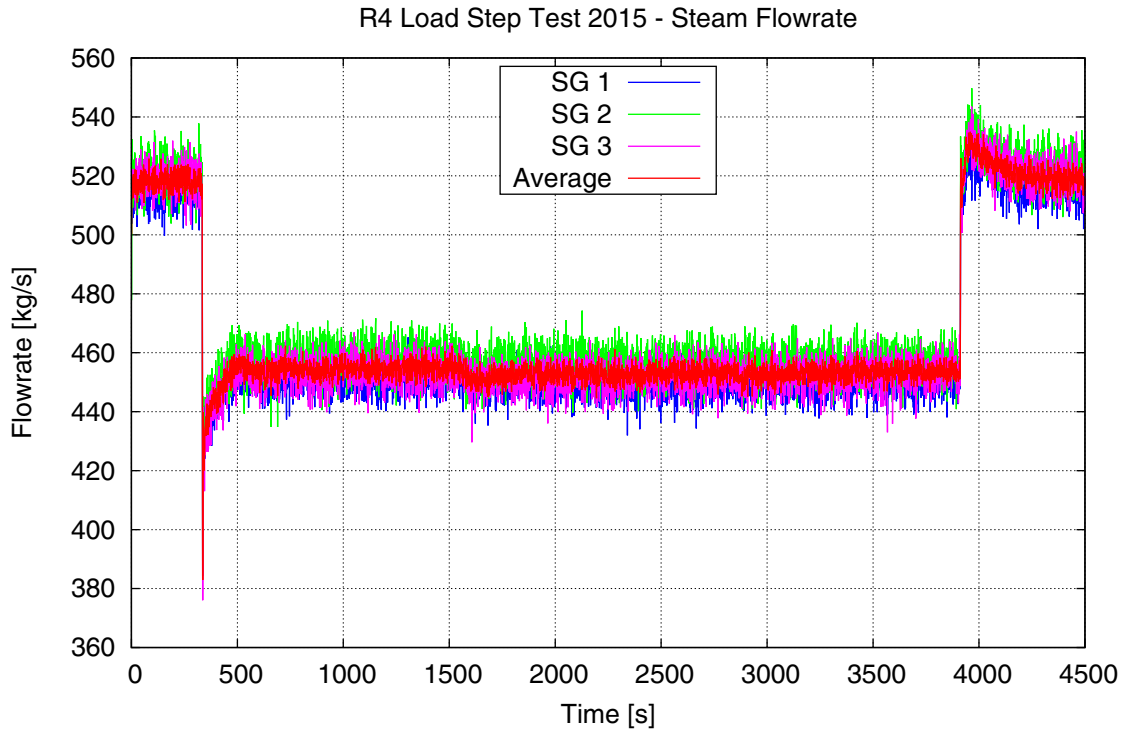
Figure 24   Steam Flowrate
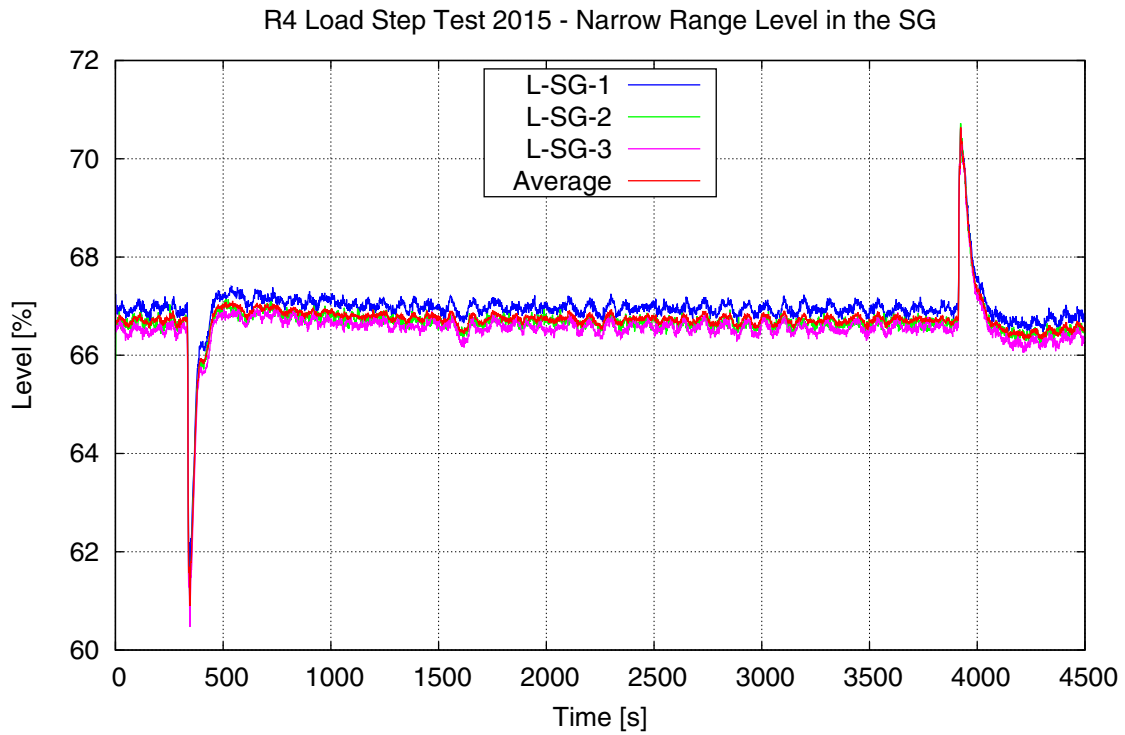
Figure 25   Narrow Range Level in the SG

3   DESCRIPTION OF THE CODE AND THE MODEL

3.1   The RELAP5 Code as an Analytical Tool

In prior agreement with SSM, the RELAP5 code has been selected as the numerical tool for the transient analysis. It has been developed for best-estimate transient simulation of light water reactor coolant systems during postulated accidents. The code originates from the Idaho National Engineering Laboratory (INEL) and first it was created for the U.S. Nuclear Regulatory Commission (NRC). Code uses include analyses required to support rulemaking, licensing audit calculations, evaluation of accident mitigation strategies, evaluation of operator guidelines, and experiment planning analysis. RELAP5 has also been used as basis for a nuclear plant analyzer (NPA). The code models specific simulations of transients in LWR systems, e.g., the coupled behavior of the reactor coolant system and the core for loss-of-coolant accidents and, operational transients such as anticipated transient without scram, loss of offsite power, loss of feedwater, station blackout, turbine trip and, loss of flow. RELAP5 is a highly generic code that, in addition to calculating the behavior of a reactor coolant system during a transient, can be used for simulation of a wide variety of hydraulic and thermal transients in both nuclear and nonnuclear systems involving mixtures of steam, water, non-condensable, and solute.

RELAP5/MOD3.3 Patch-04-jm was the latest installed version of the code [7] at the time of the analysis and it was used without any modification in the source code. RELAP5 is maintained jointly by the NRC and a consortium consisting of several countries and U.S. organizations that were members of the International Code Assessment and Applications Program (ICAP) and its successor organization, Code Applications and Maintenance Program (CAMP). Sweden is a signatory member country of the CAMP Agreement.

The RELAP5/MOD3 code is based on a one-dimensional, nonhomogeneous and non-equilibrium six-equation hydrodynamic model for the two-phase systems. The mass, momentum and energy balance equations are solved by a fast, partially implicit numerical scheme to permit economical calculation of system transients. The objective of the RELAP5 development effort from the outset was to produce a code that included important first-order effects necessary for accurate prediction of system transients but that was sufficiently simple and cost effective so that parametric of sensitivity studies were possible. The code includes many generic component models from which general systems can be simulated. The component models include pumps, valves, and pipes, heat releasing or absorbing structures, reactor point kinetics, electric heaters, jet pumps, turbines, separators, accumulators, and control system components. In addition, special process models are included for effects such as form loss, flow at an abrupt area change, branching, choked flow, boron tracking, and non-condensable gas transport.

3.2   Development of the R4 Model

3.2.1   The R3 Model as a Starting Point

A very simplified RELAP5 model was created for R3/4 by J. Eriksson [8] at Studsvik EcoSafe in 1994. About a decade later, Chalmers University of Technology took over the developmental efforts on the legacy input. The former coarse nodalization has been refined, thoroughly updated, extended, and a coupled neutron kinetic model has been prepared. A technical description of the coupled R3 model is summarized in [2]. Results of the validations have been published in a number of technical reports, international conferences, and scientific journals [9], [10], and [11].

3.2.2   Status of the Current R4 Model

The current RELAP5 model of the R4 was built on the basis of the R3 (Figure 26). Since the layouts of the R3 and the R4 units are similar, the main intention was to keep as many elements from the R3 model as possible. However, the steam generators and the pressurizer were replaced with the new AREVA-design components in 2011. The structures of these parts, especially the SGs are significantly different from those that are installed in R3. Consequently, building a new full-plant model became necessary.
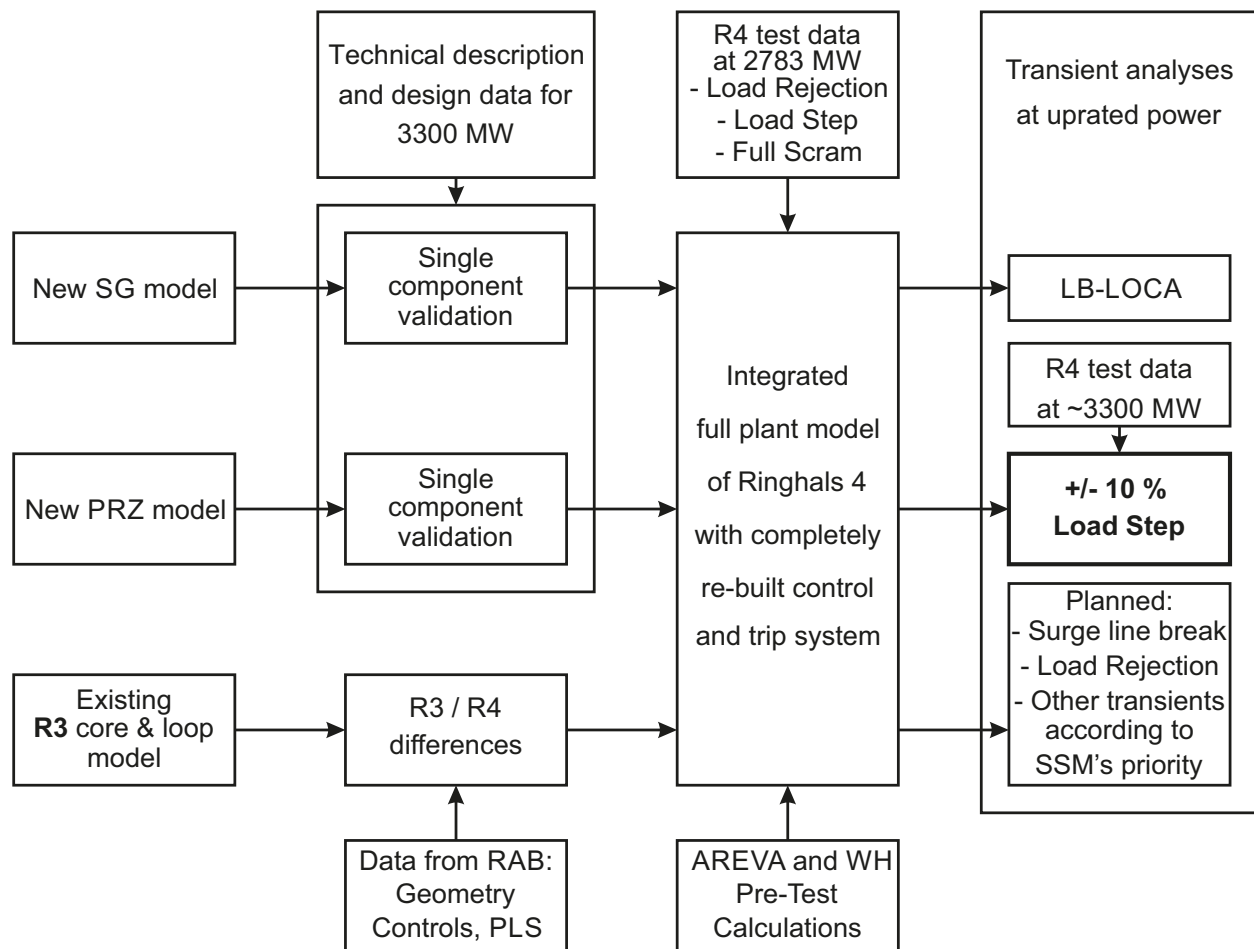
Figure 26   Process of model Development for Ringhals 4

The current R4 model represents the "state-of-the-art" and the practical experiences that have been gained by the modeling efforts over the last few years. Quality assurance is guaranteed by the results of the extensive verification and validation tests that the Ringhals models have passed successfully. A number of *startup* and *maneuverability* tests were performed with using 2783 MW_{th} before the power uprate at the end of 2011. In particular, a transient with a stepwise change of load by ± 10 % was used for validation of the new components and the related control system responses to the perturbations. The results are summarized in a conference paper [5].

The plant parameters, details of the control system data, setpoints, technical specifications and operational data were obtained from the Precautions, Limitations, and Setpoints (PLS) document of R4 [12].

3.3   Description of the Primary Side

3.3.1   The Reactor Pressure Vessel Internals

The complex structure of the reactor pressure vessel (RPV) internals of a Westinghouse-type PWR is shown in Figure 27 [13]. The core consists of 157 fuel assemblies. The fuel rods are arranged into a 17x17 matrix. The length of a fuel rod is 3.66 m.
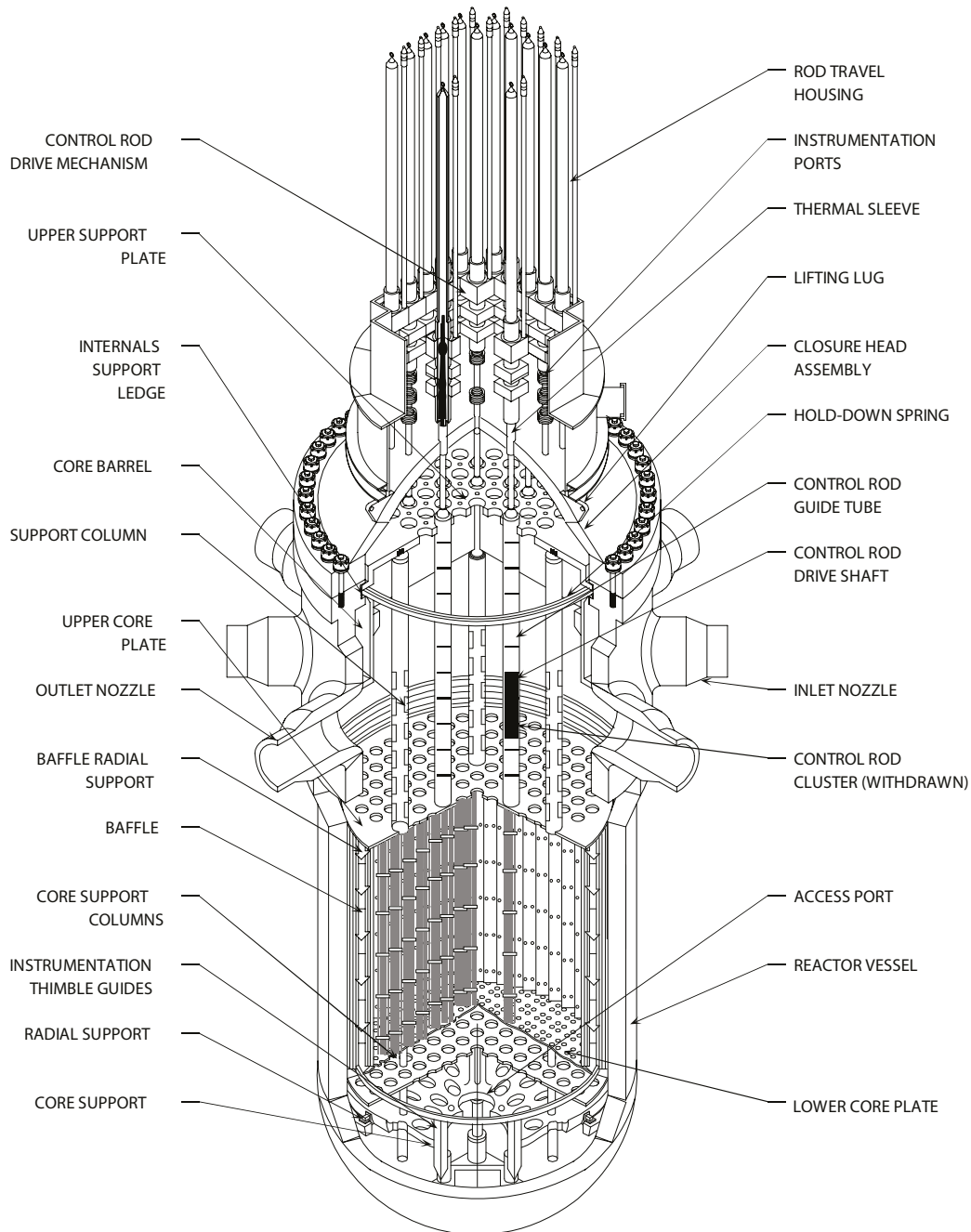
Figure 27   Internal Structure of a Westinghouse-Type PWR Pressure Vessel

In the core region, each of the 157 fuel assemblies is modeled individually, both for the hydrodynamics and for the heat structures. Such a detailed nodalization has been chosen in order to allow 1:1 coupling between the thermal hydraulic and neutron kinetic calculations.

It is assumed that a 1/3 radial section of the core of is connected to 1 loop out of 3 loops, marked with red, green, and blue colors, respectively in Figure 28. In principle, 52 and 1/3 assemblies belong to 1 loop. This means that, due to lacking triangular (120°) symmetry, the assembly in the center (no. 364) is equally split between the 3 loops. In axial direction, the active core was discretized into eight levels.
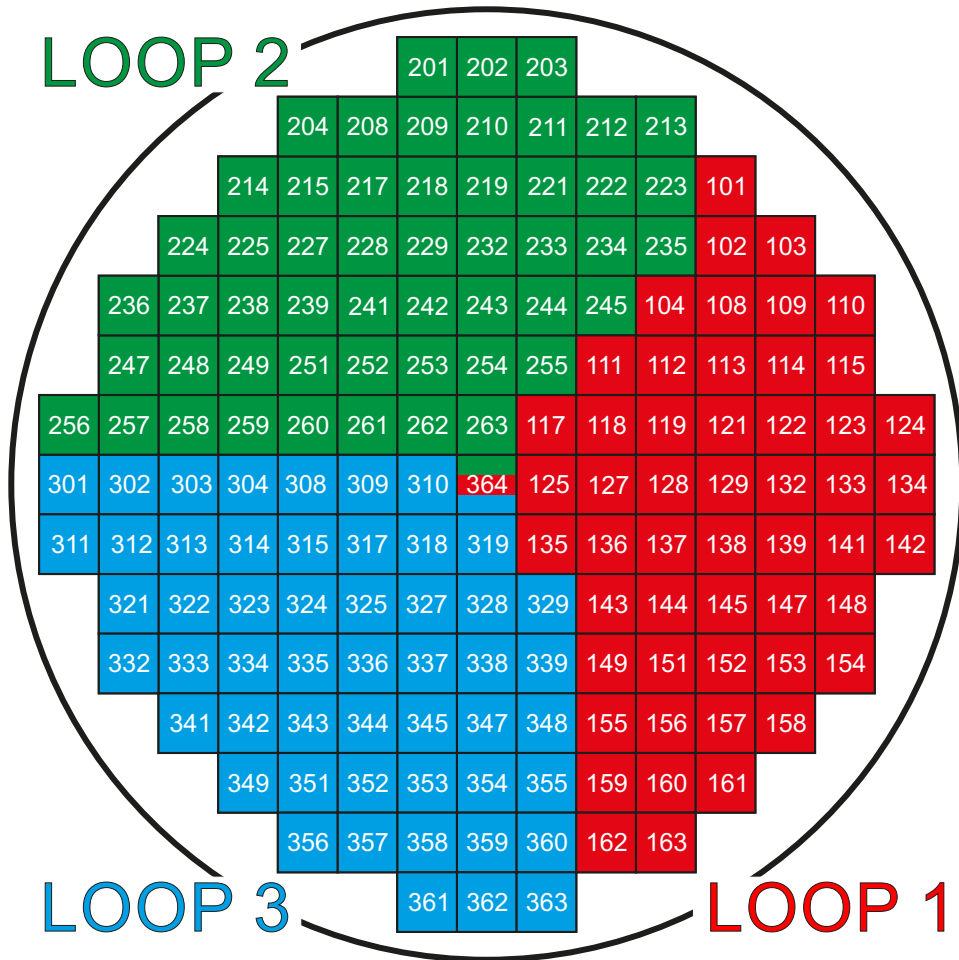
Figure 28   Numbering Scheme of the Radial Nodalization

The core inlet and outlet needed special considerations due to a limitation in RELAP5, that a "branch" component may be connected to a maximum of 9 other volumes. To overcome this limitation, 6 branches per loop were inserted to the core inlet and outlet. (Components 171-176, 271-276, 371-376 at the inlet, and 191-196, 291-296, 391-396 at the outlet on Figure 29).

It is essential that some specific phenomena, for instance an asymmetric behavior of the loops can be properly captured. For this reason, the downcomer (DC), the way as the core is split into three parallel channels in order to retain the 3-loop structure of the primary side even within the reactor pressure vessel.
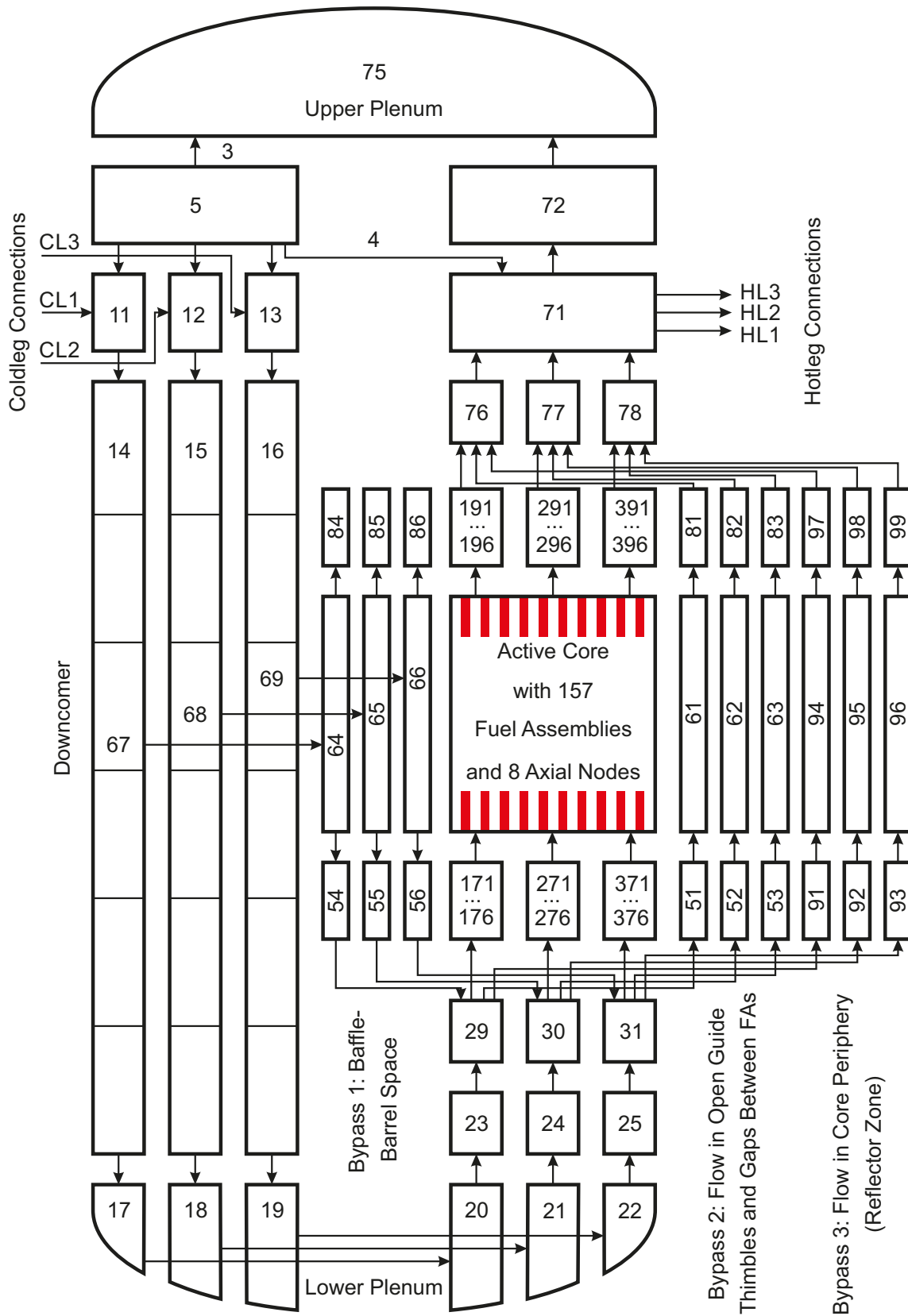
Figure 29 Nodalization of the RPV Internals

Figure 30   Nodalization of the Entire Primary Side
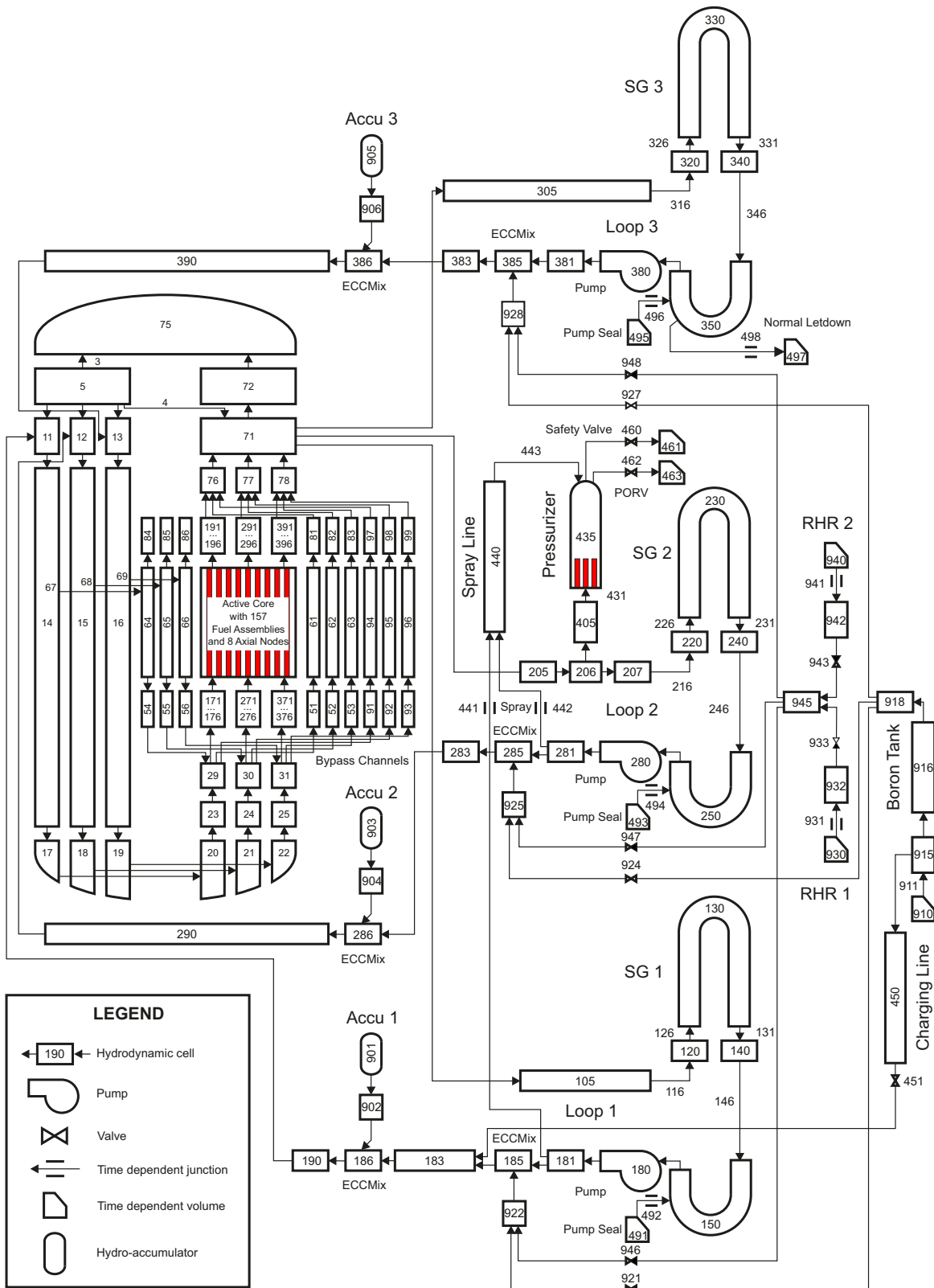
It has to be underlined that the DC is modeled in a realistic manner, including the material properties and the wall thicknesses of metallic structures. Application of 6 axial nodes in an "annulus" component provides adequate resolution for level tracking and thermal stratification. Modeling of heat transfer between the fuel assemblies, the baffle, the barrel, the DC wall, the RPV wall, and the ambient assures that the DC-related thermal hydraulic phenomena are simulated with high fidelity.

It is also important to distinguish between the coolant flowing through the fuel assemblies while being heated, and the remaining part of the main loop flow. Thus, the core has been extended with altogether three bypass channels per loop in the following manner:

- the first one is representing the baffle-barrel space,
- the second one is modeling the open guide thimbles, and
- the third channel is created for the flow path at the core periphery.

The flow resistances were set according to the plant data and therefore resulted in a realistic distribution of the pressure losses. Figure 30 shows the nodalization of the entire primary side.

3.3.2 Heat Structures in the Fuel

The radial description of the fuel rods consists of 3 materials:

- the pellet with UO2 fuel,
- the gap with He gas, and
- the cladding with zircaloy.

Altogether 9 mesh points are defined in the heat structures accordingly (Figure 31). The radial coordinates of the mesh points are indicated as distances from the center line.
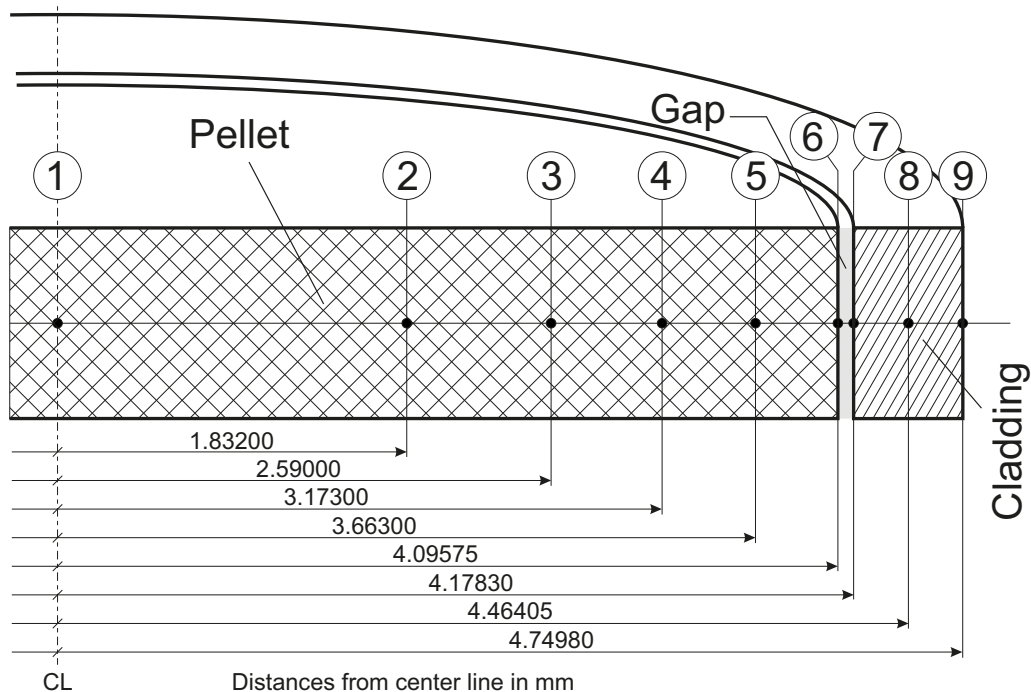
Figure 31 Geometry of the Fuel Rods with Radial Mesh Points

3.3.3   Axial Power Distribution

Distribution of the relative power in axial direction is shown in Figure 32. Altogether 8 axial nodes are used for the heat source in the active part of the core, which is the same number as of the corresponding hydrodynamic cells.
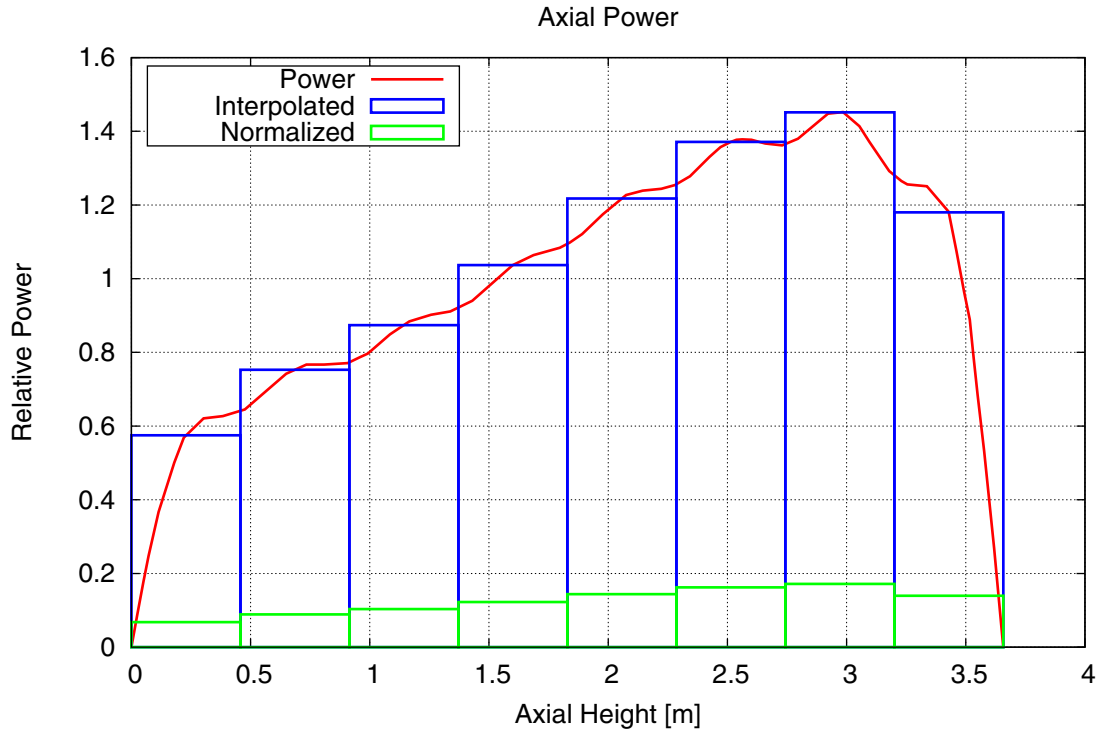
Figure 32   Power Distribution in the 8 Axial Nodes

3.3.4   The Main Circulation Pump Model

The MCPs are modeled with "pump" components available in RELAP5. The homologous curves, torque and head data were obtained from plant documentation. The model was adopted from R3 input without any modification in the updated version of the R4 input deck. Maintaining the primary side loop flowrate is achieved with controlling the velocity of the pump. A dedicated control variable (cntrlvar-180) stores the deviation of the actual loop flowrate from the setpoint value of the desired loop flowrate in kg/s. A PI controller (cntrlvar-181) determines the pump velocity in order to approach the setpoint value as close as possible.

3.3.5   The Safety Systems

One hydro-accumulator component (901, 903, and 905) is connected to each loop of the primary system through an emergency core cooling mixer component (x86). X denotes here the number of loop, i.e. 1, 2, or 3. These ECC mixers are operating in tandem with the other mixers (x85) that may inject water either from the boron tank (916) or from the residual heat removal system (930 and 940).

The primary side model is extended with a time dependent junction (498) simulating the normal letdown, and a charging line (450) and the corresponding charging valve (451).

3.3.6 Primary Side of the Steam Generators

The coolant enters to the inlet plenum (120) from the hot leg (Figure 33). The inverted U-shaped heat exchanger tubes are modeled with a single channel (130). The tube bundle model has altogether 22 cells. The cells from 130-01 to 130-10 are vertical and upwards directed. The cells 130-11 and 130-12 are simulating the U-turn of the tubes with tilted volumes at the top. The cells between 130-13 and 130-22 are again vertical but pointing downwards on the cold leg side. The outlet plenum is modeled with a branch component (140).

3.4 Description of the Secondary Side

3.4.1 Secondary Side of the Steam Generators

The feedwater is injected through the distributor, and enters to the top volume of the inner DC (505-01). The flow is downwards directed in the channel and reaches the connection junction (508) at the tube plate. It turns upwards at cold side of the riser (510). The boiler section starts with a component (530) having 4 internal cells above the divider plate. The evaporator has 2 components (535 and 538). Phase separation takes place in the separator (540).

The water droplets are diverted from the separator to the upper part of the DC, which is connected to the inlet of cell 545-04. The volume (554) is a downwards directed channel, ending in a junction (548), which connects to the outer DC component (550). The fluid is recirculated in this volume and fed into the hot side of the riser (520) at the bottom of the SG. The volume (520) is thermally associated with the hot leg side of the heat exchanger tube bundle, and also with the cold side of the riser through the divider plate. In those secondary volumes where the heat exchanger tubes are led through (510, 520, and 530) the "bundle friction" option is applied. The steam drum, the dryer, and the steam dome are modeled with 2 volumes (560 and 570) at the top of the SG. In fact, (570) is a branch component and its exit junction is connected to steam line. The upper part of the outer DC (545) appears both on the left and right sides of the nodalization.

3.4.2 The Feedwater and Steam Lines

The nodalization scheme of the entire secondary side is shown in Figure 34. The boundary conditions for the normal FW are set in a time dependent volume (581). Distribution of the FW takes place in a branch component (854). The normal FW line consists of a control valve (862, 872, and 882) and an isolation valve (864, 874, and 884), respectively in each loop. The auxiliary FW is taken from the boundary volumes (891, 893, and 895). The flowrate of the injected auxiliary FW is controlled by time dependent junctions (892, 894, and 896).

The steam line is split into 2 parts (x85 and x95), each partitioned to 10 volumes. "X" is again associated with the loop number, i.e. x = 5, 6, and 7 mean loops 1, 2, and 3, respectively. The main steam isolation valve (x94) is connecting the 2 parts together. Relatively high resolution of meshing was chosen in order to capture propagation of pressure pulses along the steam lines. Altogether 6 safety valves (x86…x91) and a relief valve (x92) are connected to the steam line, in parallel with each other. The steam lines are merging at a branch component (800). The Ringhals-4 unit has 2 turbines and 4 turbine dumps. These components are modeled in a simplified way in the current RELAP5 model. Turbine 1 and 2, and their control valves are simulated with time dependent junctions (814 and 824) and motor valves (813 and 823), respectively.
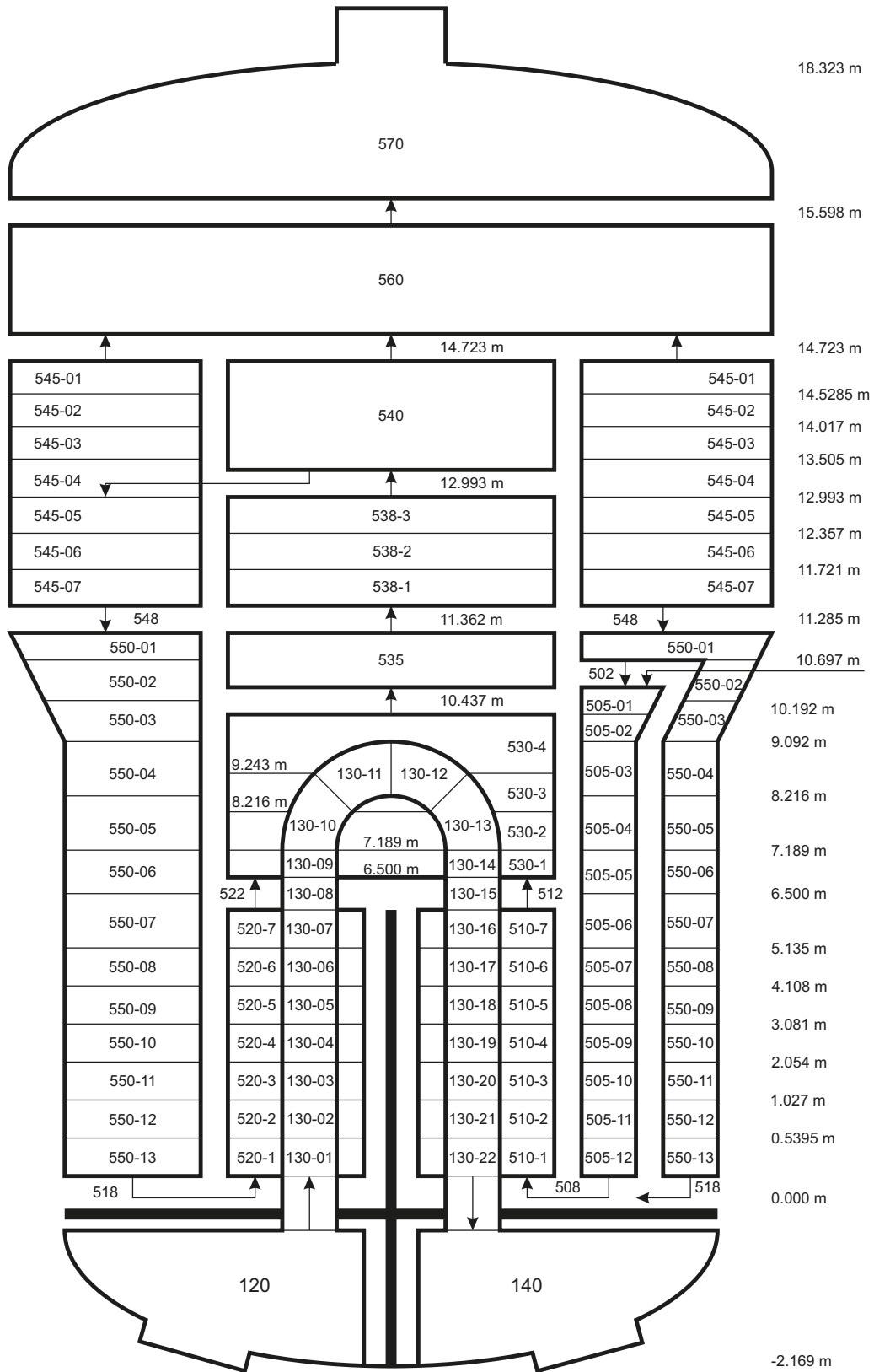
Figure 33   Nodalization Scheme of SG 1
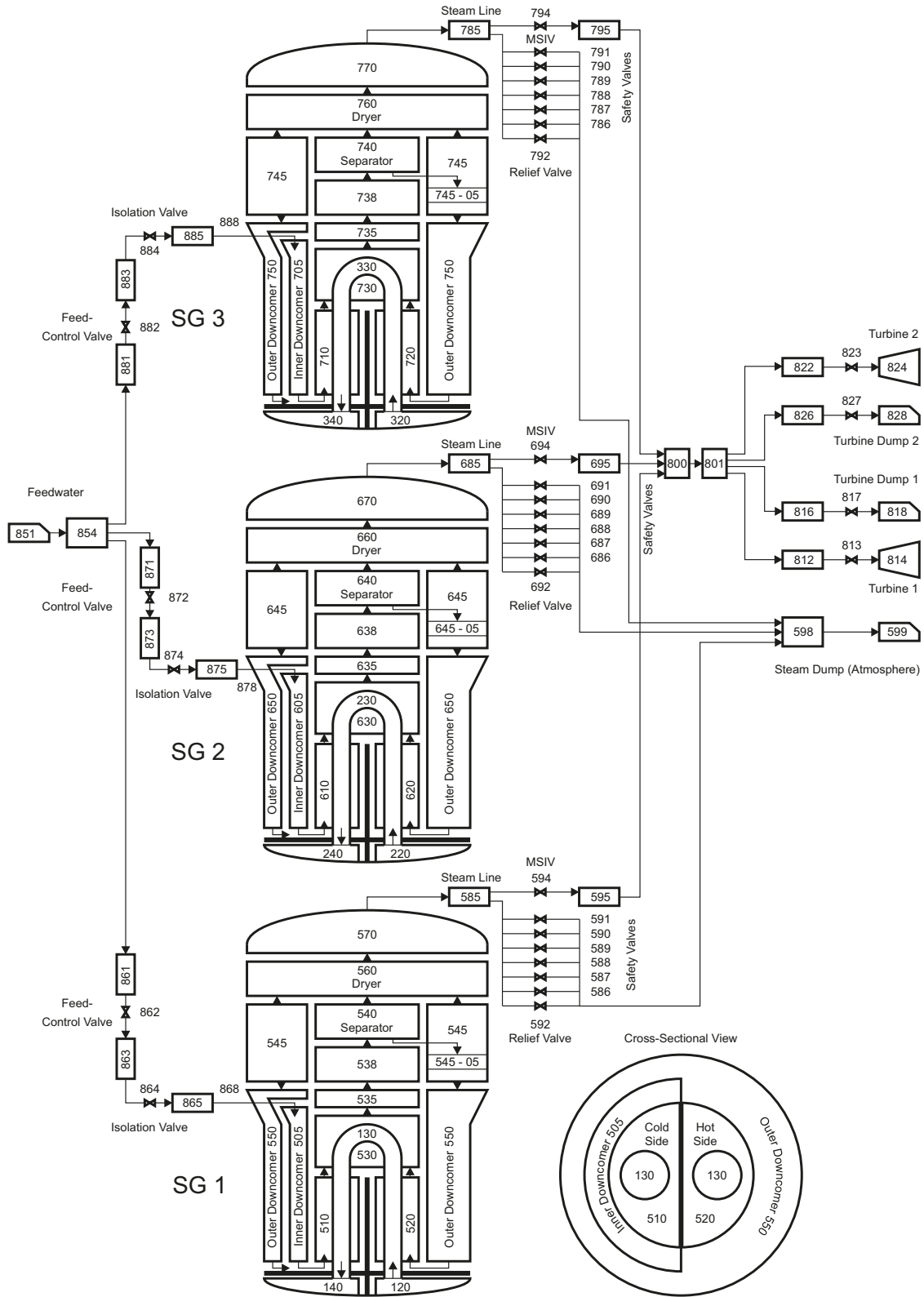
Figure 34   Nodalization Scheme of the Entire Secondary Side
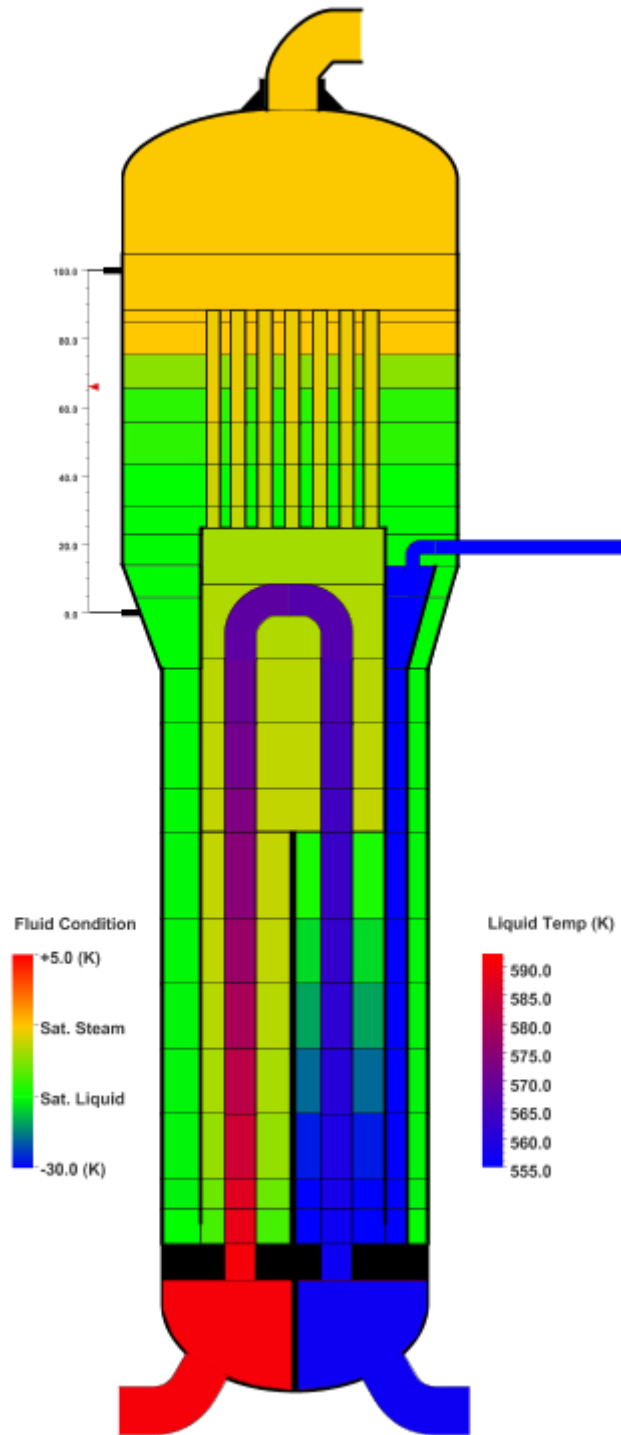
Figure 35   Fluid Conditions in the SG by the SNAP Visualization Vool
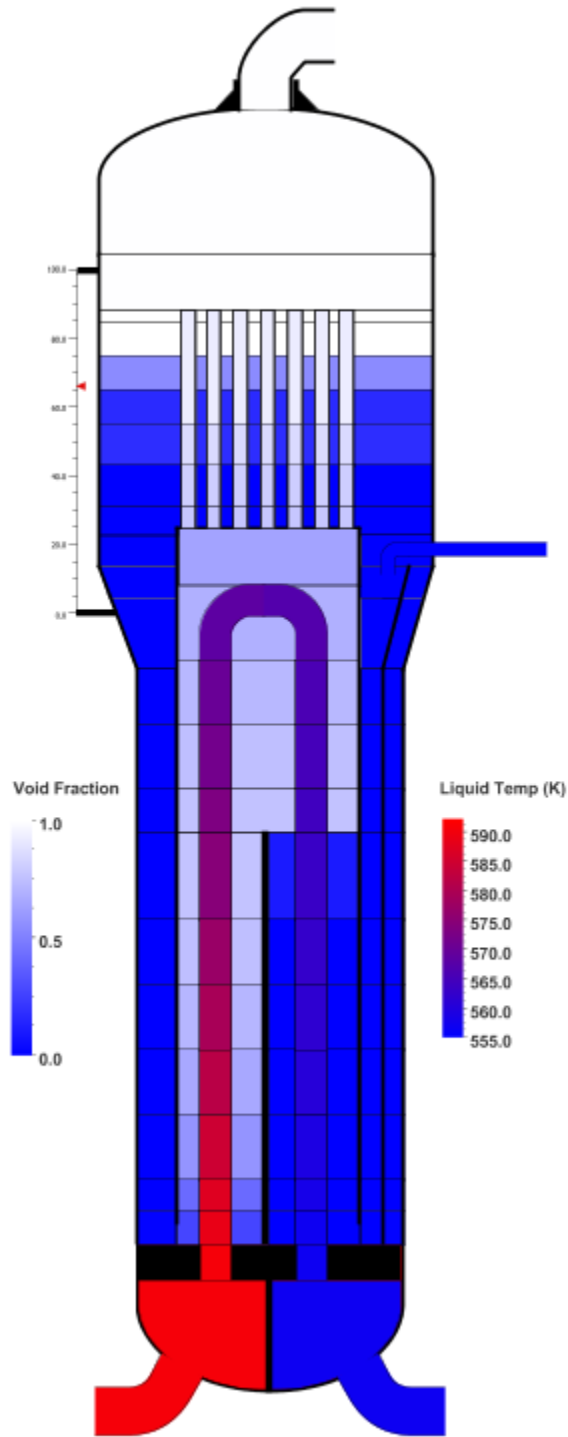
Figure 36   Void Fractions in the SG by the SNAP Visualization Tool

4 STEADY-STATE RESULTS

It is essentially important that a numerical simulation should reach perfect steady-state before initiating a transient calculation. However, looking at the measured plant data, this goal seems to be theoretical because even in the most stable and normal operation of a plant, in fact, it is in a "quasi-steady-state" condition. Consequently, the term "steady" can mean minor oscillations around a setpoint value.

4.1 Energy and Mass Balance Calculation

Exact calorimetric details of the thermal power were not available from the plant at the time of the simulations. One of the possible approaches to determine a consistent dataset is to make an estimate, using averaged data over the measured stable period of time. This "hand-calculated" dataset can satisfy the energy and mass balance equations, which will be entered to the RELAP5 input as initial conditions.

The balance calculations help also to determine those parameters that are not directly available from the measure database. For instance, the primary loop flowrate is recorded as percentage of the nominal flow but the reference (i.e. 100 %) value is not known. Still, it is necessary to enter the flowrate data in SI units (kg/s) into the RELAP5 input.

Knowing the flowrate $\dot{m}_{FW}$, temperature T_{FW}, and pressure p_{FW} of the feedwater, the enthalpy h_{FW} can be determined. With assumption of saturated steam (x_{steam} = 1) the enthalpy of the steam h_{steam} can also be determined. With neglecting the small amount of blowdown steam and averaging of the flowrates, the thermal energy $Q_{SG,sec}$ of the steam generators can be calculated.

By taking into account the considerations above, the following, reasonably simplified balance equations can be set up:

4.1.1 Balance Equations of the Secondary Side

$$\dot{m}_{FW} = 524.57 \text{ kg/s}$$
$$T_{FW} = 480.92 \text{ K}$$
$$p_{FW} = 70.0 \text{ bar}$$
$$h_{FW} = 0.889723 \cdot 10^6 \text{ J/kg}$$
$$\dot{m}_{steam} = 518.17 \text{ kg/s}$$
$$p_{steam} = 64.31 \text{ bar}$$
$$x_{steam} = 1$$
$$h_{steam} = h'' = 2.7797 \cdot 10^6 \text{ J/kg}$$
$$\bar{m} = \frac{\dot{m}_{FW} + \dot{m}_{steam}}{2} = 521.37 \text{ kg/s}$$
$$Q_{SG,sec} = \bar{m}(h_{steam} - h_{FW}) = 985.377 \text{ MW}$$
$$\sum_{i=1}^{3} Q_{SG,sec,i} = 3 \cdot N_{SG} = 2956.132 \text{ MW}$$

4.1.2 Balance Equations of the Primary Side

With assumption of the PRZ pressure p_{PRZ} to be the primary system pressure, and knowing the temperatures of the hot leg T_{HL} and of the cold leg T_{CL}, the enthalpy difference Δh can be determined. Neglecting the losses of heat transfer between the primary and secondary sides, as well as the additional heat generated by the main circulation pumps, we can calculate the loop flowrate $\dot{m}_{loop}$ from the SG thermal energy Q_{SG}, according to the following simplified equations:

$$p_{PRZ} = 154.99 \text{ bar}$$
$$T_{HL} = 593.68 \text{ K}$$
$$T_{CL} = 556.51 \text{ K}$$
$$h_{HL} = 1.45632 \cdot 10^6 \text{ J/kg}$$
$$h_{CL} = 1.24997 \cdot 10^6 \text{ J/kg}$$
$$\Delta h = h_{HL} - h_{CL} = 0.20635 \cdot 10^6 \text{ J/kg}$$
$$Q_{SG,prim} = m_{loop}\Delta h$$
$$Q_{SG,prim} = Q_{SG,sec} = 385.377 \cdot 10^6 \text{ W}$$
$$\dot{m}_{loop} = \frac{Q_{SG,prim}}{\Delta h} = \frac{985.377 \cdot 10^6 \text{ W}}{0.20635 \cdot 10^6 \text{ J/kg}}$$
$$\dot{m}_{loop} = 4775.27 \text{ kg/s}$$
$$\dot{m}_{total} = \sum_{i=1}^{3} \dot{m}_{loop,i} = 3 \cdot \dot{m}_{loop} = 14\,325.81 \text{ kg/s}$$

4.1.3 Strategies to Reach Steady-State

As in any numerical plant analysis, the basic assumption is that the unit is operating under steady-state before moving out from stable conditions. Therefore, it is essential to provide a set of proper initial conditions prior to the transient initiation. This aim can be achieved by running the code long enough, while the control systems are actuated and converging the system to a sufficiently stable condition. This method is in accordance with the procedure suggested by the code User Guidelines, instead of using the "steady-state" option of the input, which may result in premature termination of the run.

The following strategies have been applied:

- The core heating power (2956.1 MW) is kept constant by the user-given heat source data in a fuel bundle. Control variable 001 specifies this boundary condition (BC).
- For maintaining the primary system pressure (Figure 37) close to the setpoint value, the PRZ pressure control system is driven by a control signal (Figure 39), the same way as in the plant: i.e. by spraying of coolant taken from the cold legs or heating the system up by the proportional heaters (Figure 40).
- The desired primary side level (Figure 38) is achieved by controlling the PRZ level control system. Charging of the coolant (Figure 41) is provided from the chemical and volume control system (CVCS). The PRZ level program is always a function of the actual average loop temperature (Figure 42).

- The temperatures in the hot leg (Figure 43) and cold leg (Figure 44) are not controlled. These are derived quantities in the code calculation.
- Concerning the primary side loop flowrate, the pump speed is controlled by monitoring the difference between the actual loop flowrate and the prescribed value. The pump rotation is adjusted by a PI controller accordingly.
- On the secondary side, the SG level control system is regulating the feedwater flowrate (Figure 45) and steam flowrate (Figure 46) in order to keep the SG level (Figure 47) at the necessary elevation. Deviations between the feedwater flows and the steam flows are sensed, and the level is compared to the actual setpoint value, which is a function of the reactor power. The feedwater control valve (FCV) is then actuated by modifying its cross-sectional area for injection of the appropriate amount of feedwater.
- The secondary side pressure (Figure 48) is given by a constant boundary condition. The turbine model is a simplified time dependent volume with a pressure boundary.

The parameters of the steady-state case are summarized in Table 1. Deviations of the achieved values from the desired ones are very small. Therefore, it can be concluded that the plant parameters have converged to a stable condition, which satisfies the expected heat balance between the primary and secondary sides.

Plots of the initial search run are shown in Figure 37 … Figure 48.

Table 1   Parameters at the End of the Steady-State Run

Parameter	Unit	Desired	Achieved	Diff. [%]	Parameter in RELAP
Reactor power	MW$_{th}$	2956.1	2956.1	0.0000	cntrlvar-001 (BC)
Primary pressure	bar	154.99	154.998	0.0052	p-435120000
PRZ level	%	41.94	42.33	0.9213	cntrlvar-430
PRZ charging flow	kg/s	5.6011	5.5981	0.0536	mflowj-451000000
PRZ prop. heater	%	53.14	54.02	1.6560	cntrlvar-411
Hot leg temperature	K	593.68	593.67	0.0017	tempf-120010000
Cold leg temperature	K	556.51	556.42	0.0162	tempf-140010000
Average temperature	°C	301.94	301.98	0.0132	cntrlvar-434
Loop mass flowrate	kg/s	4775.27	4772.56	0.0568	mflowj-180010000
Feedwater flowrate	kg/s	521.37	519.32	0.3932	mflowj-868000000
Steam flowrate	kg/s	521.37	519.39	0.3798	mflowj-594000000
SG level	%	66.71	66.71	0.0000	cntrlvar-502
SG pressure	bar	64.31	64.40	0.1399	p-570010000

4.2 Plots of the Steady-State Convergence

R4 Load Step Test 2015 - Pressure in the PRZ
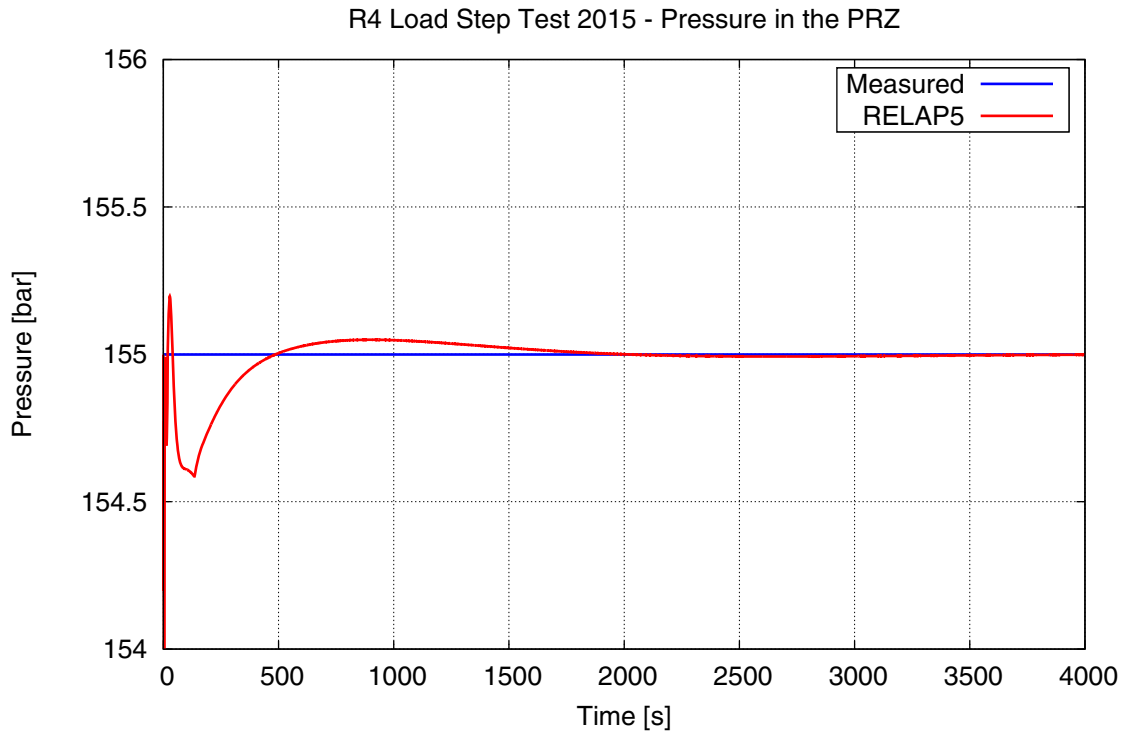
Figure 37   Pressure in the Pressurizer

R4 Load Step Test 2015 - Level in the PRZ
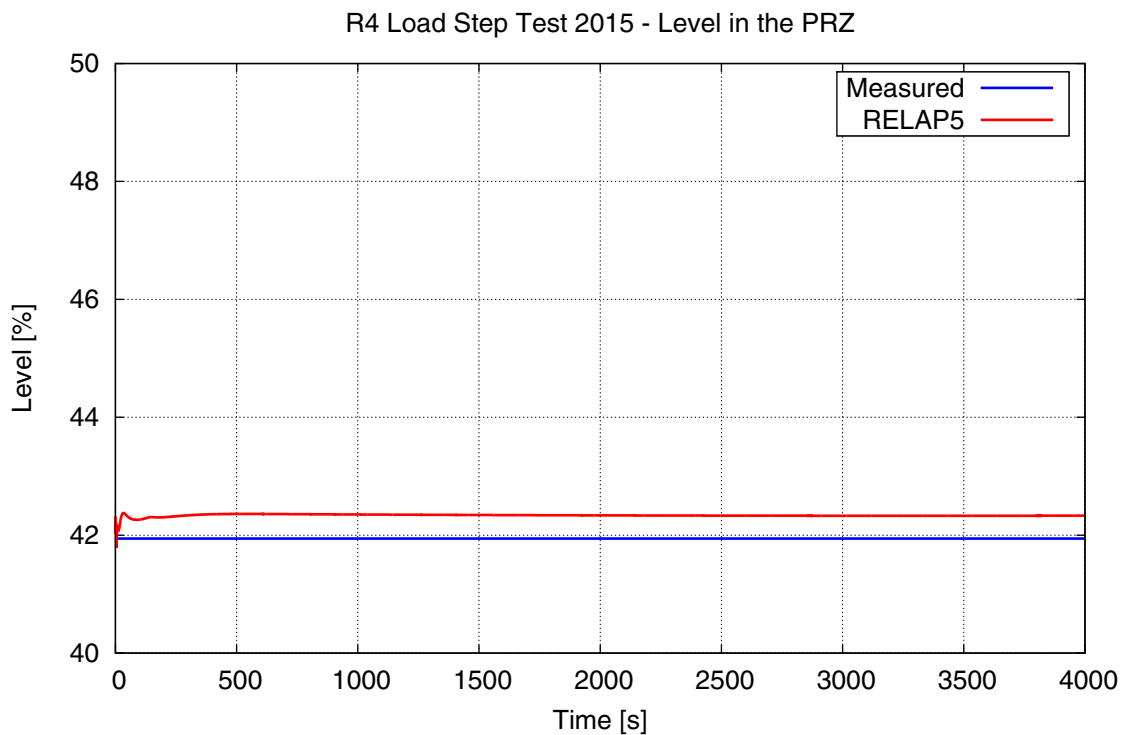
Figure 38   Collapsed Level in the Pressurizer
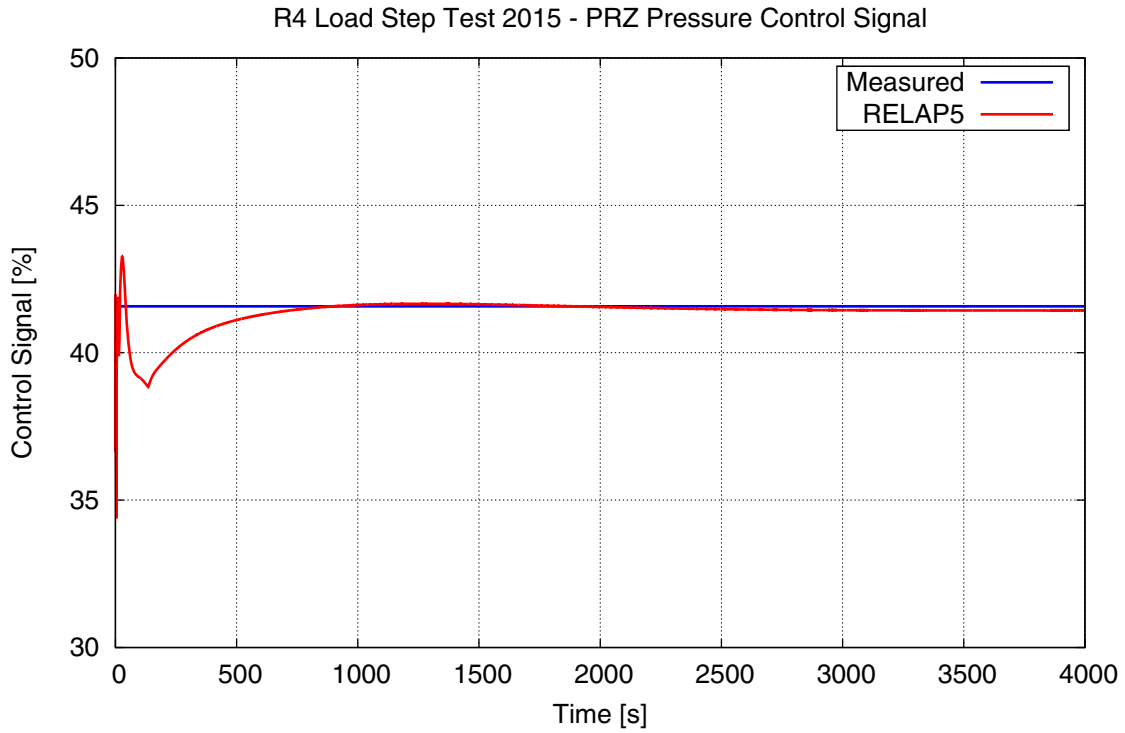
Figure 39   PRZ Pressure Control Signal
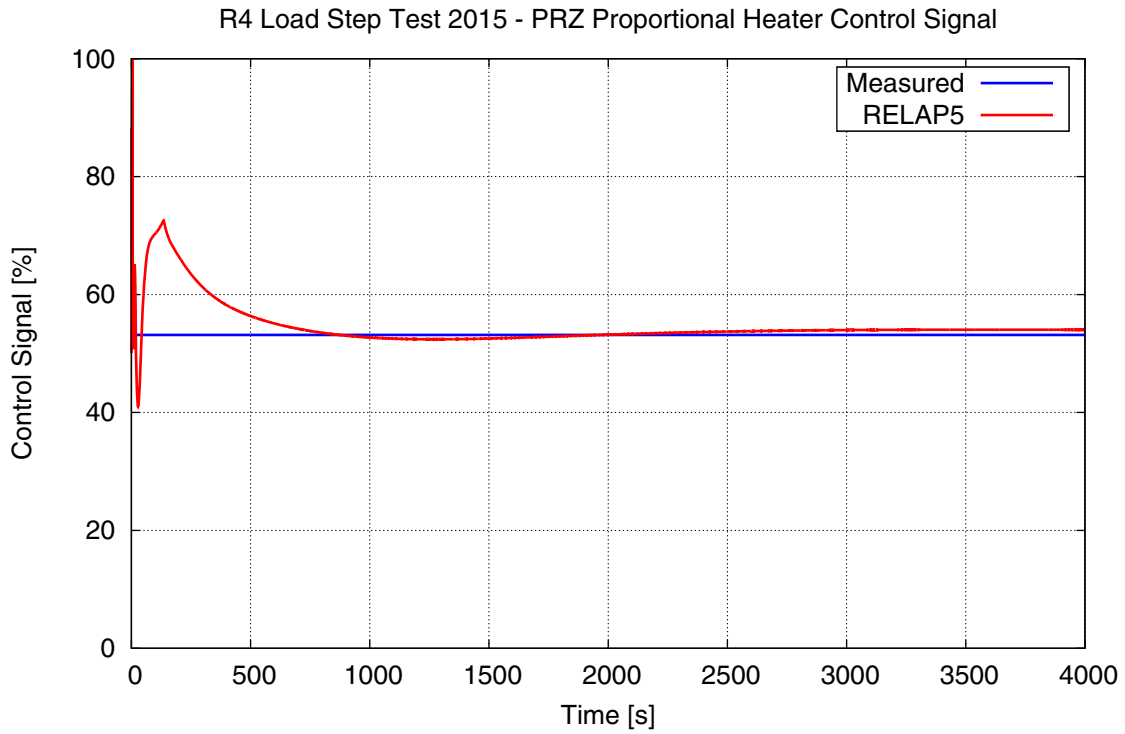
Figure 40   PRZ Proportional Heater Signal
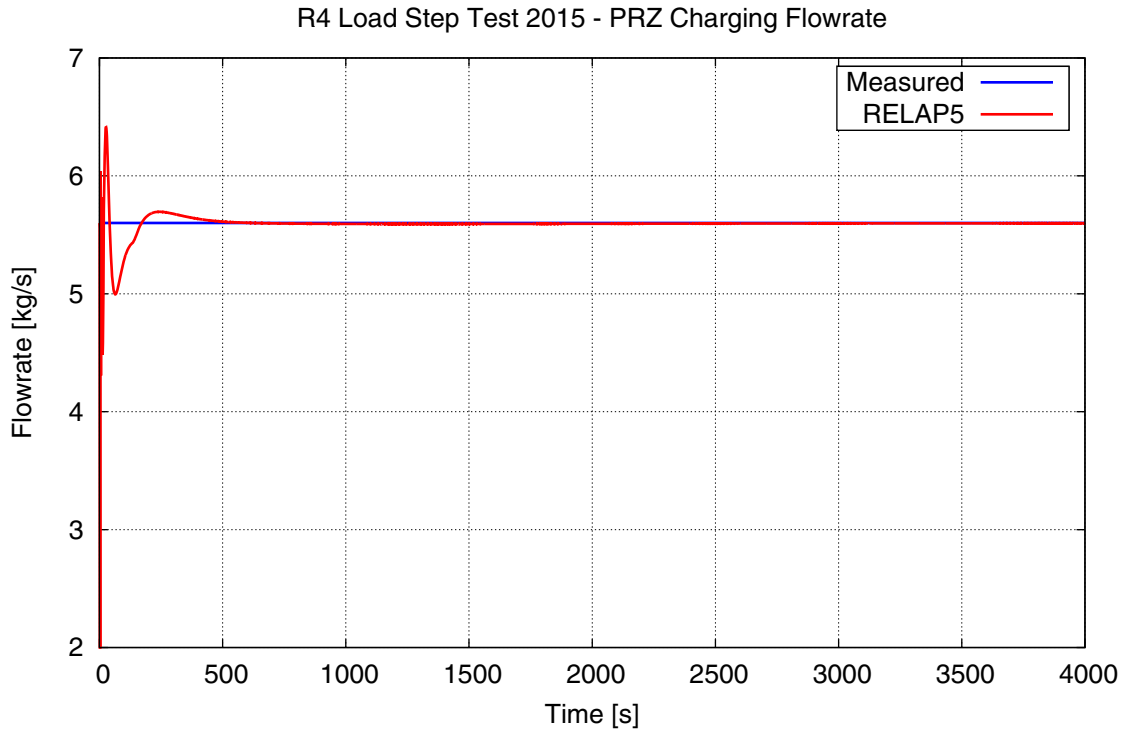
Figure 41   Charging Flowrate of the PRZ
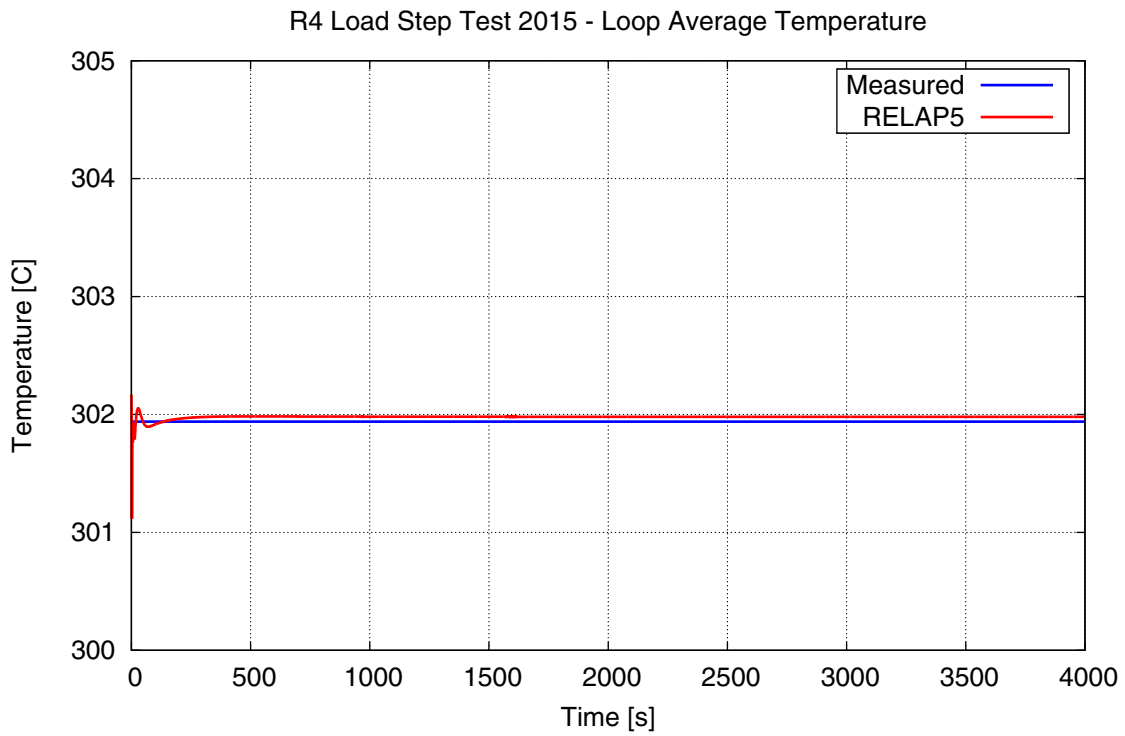
Figure 42   Average Temperature in the Loop
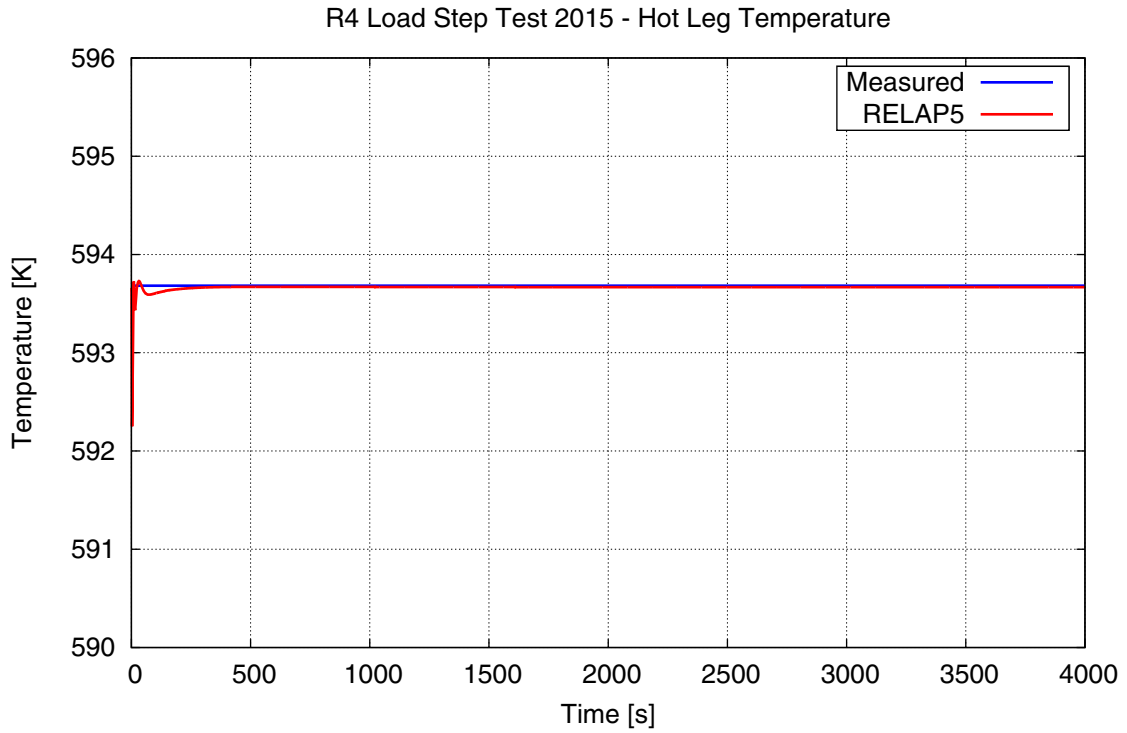
Figure 43   Temperature in the Hot Leg
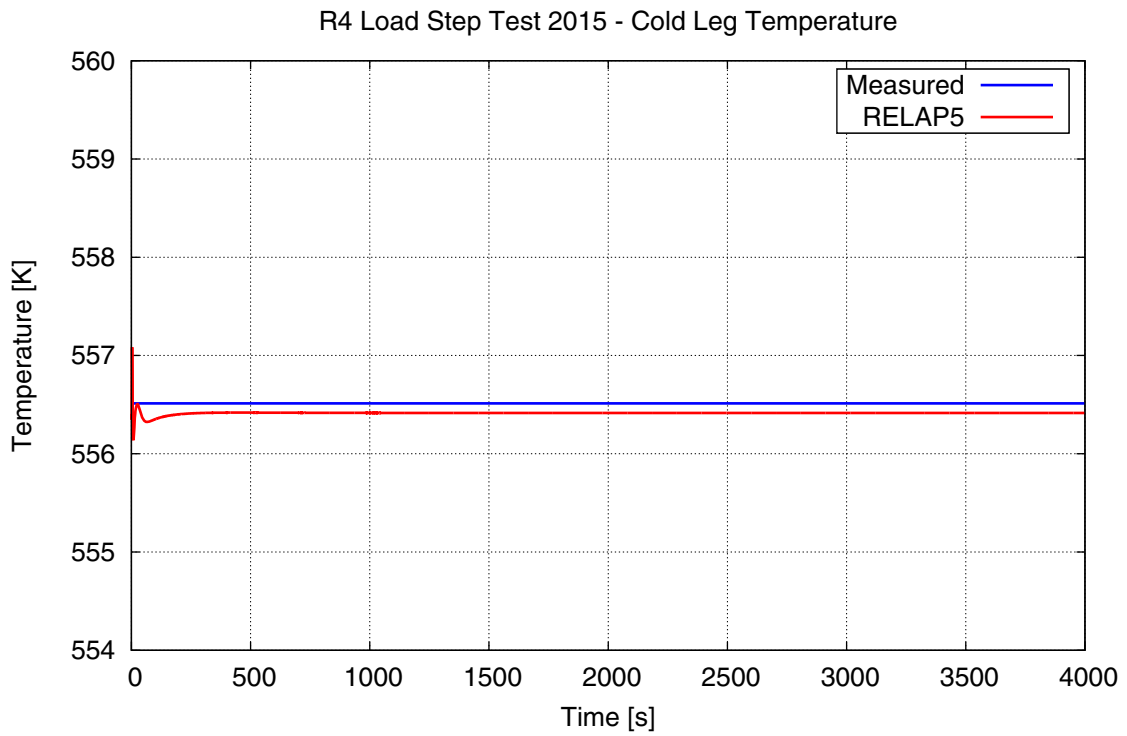
Figure 44   Temperature in the Cold Leg

R4 Load Step Test 2015 - Feedwater Flowrate
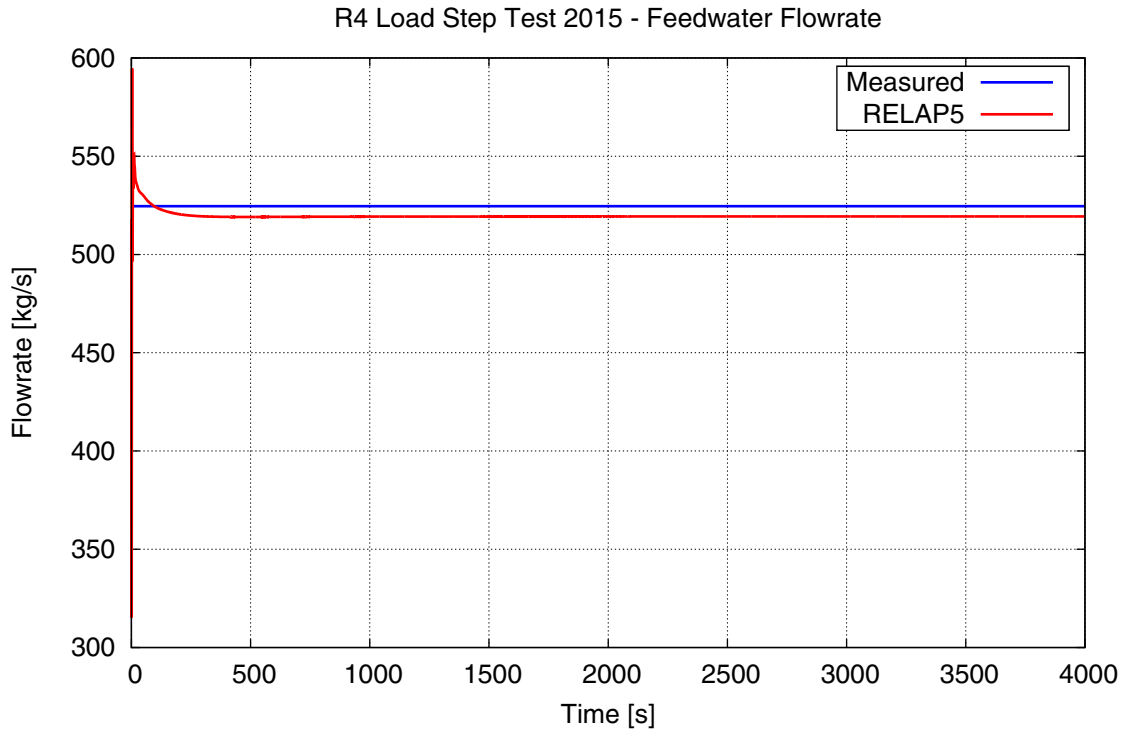
Figure 45   Feedwater Flowrate to the SG

R4 Load Step Test 2015 - Steam Flowrate
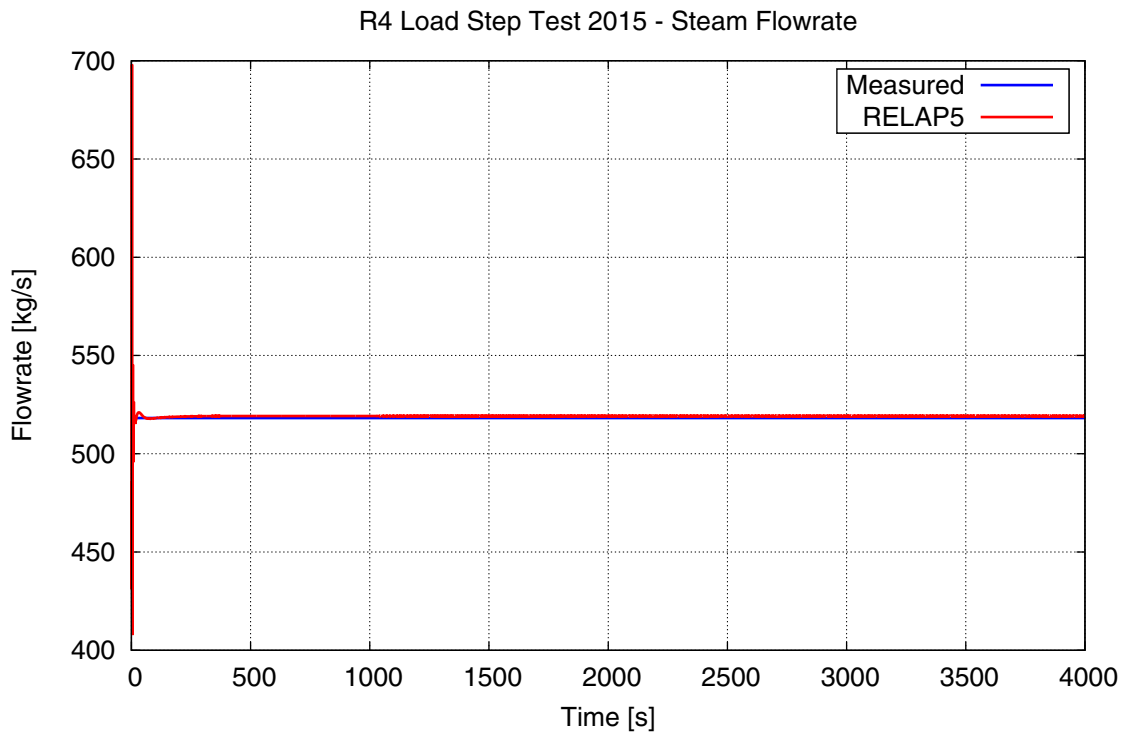
Figure 46   Steam Flowrate from SG
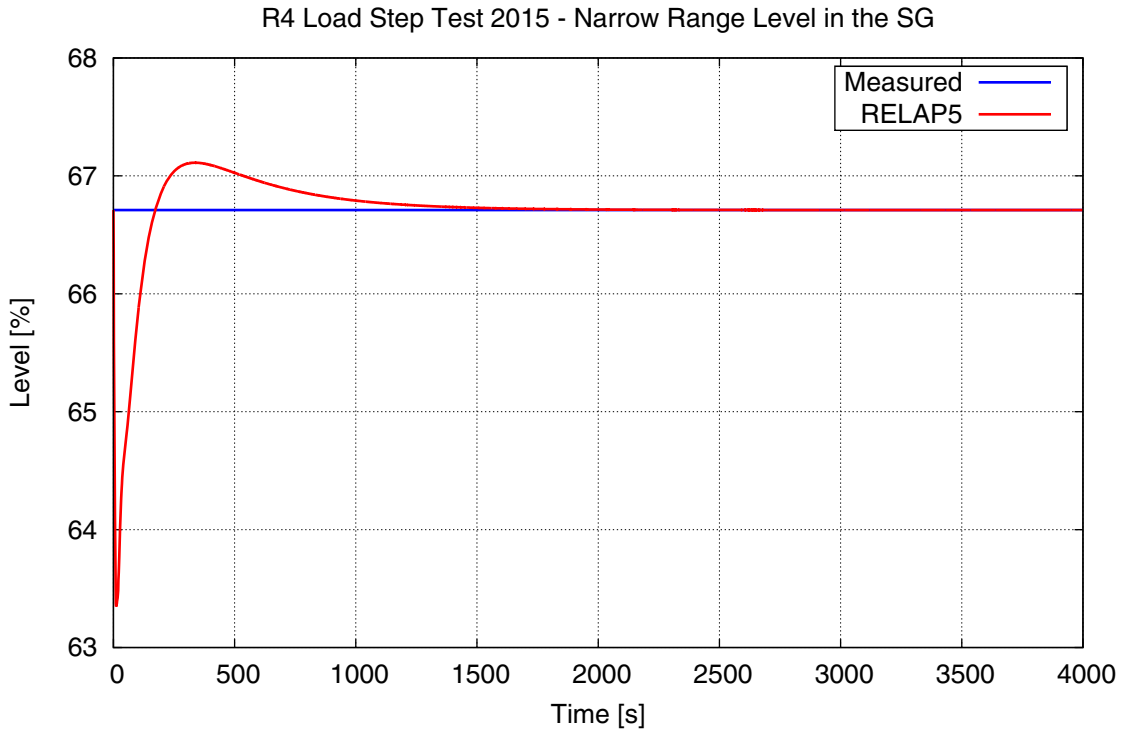
Figure 47   Narrow Range Level in the SG
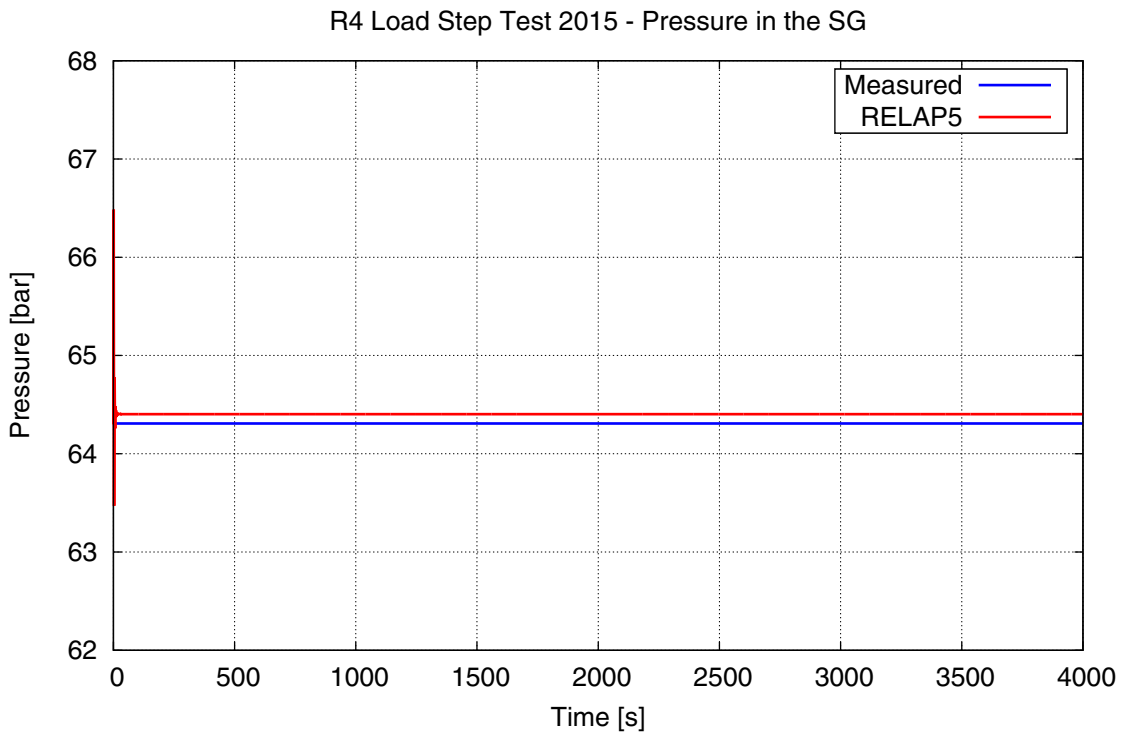
Figure 48   Pressure in the SG

5 ANALYSIS OF THE TRANSIENT

5.1 Boundary Conditions

In many computer code calculations attempting to simulate full-plant transients it is obvious that some parameters are not available due to lacking measurement, documentation, or inaccessible information. In some cases, this shortcoming can be bypassed with derivation of the missing data from other known variables. In a few calculations, it is enough to approximate unavailable data with constants or simple functions. Applications of boundary conditions are natural parts of the transient simulations, and this approach is discussed in the following paragraphs.

5.1.1 Heat Source Boundary Condition

It is important to emphasize that the simulation in the current study used a so called *stand-alone* model of Ringhals 4. It means that only the thermal-hydraulic features of RELAP5 were applied, without any internal neutronic feedback or without coupling to an external neutronic code, such as PARCS. (There are intentions to prepare a neutron kinetic model of Unit 4 in the future). This fact has put some limitation on the present analysis because it was not possible to take the minor power changes into account, which were originating from control rod movements. Note that with changing coolant temperatures, the density, the moderation, and the power are also changing. These effects were interacting with the power control and the rod drive mechanism, which was not modeled in this stand-alone simulation. Nevertheless, the core heating power is also in strong correlation with the temperature difference (ΔT) of the loop (Figure 49), and both the hot leg temperature and cold leg temperature were measured quantities. Consequently, the thermal power was approximated with a user-given input, based on the loop ΔT, as an estimation. The normalized heat source is shown in Figure 50, with respect to 2956.13 MW.

5.1.2 Turbine Pressure Boundary Condition

As it has been mentioned before, the secondary side model of Ringhals 4 is not a closed loop as it is in the plant. A real turbine is far too complex to model in the present analysis. Therefore, the components between the turbine and the feedwater pump are modeled in a simplified manner. The turbine is replaced with a pressure boundary condition, assuming saturated steam and pressure, according to the curve in Figure 51.

5.1.3 Turbine Control Valve Opening Boundary Condition

Features of the turbine control valve (TCV), such as opening vs. stem position, are not known. In fact, throttling of the turbine is driven by a very sophisticated mechanism. Adequate modeling of the TCV and the related controls are beyond the scope of the present study. For achievement of proper conditions, position of the TCV was assumed according to the curve in Figure 52.

5.1.4 Feedwater Temperature Boundary Condition

Temperature of the feedwater is always a function of the actual load. Due to the simplifications mentioned before, the turbine discharges and the feedwater pre-heaters are not part of the current model. Consequently, temperature of the feedwater is provided for the input with a boundary condition. The time function of the temperature is depicted in Figure 53.
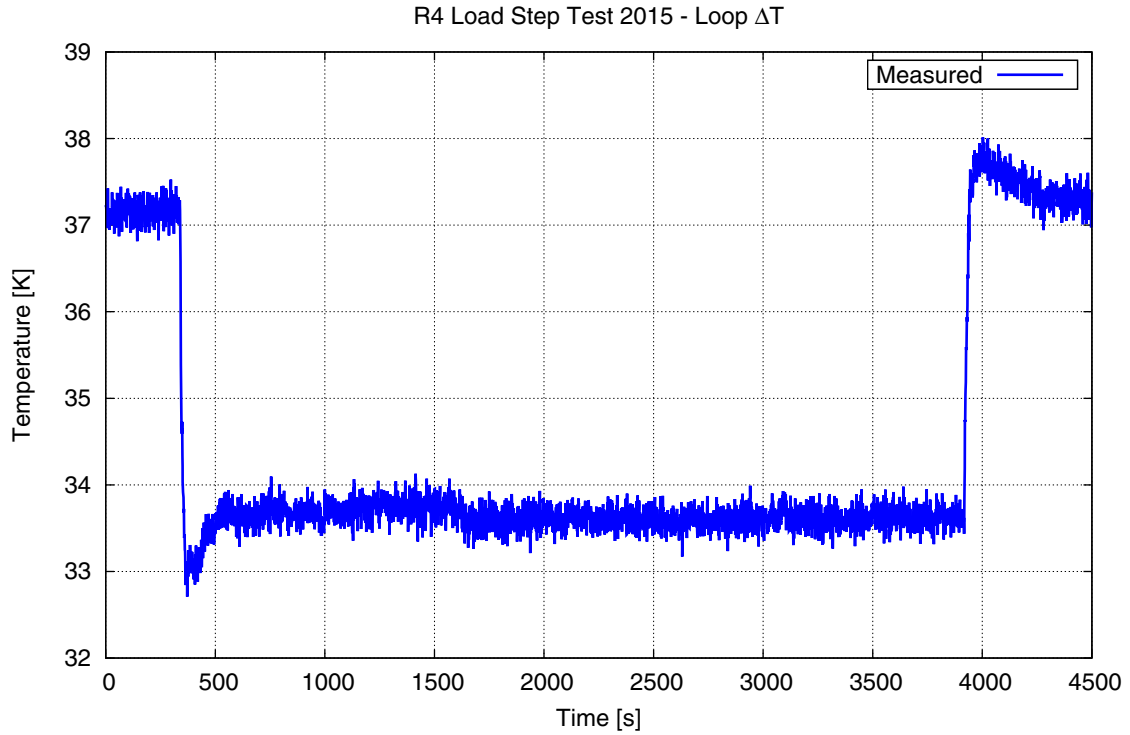
Figure 49   Temperature Difference in the Loop
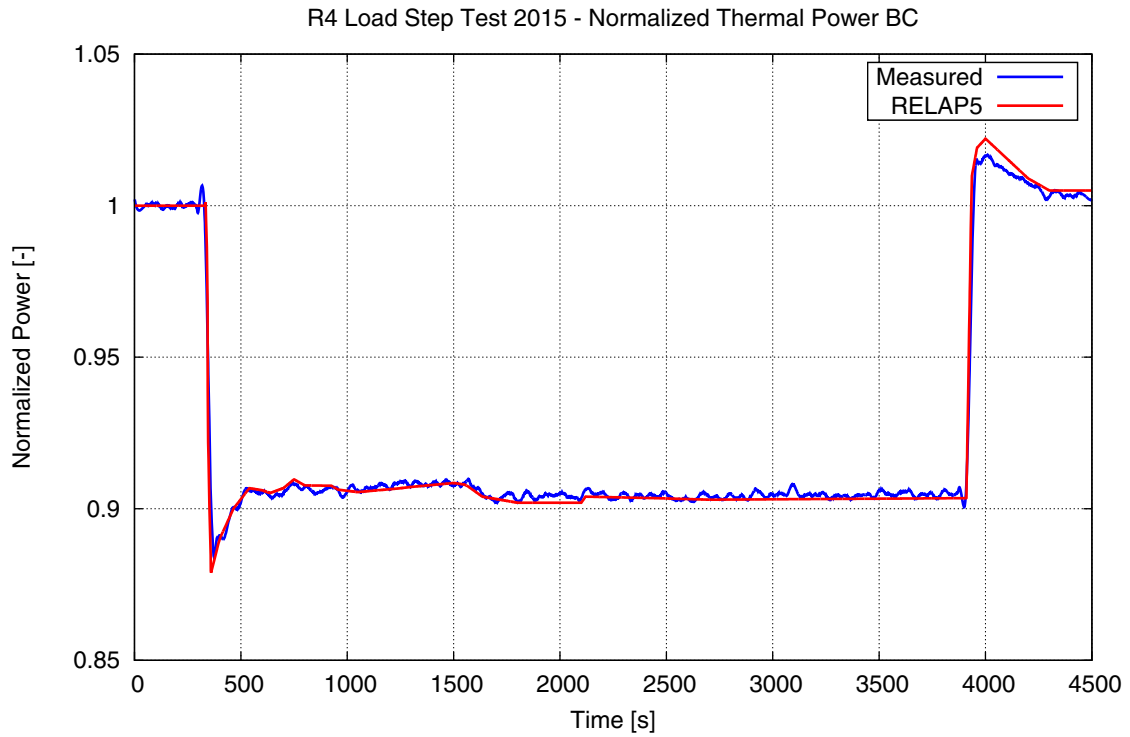
Figure 50   Normalized Thermal Power as a Boundary Condition
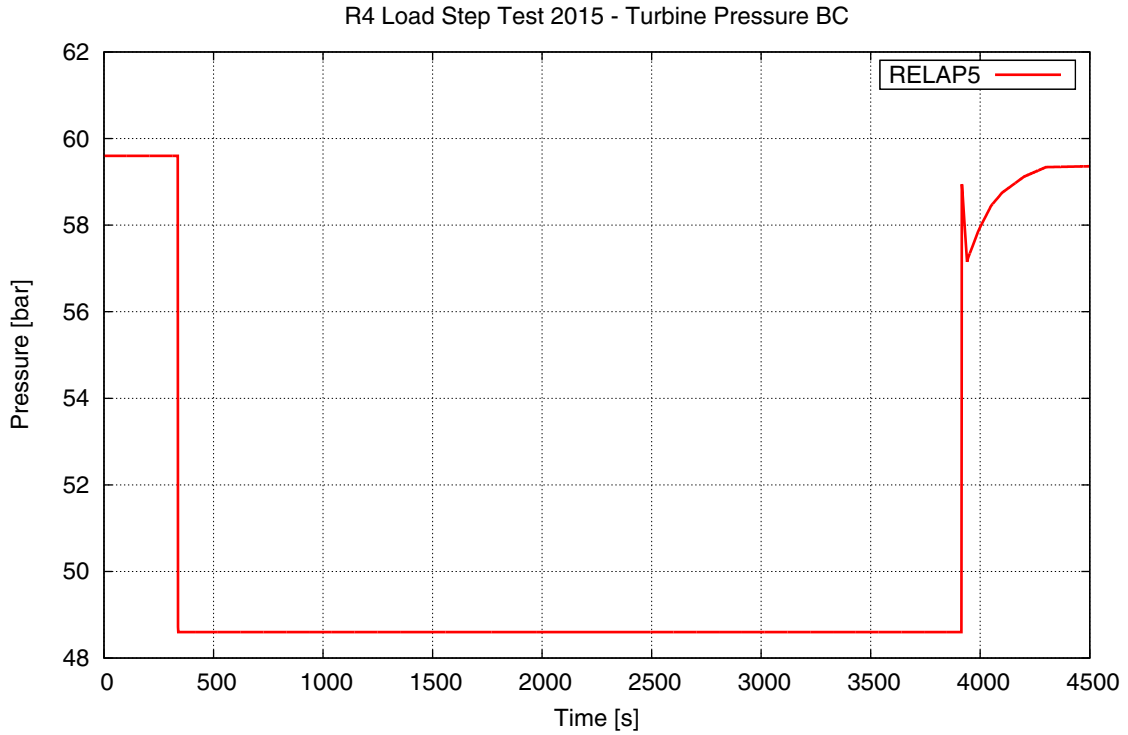
Figure 51   Turbine Pressure as a Boundary Condition
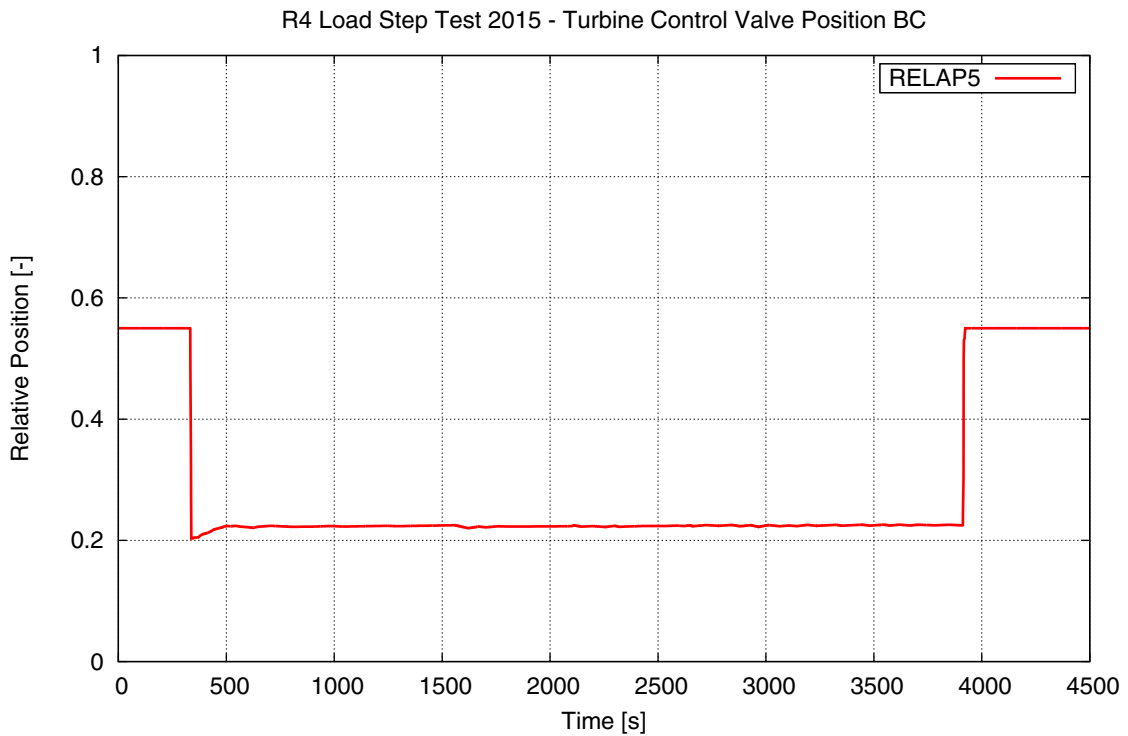
Figure 52   Turbine Control Valve Position as a Boundary Condition
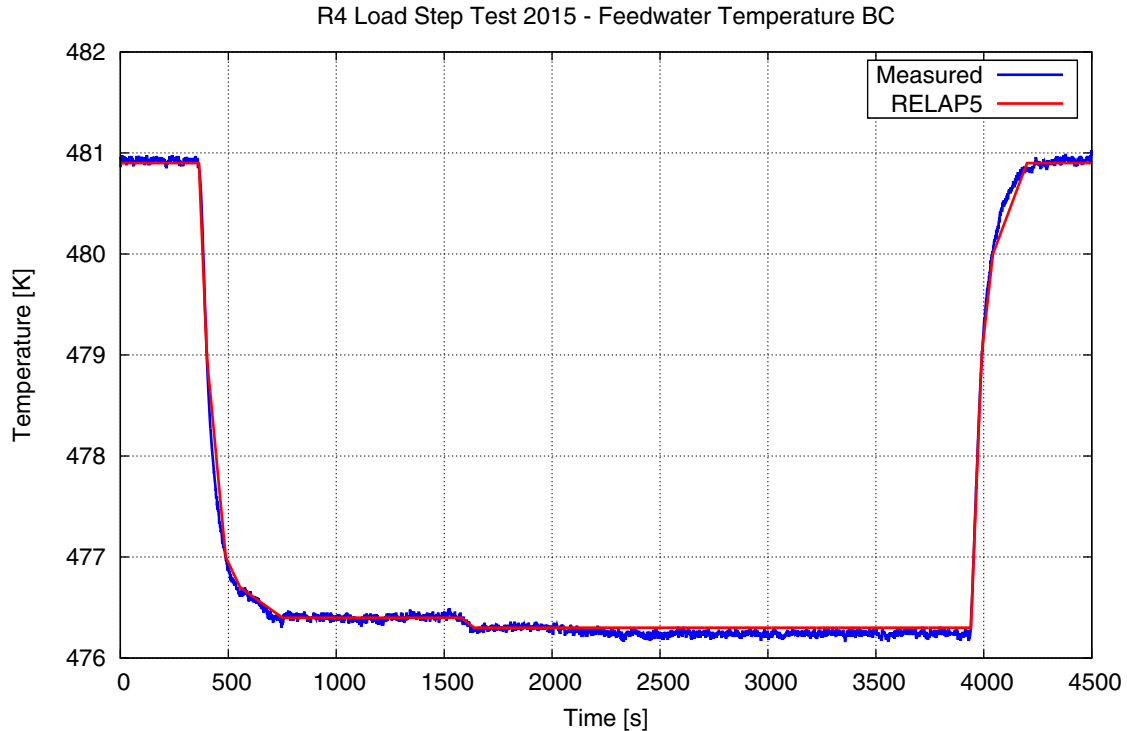
Figure 53   Feedwater Temperature as a Boundary Condition

5.2   Discussion of the Transient Results

Calculation of the transient began with restarting the simulation from the end point of the steady-state run. In the transient input, the "*reset*" option was used on card number 100 and restart number of "*-1*" was given on card number 103. The SSDTT flag was set to "*00032*" on card 201.

The main characteristic periods of the transient can be observed in the calculation, namely:

1. Stable operation at high power
2. Power reduction
3. Operation at reduced power
4. Power increase
5. Operation at restored power

The first period of stable operation is basically an extension of steady-state. At approx. 333 s, the instant power reduction resulted in a large peak, followed by a sudden fall of the PRZ pressure (Figure 54). The control system of the PRZ generates a signal from the setpoint deviation. The signal shown in Figure 55 drives the opening of pressurizer spray valve, the power of the proportional heaters, and the on/off heaters. The magnitude of pressure changes first deactivated the PRZ proportional heaters (Figure 56) temporarily reaching zero power. Soon after that, the sudden pressure increase triggered the PRZ spray system (Figure 57) for a few seconds. Simultaneously, the proportional heaters became powered at their maximal capacity. A peak was experienced in the PRZ level (Figure 58) during the power reduction. While the primary system level was modeled with good accuracy, the charging flowrate (Figure 59) showed larger deviations limited to *the period of power changes*. This discrepancy is discussed further in section 5.4.

Concerning the coolant temperatures, a similar behavior can be observed. The loop average temperature (Figure 60, note in [°C]) and the cold leg temperature (Figure 62) show higher peaks, while the hot leg temperature (Figure 61) increase is almost negligible. With respect to the fluid temperatures, a general trend of slow decrease characterizes the quasi-steady period at reduced power.

When the power was suddenly restored, the PRZ parameters reacted the opposite way, compared to the up-step. A large negative peak was followed by a surge in the pressure within a few tens of seconds. Just before 4000 s of transient time, the low PRZ pressure required energizing of the proportional heaters. This had an immediate effect on the primary side pressure and activation of the spray system became necessary. Injection of cold water by the spray system was maintained for ~250 s, which brought the PRZ pressure constantly down until the end of the transient.

On the secondary side, the pressures measured in the SG steam dome (Figure 63) and in the steam line are very well simulated by the code, though the latter is somewhat underestimated. This indicates that sources of pressure losses (such as the flow restrictor or the main steam isolation valve) have to be carefully examined and adjusted.

While the feedwater flowrate (Figure 64) is almost perfectly calculated, the corresponding steam flowrate (Figure 65) is a bit higher than the measured value. This can be explained by the fact that the "missing" few kg/s is nearly the same amount as a blow-down, which is extracted from the secondary system for purification. Since the blow-down discharge is not part of the model, the real mass flows are accurately calculated by the code.

Large peaks are often present in many numerical simulations. In some cases these are not realistic, or at least their sources are unknown. Such peaks can be observed both in the calculated flowrates of feedwater and steam. This phenomenon may be a consequence of a sudden closure or opening of a valve. Alternatively, it can be attributed to the derivative component of the modeled SG feed control system, which is reacting to large instant changes in such a way. Further investigations are necessary on this issue.

Another parameter, the SG level (Figure 66) is a good indicator for good simulation of the mass balance in the secondary side. The simulated narrow range SG level follows very well the dynamical changes of measured level. This is an evidence for properly designed and well-functioning model of the SG level control system.

It has to be noted that most of the measured signals contained high level of noise, making the comparison very difficult. For reduction of the measurement noise in the previous plots, the Savitzky-Golay filtering algorithm was applied with using MATLAB. The unfiltered, raw test data were plotted in Chapter 2 of this document.

5.3   Plots of the Transient Calculation

R4 Load Step Test 2015 - Pressure in the PRZ
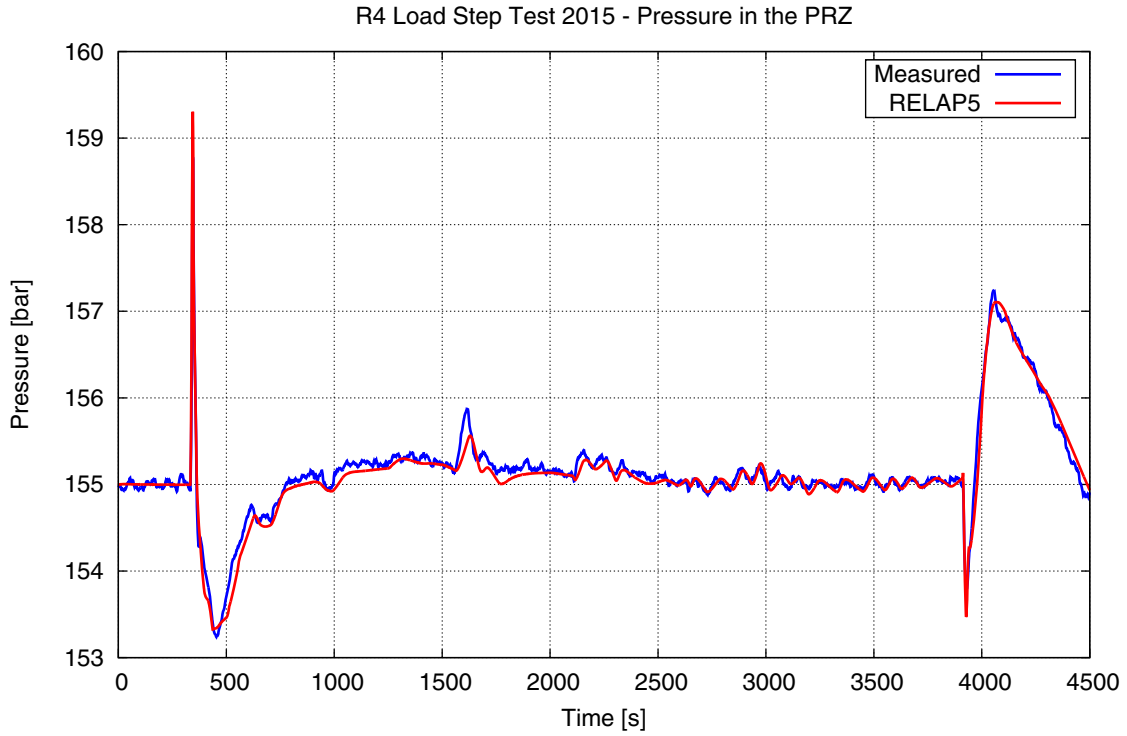
Figure 54   Pressure in the PRZ

R4 Load Step Test 2015 - PRZ Pressure Control Signal
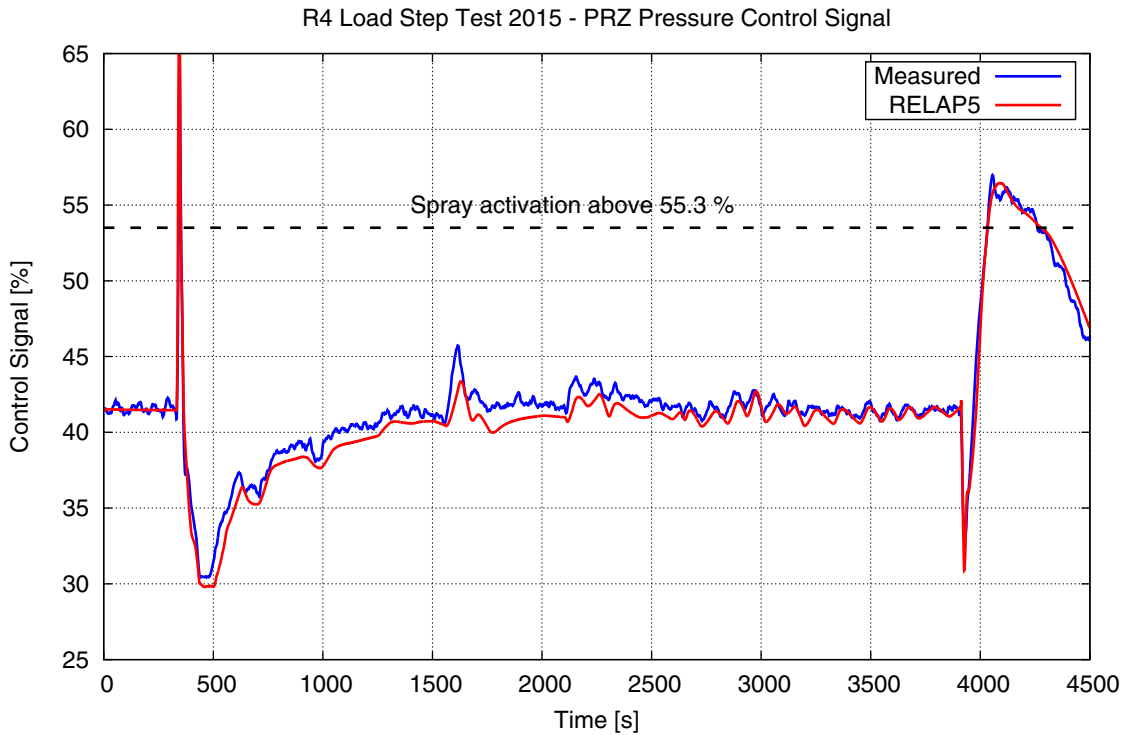
Figure 55   PRZ Pressure Control Signal
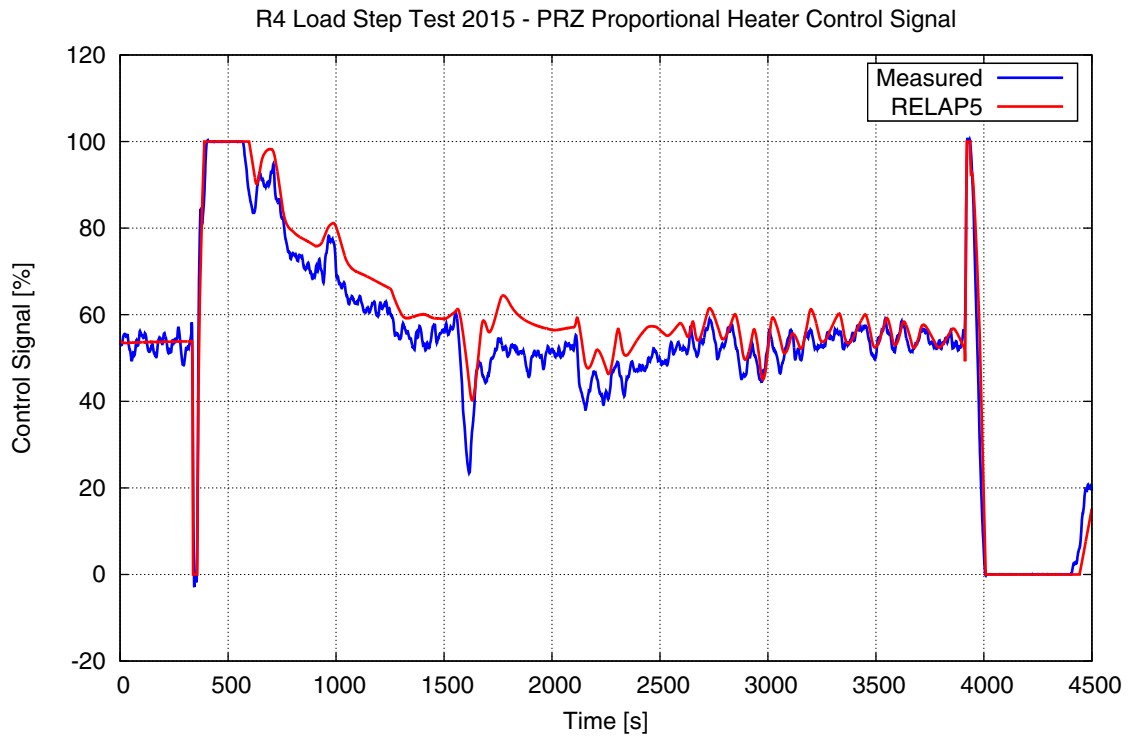
Figure 56   PRZ Proportional Heater Signal
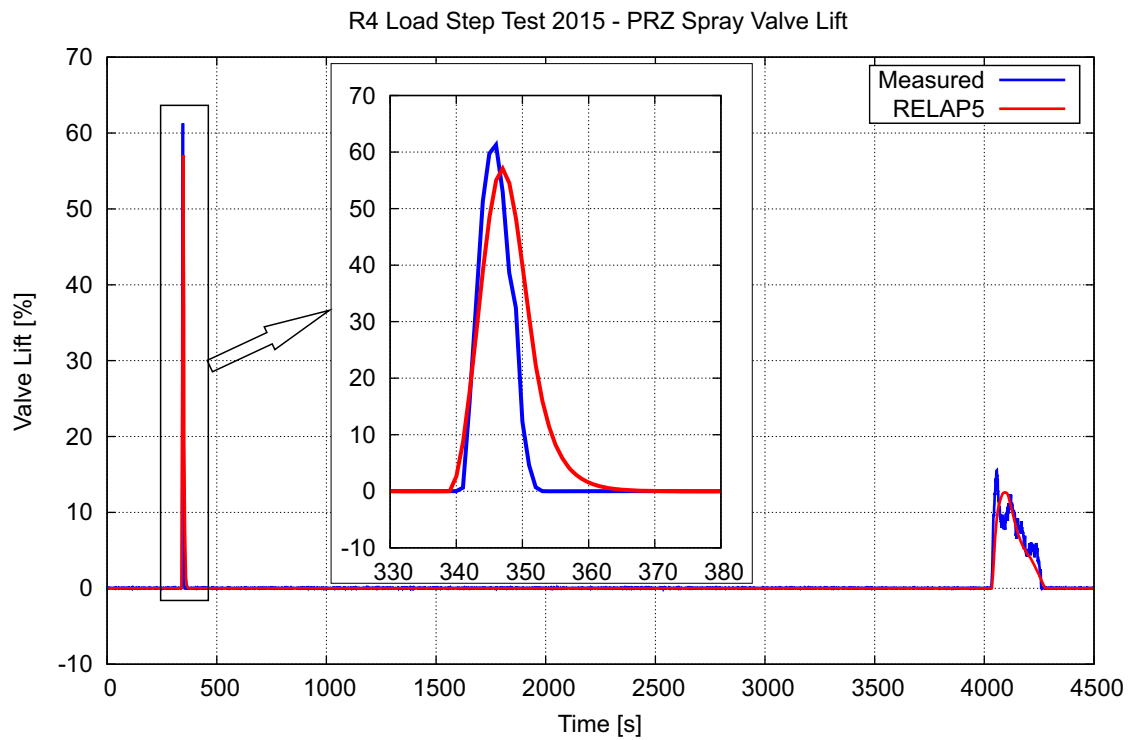
Figure 57   PRZ Spray Valve Lift with Zooming on a Large Peak at ~345 s
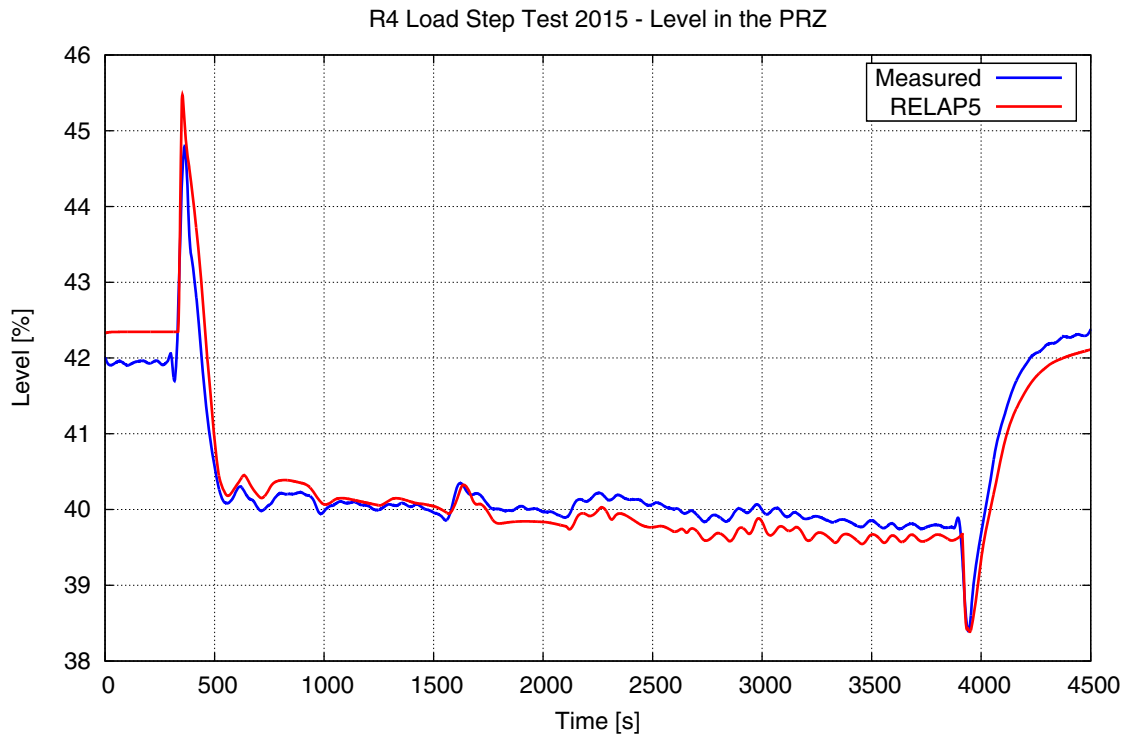
Figure 58   Level in the PRZ
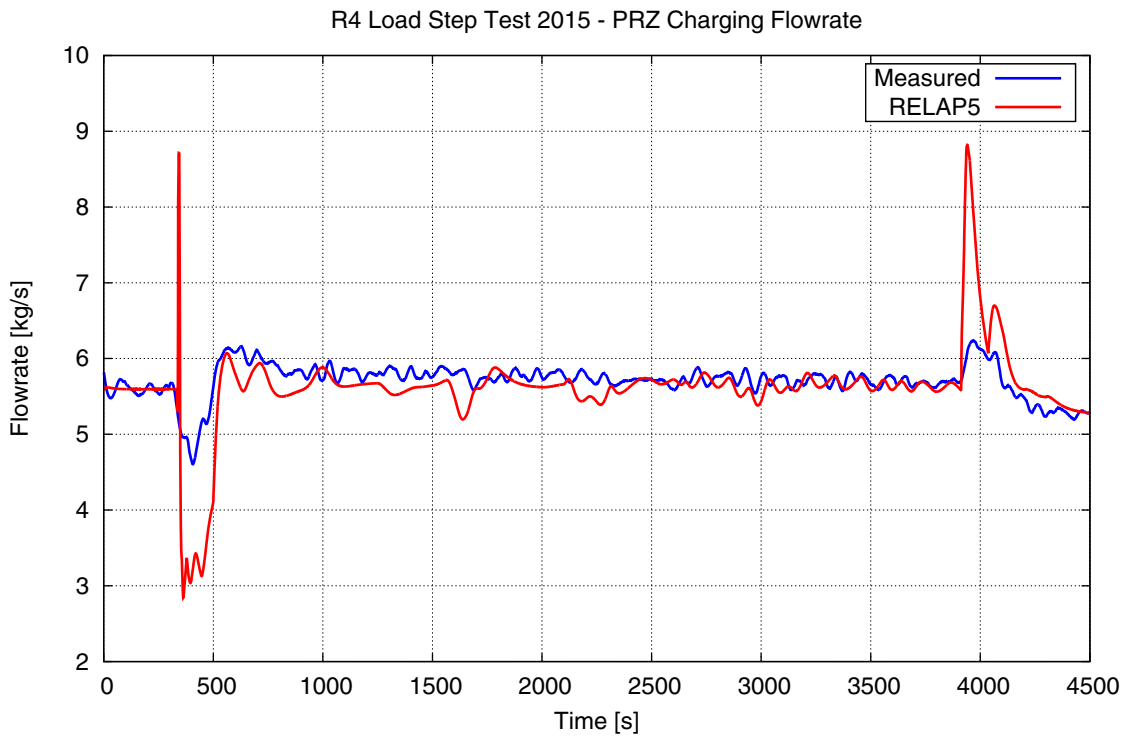
Figure 59   PRZ Charging Flowrate
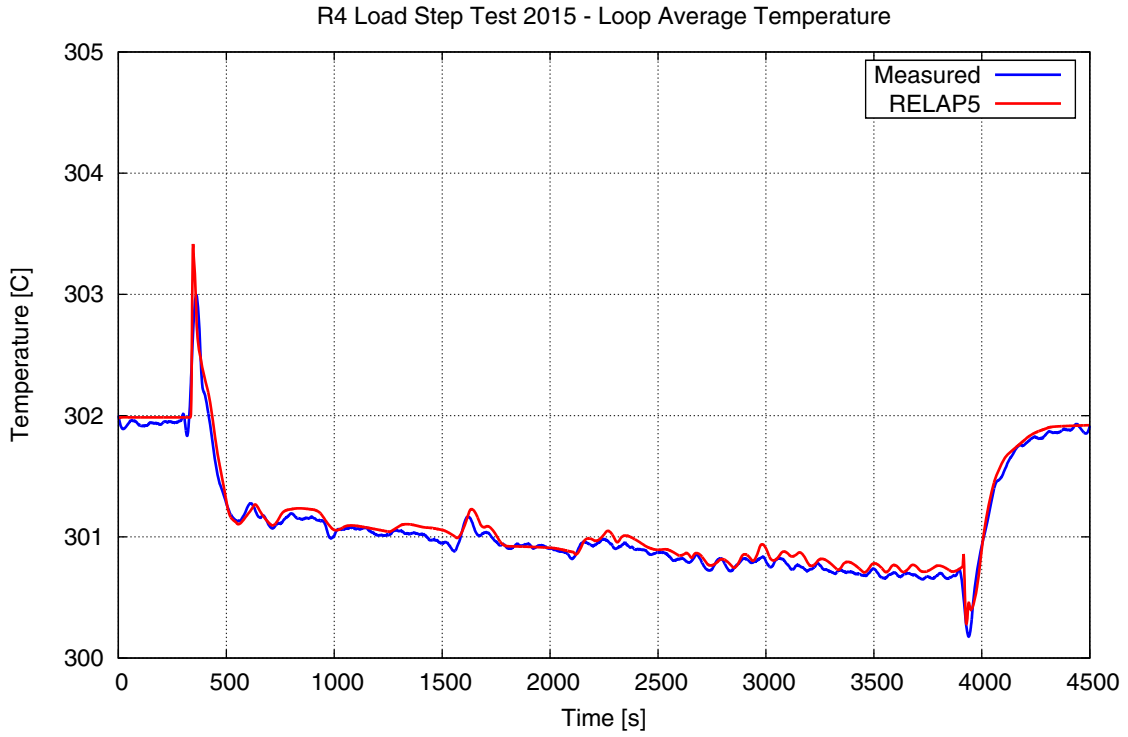
Figure 60   Loop Average Temperature
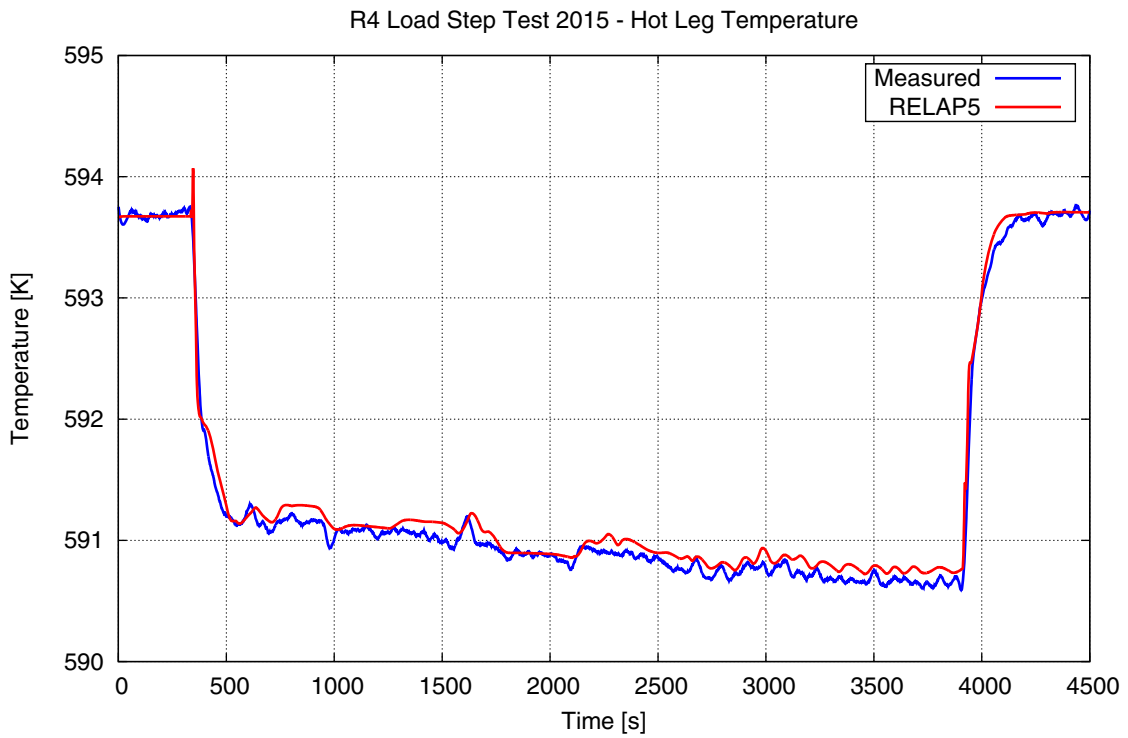
Figure 61   Hot Leg Temperature
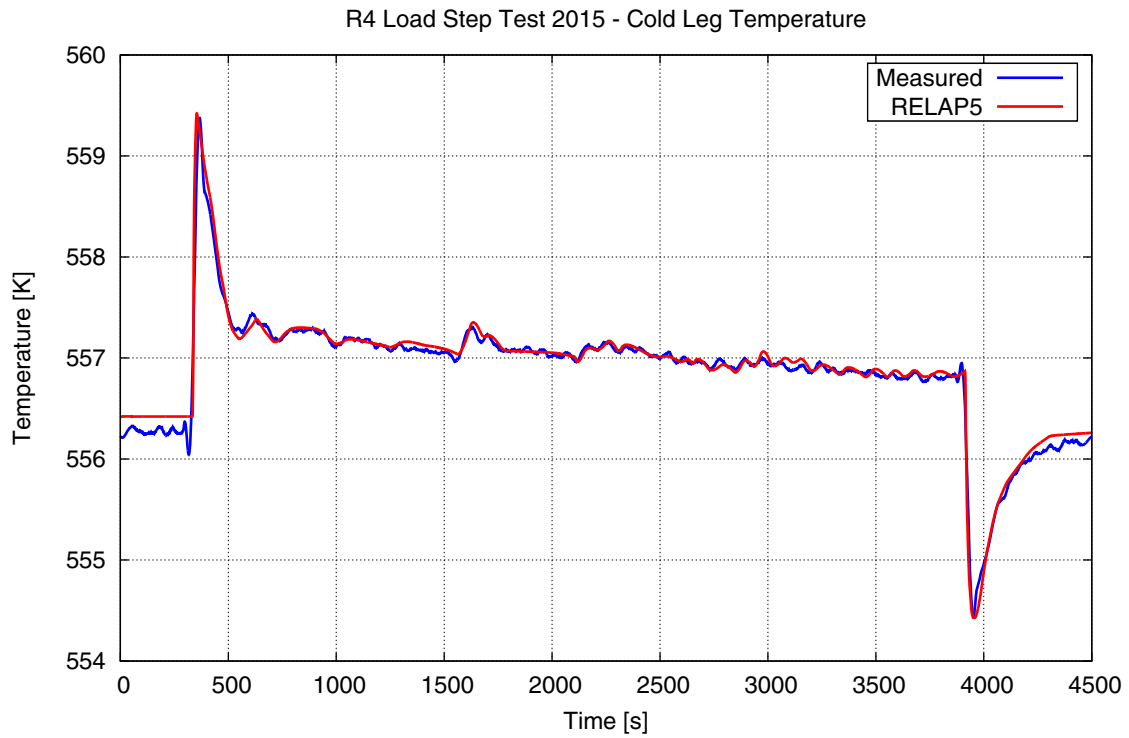
Figure 62   Cold Leg Temperature
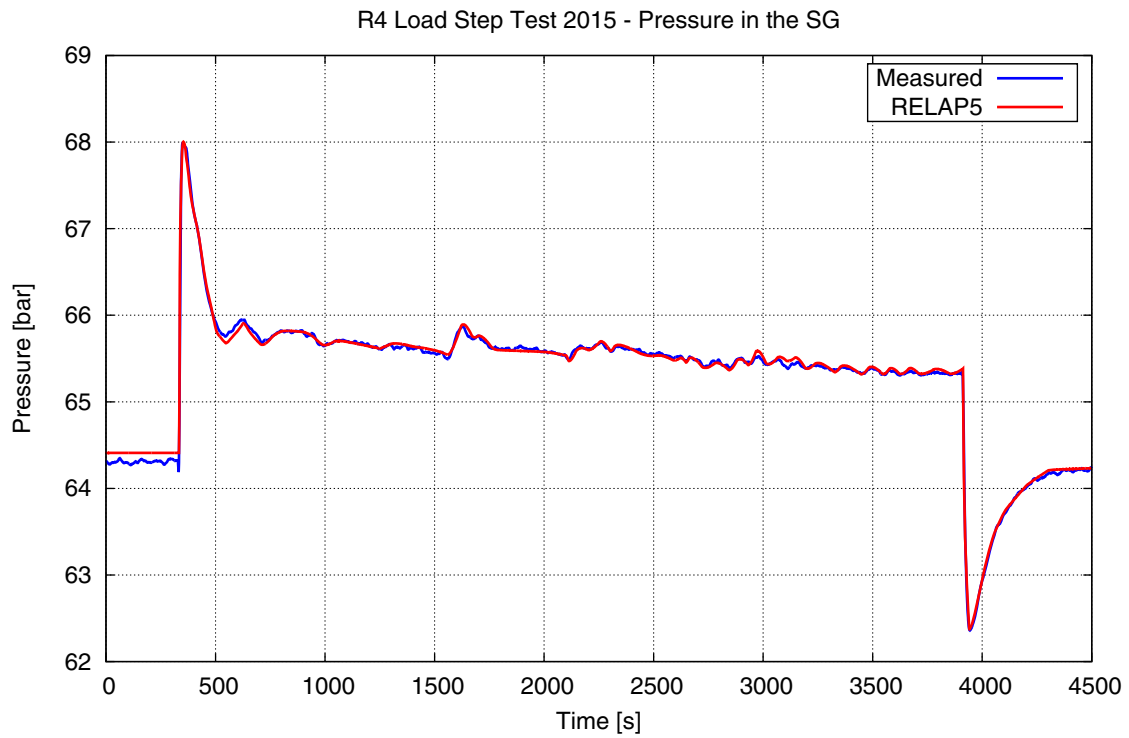
Figure 63   Pressure in the SG
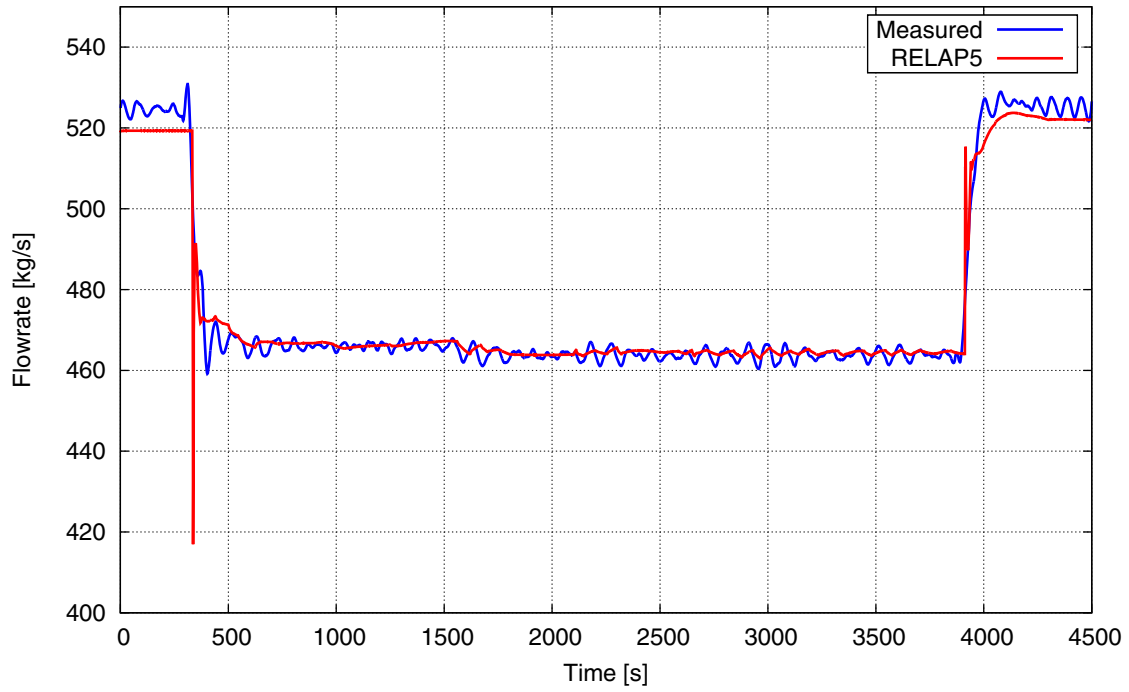
Figure 64   Feedwater Flowrate
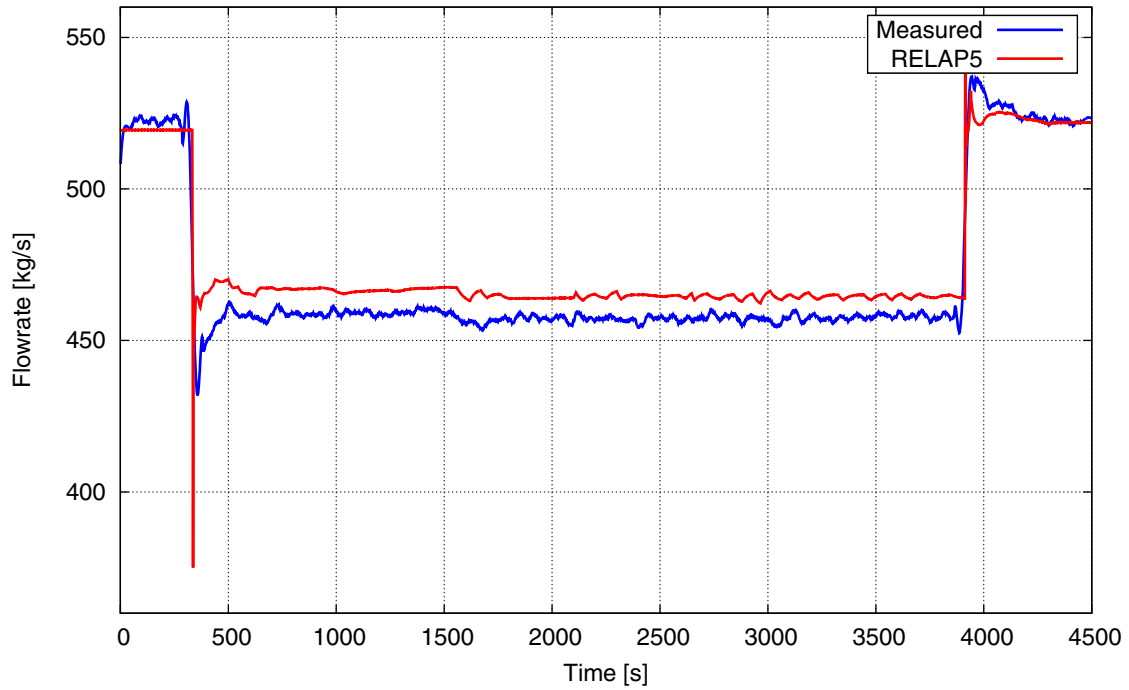
Figure 65   Steam Flowrate
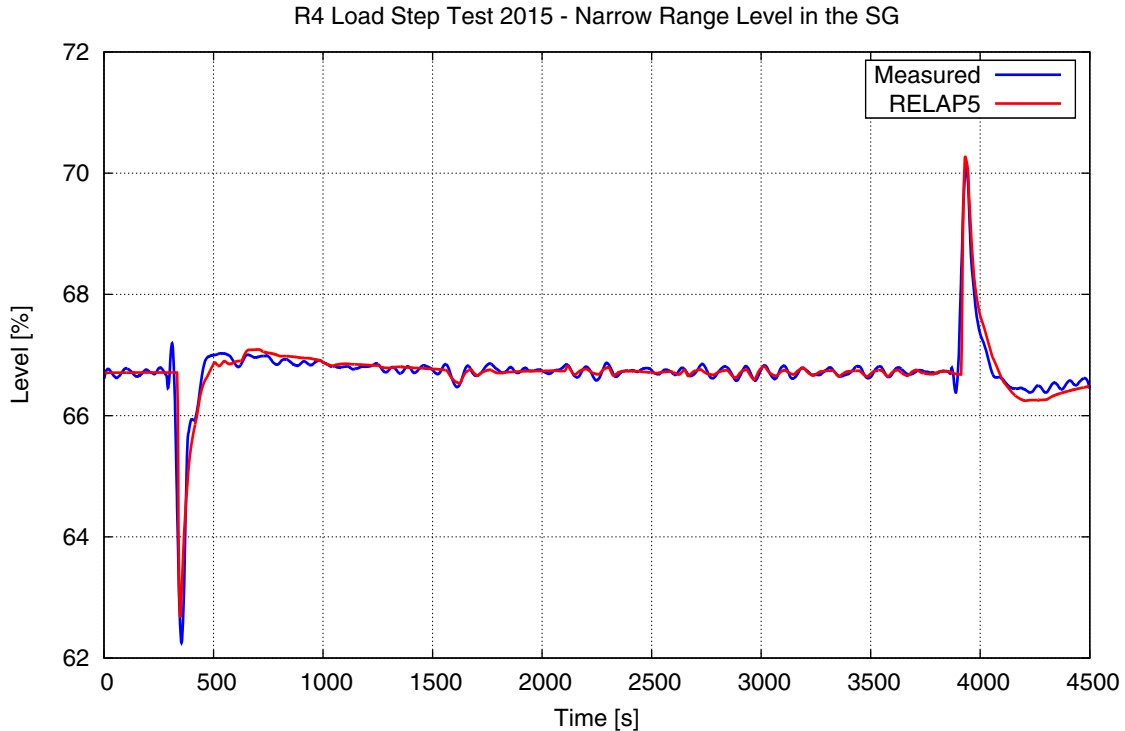
Figure 66   Narrow Range Level in the SG

5.4   Modeling Problems with the PRZ Level and the Charging Flow

As it was shown in Figure 58, the code managed to simulate the PRZ level with a good accuracy. However, this was achieved with much lower charging flowrate during the down-step of the power and on the contrary, with overestimated charging flow during the power up-step (Figure 59). No explanation has been found, yet for such a behavior. In particular, it is interesting that the necessary charging flow is simulated quite well in the other periods of the transient.

Another mismatch was detected in connection to the PRZ. As it can be clearly recognized in Figure 67, the actual measured levels are scattered within a bounding range of more than 1.5 %. Most likely, these signals (40313LT-459, 40313LT-460, and 40313LT-461) were calibrated purposely in such a way. However, the signal of the desired setpoint level (i.e. the "level program", which is a function of the loop average temperature) is always out of measured bounding range. The value determined by the level program is practically less than the lowest measured signal of 40313LT-460. This phenomenon caused difficulties in proper modeling of the PRZ level.

Mismatching between the level setpoint and the actual levels is further confirmed in Figure 68. It can be observed that the lowest measured level signal (40313LT-460) shows the strongest correlation with the setpoint value documented in the PLS. However, even this relatively good correlation is limited to a small range of loop average temperatures. Consequently, the modeled control system may struggle to find the correct level setpoint for the PRZ. This is affecting the amount of charging water to be injected into the primary system. As a future activity, this phenomenon will be investigated and improved at a later stage of the R4 RELAP5 model development.
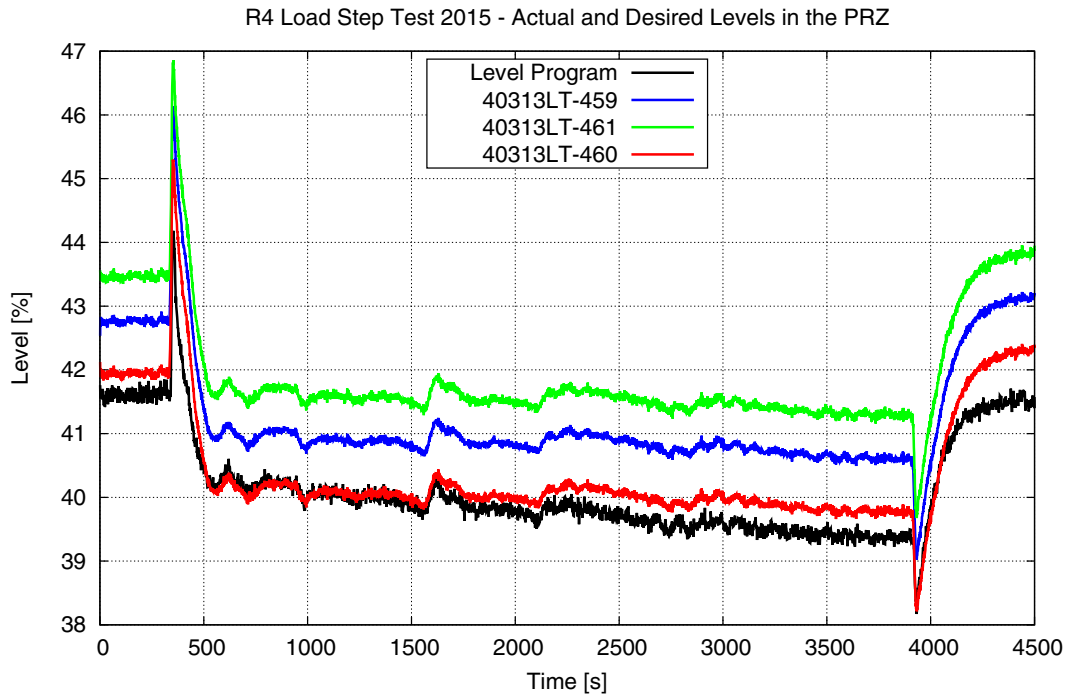
Figure 67   Actual and Desired Levels in the PRZ
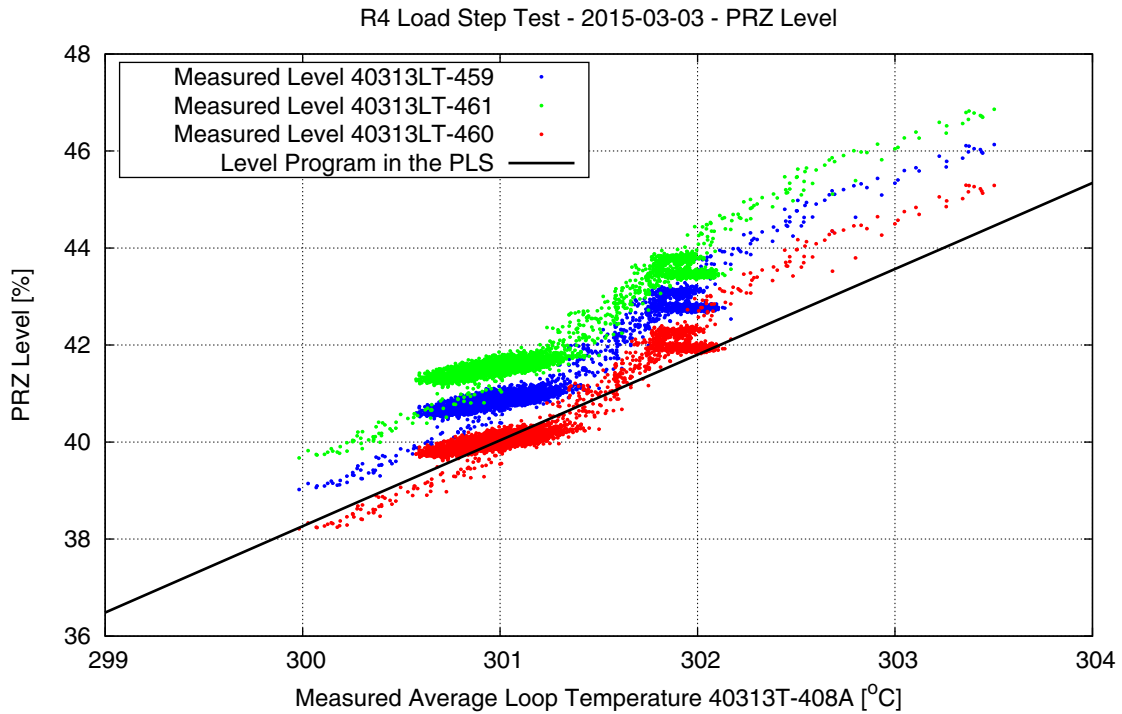
Figure 68   Measured Levels and the Setpoint vs. Loop Average Temperature

5.5   Run Statistics

In a numerical simulation of a transient, it is always important to have information about the stability and smoothness of the calculation. The two plots in Figure 69 describe the relationship between the actual time step and the Courant-limit time step. The former one is practically constant (0.025 s), which is the same as the requested time step. The latter one is nearly constant, and it is just slightly higher than the actual time step. The fact, that the actually used time step is never reduced, it indicates that the calculation is running smoothly. On the other hand, the two time steps values were very close to each other. Consequently, the calculation was performed quite "economically" because the requested time step was set to just 0.002 s less than the value allowed by the Courant-limit. The initial reduction of the time step is due to resetting from the end-point of the steady-state. The final reduction is a consequence of the requested termination of the run exactly at 4500 s, resulting in a shortened time step.
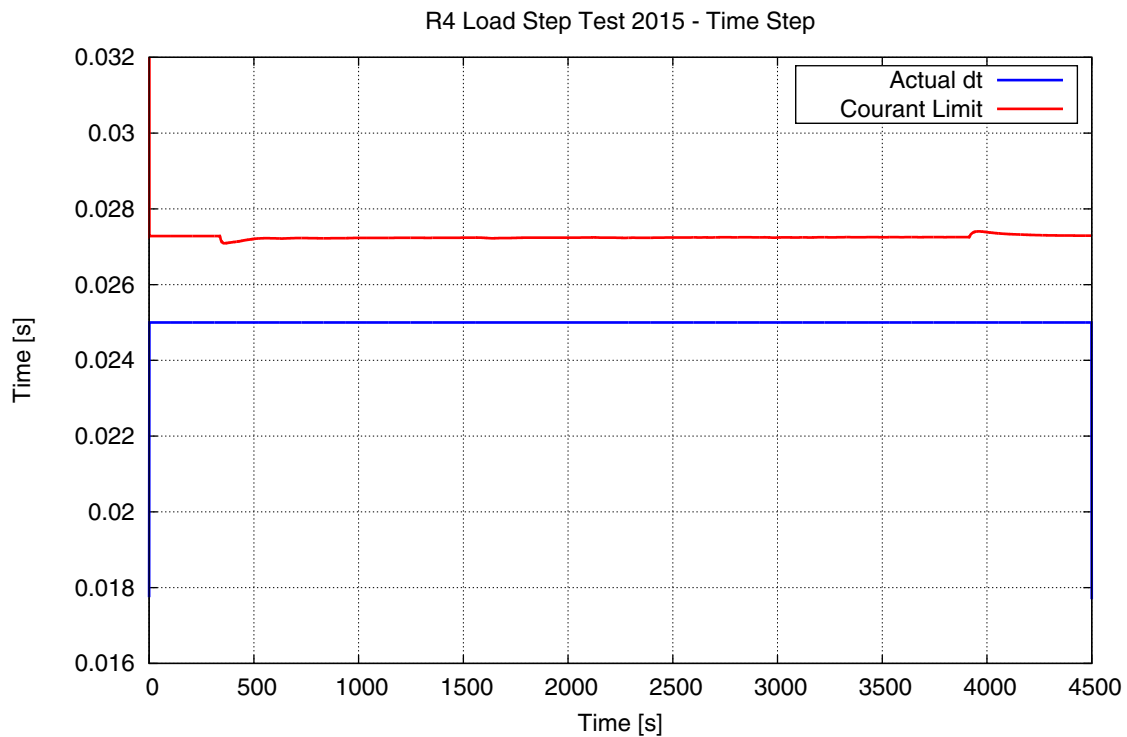
Figure 69   Actual and Courant Limit Time Steps

The calculations were performed on a computer with a 3.5 GHz 4 cores Intel i7 4770K processor and 32 GB RAM running Ubuntu version of Linux. The total consumed CPU time was 3167 s for altogether 300121 attempted advancements. The ratio between the CPU time and the transient time is 3167 s / 4500 s = 0.7038.

6 QUANTIFICATION OF SIMULATION ACCURACY

6.1 Fast Fourier Transform Based Method (FFTBM) Analysis

Fast Fourier Transform Based Method (FFTBM) is a method used for the quantification of "goodness" both for a particular variable prediction and overall model predictions. The basis of FFTBM is the calculation of the relative error between calculated and measured (test) data in the frequency domain. Thus, FFTBM can become a very useful aid on the search of discrepancy sources. In addition it can be used as an aid to tackle practical issues related with the models used, such as the fidelity of the nodalization needed, margin for simplifications or further improvements, etc. [14].

For the FFTBM analysis JSI FFTBM Add-in 2007 is used. It is an Excel-2007 add-in developed by Jožef Stefan Institute in Ljubljana by Dr. Andrej Prošek.

6.1.1 Average Amplitude

Average Amplitude (AA) is the basic measure used for FFTBM analysis. Supposing that the difference between the calculated $F_{cal}(t)$ signal and the experimental one $F_{exp}(t)$ reads in the time domain as:

$$\Delta F = F_{cal}(t) - F_{exp}(t),$$

then the average amplitude AA is calculated as:

$$AA = \frac{\sum_{n=0}^{2^m} |\tilde{\Delta F}(f_n)|}{\sum_{n=0}^{2^m} |\tilde{F}_{exp}(f_n)|},$$

where $\tilde{\Delta F}(f_n)$ and $\tilde{F}_{exp}(f_n)$ the discrete Fourier transformation of ΔF and F_{exp} as calculated by FFT algorithm respectively. Average amplitude could be interpreted as an integral measure that keeps track of the relative magnitude of the discrepancy between the experimental and calculated variable over a time interval.

The following statements can be made for variables predictions based on average amplitude:

- $AA \leq 0.3$ corresponds to very good variable prediction.
- $0.3 < AA \leq 0.5$ corresponds to good variable prediction.
- $0.5 < AA \leq 0.7$ corresponds to poor variable prediction.
- $AA > 0.7$ corresponds to very poor variable prediction.

This criterion refers to one variable. However, it is often needed to assess the overall prediction capability of a model based on N_{var} number of variables. Thus, the total average amplitude AA_{tot} for all of the variables of interest can be computed as:

$$AA_{tot} = \sum_{i=1}^{N_{var}} (w_f)_i \cdot AA_i,$$

where $(w_f)_i$ the (normalized) weighting factor of the $i-th$ variable of interest. The selection of weighting factors is a matter of subjective engineering judgment and should be specified for the transient of interest. The AA criterion mentioned above can be applied for AA_{tot} to assess the overall prediction "goodness" of the model.

6.1.2 Additional Measures for Accuracy Quantification

The following additional measures can assist the accuracy quantification within the FFTBM context:

- variable accuracy VA_i, $i = 1, 2, ..., N_{var}$
- minimal and maximal variable accuracy VA_{min} and VA_{max}
- number of discrepancies ND

Variable accuracy VA_i of the $i-th$ variable of interest shows what the total average amplitude AA_{tot} would be if the rest of the chosen variables all have the same weighting factor $(w_f)_i$ and average amplitude AA_i. Therefore, it is designated as:

$$VA_i = AA_i \cdot (w_f)_i \cdot N_{var}$$

It should be mentioned that the criterion for AA is applicable for VA_i too. Minimal variable accuracy VA_{min} and maximal variable accuracy VA_{max} indicate the minimum and the maximum variable accuracy among the accuracy amplitudes AA_i, $i = 1, ..., N_{var}$ of the N_{var} chosen variables. Consequently, they are defined as:

$$VA_{min} = \max\{VA_i\}, i = 1, ..., N_{var}$$

and

$$VA_{max} = \min\{VA_i\}, i = 1, ..., N_{var}.$$

Minimal variable accuracy VA_{min} is used to define the number of discrepancies ND. It is accepted that the acceptability limit for a calculation is 0.4 and thus, $AA_{tot} < 0.4$. Hence, the number of discrepancies ND is equal with the number of variables for which $VA_i > 0.4$. It is obvious that $ND = 0$ when $VA_{min} < 0.4$. It should be mentioned that a prerequisite for the application of FFTBM is that the average amplitude of the primary pressure is $AA < 0.1$ due to the significant influence of this variable in the system.

6.1.3 Signal Mirroring

Discrete calculated and discrete experimental signals are mirrored in the time domain in order to avoid an inherent weakness of the original FFTBM method that produced unphysical AA results [15]. AA (AA_i or AA_{tot}) should exhibit an overall increasing monotonous trend with increasing time window, since it is an integral discrepancy measure throughout the increasing time window interval. Consequently as time window increases, addition of discrepancies of the newly added time slots occur, which is why AA should monotonically increase. However this does not happen when the last and the first point of the discrete signal differ significantly. FFT multiplies the discrete signal so as to create a periodic infinite signal. As a result, any difference between the first sample of each period with the last sample of the previous period increases the frequency content of AA, distorting it significantly.

6.1.4 FFTBM Analysis Methodology

The transient is divided in phenomenological windows for which the relevant thermal-hydraulic aspects (RTA) are identified. Variables that best describe the RTA are chosen. Then the weighting factors of the variables are set. Average amplitude AA_i for each of the chosen variables as well as the total average amplitude AA_{tot} are calculated using the increasing time window approach. In increasing time window approach the transient is divided in equal and successive time slots. Increasing time windows are then constructed by addition of successive time slots so that the first time window corresponds to the first time slot, the second time window to the addition of the two first time slots etc. Hence, the last time window corresponds to the whole duration of the transient. AA_i for $i = 1, \dots, N_{var}$ and AA_{tot} are calculated for each time window and plotted as function of time [16]. This time window approach allows better tracking of the evolution of AA_i or AA_{tot}, especially for transients with few phenomenological windows.

The transient is separated in five phenomenological windows same as it was described in the previous sections. Since the purpose of the Load Step Test is, among others, to check the ability of the control systems to mitigate the transient, selection of variables and their weighting factors takes place accordingly. Hence, 20 variables were chosen (Table 2) that are descriptive also for the most important RTAs. Most of them appear as inputs or outputs in the modelled PRZ level and pressure controllers, as well as in SG level controller.

Concerning the selection of weighting factors, a scale between 0 and 4 is used to assess the importance of the selected variables. Input variables of the controllers are assigned to a significance factor of 4. Variables appearing as controller outputs are assigned to a significance factor of 3 and the rest of the selected variables to a significance factor of 2. Then the significance factors are normalized (so that their summation equals one). For the FFTBM calculations 15 increasing time windows are considered with 300 s increments.

6.2 Results of the FFTBM Analysis

Evolution of each variable of average amplitude as function of time and in addition, of the total average amplitude, are presented in the following figures. The average amplitude and variable accuracy results for the last time window, 0 - 4500 s, representative of the whole transient, are presented in Table 2.

It can be observed in Figure 71 - Figure 79 that jumps of average amplitudes occur in most of the variables, as well as in total average amplitude, during the second increasing time window of $0 - 600$ s. This time window includes the sudden power *decrease* phase of the transient. However, such a significant average amplitude variations could not be observed in the increasing time window including the power *increase* phase. Thus, it seems that the model performs better after the step of power reduction.

As Table 2 and Figure 80 indicate, the total average amplitude is below 0.3. Consequently, the overall model predictions can be characterized as "*very good*". Furthermore, it can be seen that the first 14 variables have average amplitude below 0.3 and their predictions can be marked as "*very good*". Among those 14 variables, 11 are static quantities, such as pressures, temperatures and PRZ/SG collapsed levels, which have average amplitude equal or below 0.1. This demonstrates an excellent ability of the code to predict static variables. For the rest of the variables, comprising of steam mass flowrates, charging flowrate and spraying control signal, the average amplitudes remain under the acceptability limit 0.4, and their predictions can be marked as "*good*", except the charging flowrate.

Table 2   Variables, Weighting Factors and Results of the 0-4500 s Interval

No.	Variable	w_f	AA	0 – 4500 s VA
1	Primary pressure	0.06	0.017848	0.019831
2	Level in PRZ	0.06	0.090816	0.100907
3	Pressure in SG-1	0.03	0.024022	0.013345
4	Pressure in SG-2	0.03	0.027866	0.015481
5	Pressure in SG-3	0.03	0.026025	0.014458
6	Level in SG-1	0.06	0.089762	0.099736
7	Level in SG-2	0.06	0.096436	0.107151
8	Level in SG-3	0.06	0.093780	0.104200
9	Average temp. in loop-1	0.06	0.007577	0.008419
10	Average temp. in loop-2	0.06	0.007702	0.008557
11	Average temp. in loop-3	0.06	0.007964	0.008849
12	Feedwater flow in SG-1	0.06	0.263144	0.292382
13	Feedwater flow in SG-2	0.06	0.250198	0.277998
14	Feedwater flow in SG-3	0.06	0.266469	0.296077
15	Spraying control signal	0.04	0.495459	0.412882
16	Steam line-1 flow-rate	0.06	0.316915	0.352128
17	Steam line-2 flow-rate	0.06	0.363501	0.403890
18	Steam line-3 flow-rate	0.06	0.335377	0.372641
19	Charging flow-rate	0.06	1.050899	1.167666
20	Proportional heaters capacity	0.04	0.356188	0.296824
Total			0.22	

Charging flowrate is the only variable that is very poorly predicted which consolidates the suspicions about the PRZ level controller. The spraying output signal lies in the "*good*" prediction margin but above the acceptability limit. The level and the pressure in the PRZ and as a result the amount of spraying, are affected by the quantity of the water injected in the primary side and thus, by the PRZ level controller.

Looking at the VA data column of Table 2, it can be observed that the variable accuracies of 17 among the 20 chosen variables have variable accuracies below the acceptability limit, 15 of which exhibit $VA < 0.3$. Thus it also reflects the good quality and maturity of the model. The number of discrepancies ND in most of increasing time windows is equal to 2, mostly due to charging flow and secondly due to the spraying control signal. In the time window of 0 - 3000 s and beyond, $ND = 3$ due to the two variables mentioned above plus the steam flowrate in loop-2.

It is worth mentioning that the predictions of steam flows are considered "*good*" ($AA < 0.4$) but they can be further improved. The plant operators admit that the pressure losses in the steam line is greater than they expected. Thus, improvement of this factor should improve the agreement between measured and calculated steam flows which will culminate in the steam flows average amplitudes to become less than 0.3.

To conclude, the overall code predictions are very good as indicated by the total average amplitude diagram ($AA_{tot} < 0.3$ throughout the duration of the transient) and the code can be characterized as very reliable and of high quality. Nonetheless, there is still a margin for improvements, especially regarding the modeled PRZ level controllers.
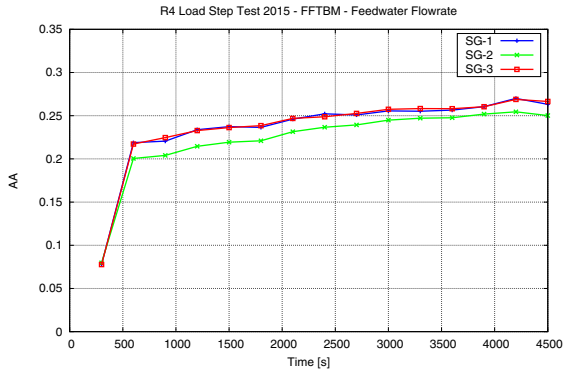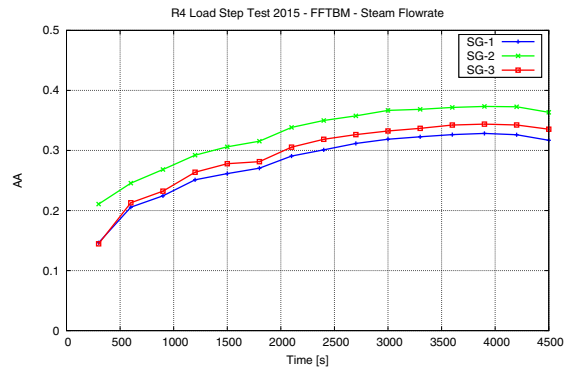
Figure 70   AA of Feedwater Flowrate
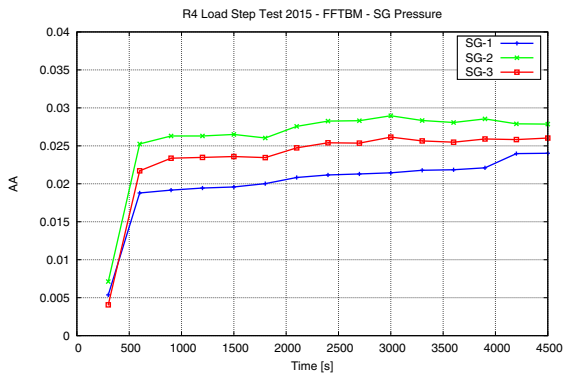

Figure 71   AA of Steam Flowrate

Figure 72   AA of SG Pressure
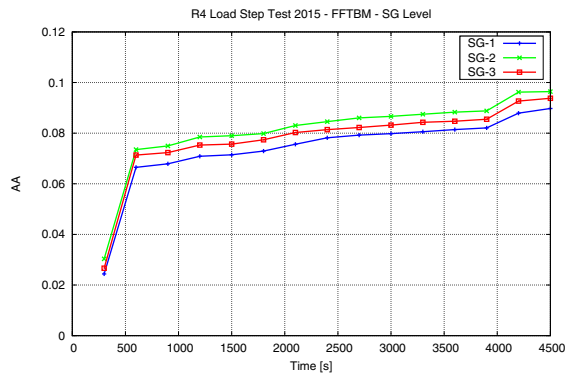

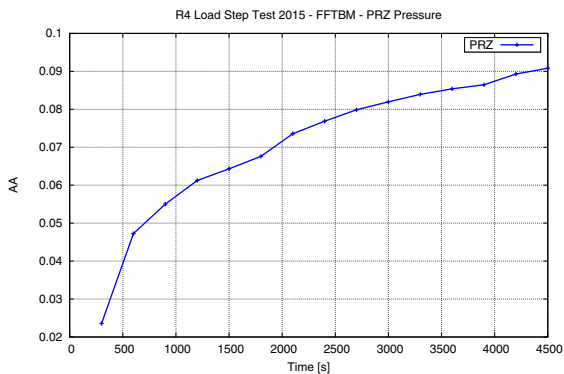**Figure 73   AA of SG Level**

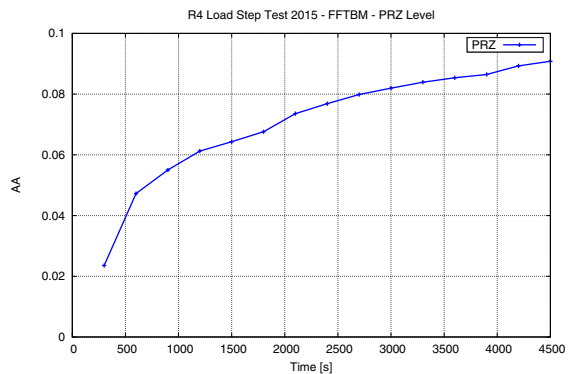**Figure 74   AA of PRZ Pressure**

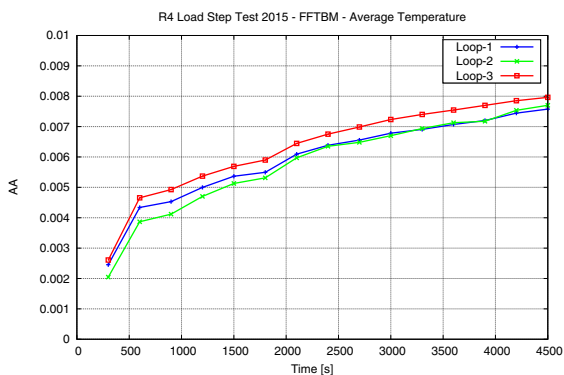
Figure 75   AA of PRZ Level

Figure 76   AA of Average Temperature
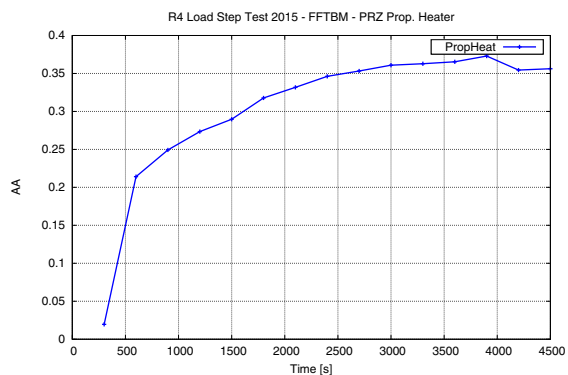

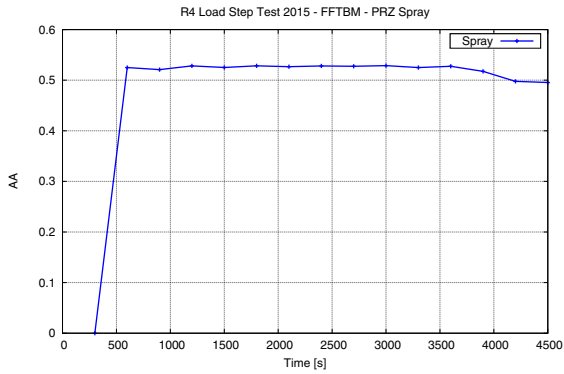**Figure 77   AA of PRZ Prop. Heater Signal**

Figure 78   AA of PRZ Spray Signal
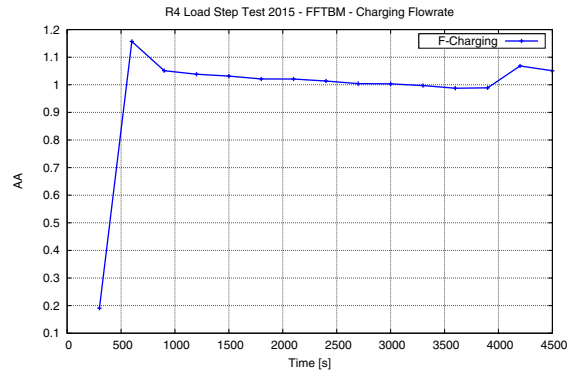

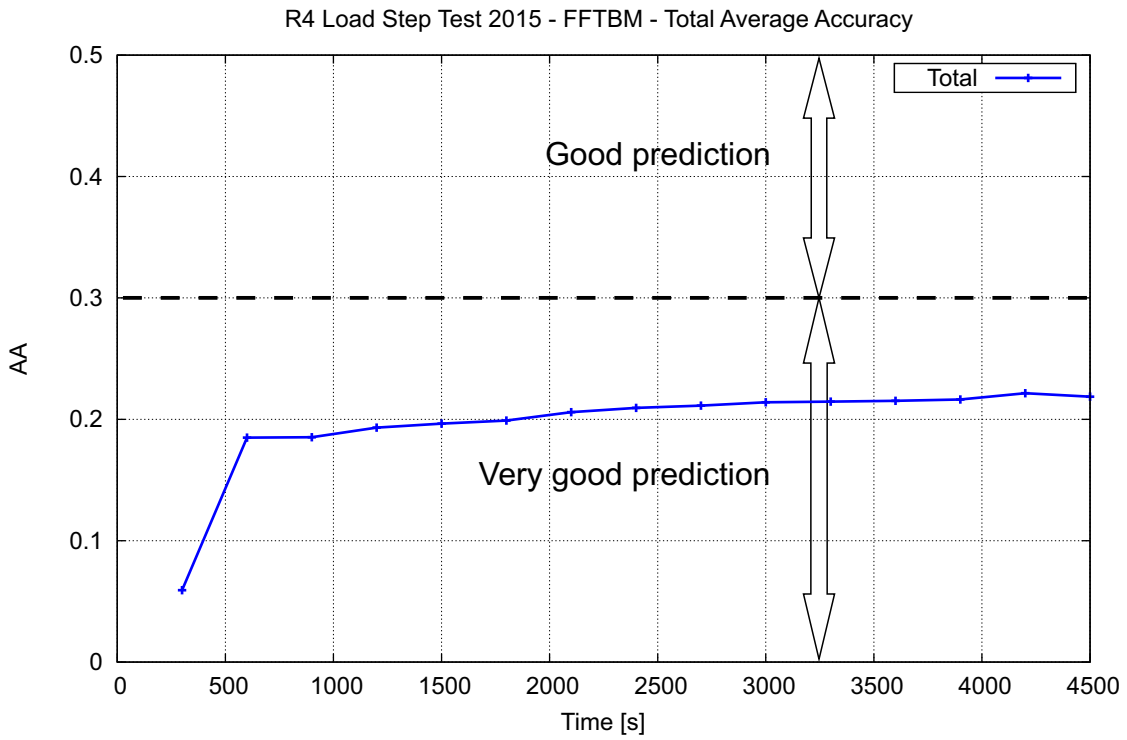**Figure 79   AA of Charging Flow**

Figure 80   Total Average Accuracy

7 CONCLUSIONS

An important stage of the R4 model development process has been summarized in the current study. Incorporation of the new components (i.e. the AREVA design SGs and the PRZ) into the full plant model was a challenging task and this was the second opportunity to validate the new model against a startup test. Prior experiences with the prototype geometries could be utilized in the present Report.

On the basis of the presented steady-state and transient results, it can be concluded that the over-all performance of the R4 RELAP5 model is good. The general trends during the 5 distinguishable parts of the transient were well predicted by the code. Quantitative matching of the parameters was satisfactory, which resulted in a successful validation of the model, as well as the code. The primary to secondary side energy transfer was sufficiently well simulated. The Ringhals 4 model is suitable for analysis of other types of transients already in its current state of development.

However, as always, there is a margin for improvement. For instance, application of FFTBM tool has revealed that characteristics of some control valves need to be obtained and examined because this is a critical parameter, which is influencing the general behavior of the transients. The calculated charging flow showed the largest deviations during the sudden power changes. This can be partly attributed to the problematic level program of the PRZ.

8 REFERENCES

1.   IAEA Technical Working Group, *Power uprate in nuclear power plants : guidelines and experience*. IAEA nuclear energy series, 2011, Vienna, International Atomic Energy Agency. 104 p.

2.   Agung, A. and Bánáti, J.,*Technical Description of the Coupled PARCS/RELAP5 Model for the Ringhals-3 NPP*. Division of Nuclear Engineering, Chalmers University of Technology, Gothenburg, Sweden. 2013. p. 41.

3.   Bánáti, J., *Technical Description of the RELAP5 Model for the Ringhals 4 NPP*. 2013, Division of Nuclear Engineering, Chalmers University of Technology. p. 53.

4.   Bánáti, J., *Validation of the RELAP5 Model of Ringhals 4 against the 2011-12-14 ± 10% Load Step Test*. Division of Nuclear Engineering, Chalmers University of Technology. Report No.: CTH-NT-315. 2013. p. 42.

5.   Bánáti, J. and M. Holmgren, *Validation of RELAP5/Mod3.3 against a Load Step Transient at Ringhals 4 NPP*, in *16th International Meeting on Nuclear Reactor Thermal Hydraulics (NURETH-16)*. ANS. Chicago, IL, USA, Aug. 30 - Sep. 4, 2015. p. 4548-4561.

6.   Stathis, A., *Analysis of a Load Step Test at Ringhals 4 using RELAP5 - Code Validation and Verification*, Division of Nuclear Engineering. Chalmers University of Technology, Gothenburg, Sweden. 2015

7.   Information Systems Laboratories Inc., *RELAP5/MOD3.3 code manual, Patch 04, Vols. 1 to 8*. 2010, US Nuclear Regulatory Commission

8.   Eriksson, J., *RELAP/MOD3 base model for the Ringhals 3/4 plants.* Report STUDSVIK/ES-94/14, Studsvik Eco & Safety AB. 1994.

9.   Bánáti, J., et al. *Analysis of a Loss of Feedwater Case at the Ringhals-3 NPP Using RELAP5/PARCS Coupled Codes*. ICONE-16 Proceedings of the 16th International Conference on Nuclear Engineering, Paper No.: ICONE16-48116, Vol 3. Orlando, Florida, USA. May 11–15, 2008. ASME.

10.   Bánáti, J., et al., *Analysis of a Loss of Normal Feedwater Transient at the Ringhals-3 NPP using RELAP5/Mod3.3*, International Agreement Report (NUREG/IA-0234). 2010, U. S. Nuclear Regulatory Commission.

11.   Agung, A., et al., *Validation of PARCS/RELAP5 coupled codes against a load rejection transient at the Ringhals-3 NPP.* Nuclear Engineering and Design, 2013. **257**: p. 31-44.

12.   Vattenfall, *Ringhals 4 Reactor PLS - Precautions, Limitations and Setpoints for Nuclear Steam Supply and Balance of Plant Systems* (v.35.0). 2015.

13.   USNRC, *Pressurized Water Reactor Systems - Reactor Concepts Manual*. 2003.

14.   Prošek, A., F. D'Auria, and B. Mavko, *Review of quantitative accuracy assessments with fast Fourier transform based method (FFTBM).* Nuclear Engineering and Design, 2002. **217**(1–2): p. 179-206.

15.   Prošek, A., M. Leskovar, and B. Mavko, *Quantitative assessment with improved fast Fourier transform based method by signal mirroring.* Nuclear Engineering and Design, 2008. **238**(10): p. 2668-2677.

16.   Prošek A., M.B., *Quantitative Code Assessment with Fast Fourier Transform Based Method Improved by Signal Mirroring*, International Agreement Report (NUREG/IA-0220). 2009, U.S. Nuclear Regulatory Commission.

2. TITLE AND SUBTITLE

Validation of RELAP5 Model of Ringhals 4 against a Load Step Test at Uprated Power

5. AUTHOR(S)

J. Bánáti and A. Stathis

6. TYPE OF REPORT

Technical

7 PERIOD COVERED (Inclusive Dates)

8. PERFORMING ORGANIZATION   NAME AND ADDRESS (If NRC, provide Division, Office or Region, U. S. Nuclear Regulatory Commission, and mailing address; if contractor, provide name and mailing address.)

Chalmers University of Technology
Department of Applied Physics
Division of Nuclear Engineering
SE – 41 296 Gothenburg, Sweden

11. ABSTRACT (200 words or less)

After finishing the large component replacement project of the steam generators and the pressurizer, the Unit 4 of the Ringhals Nuclear Power Plant was operated in test mode between 2011 and 2014. In order to reach the ultimate goal of power uprate, and obtain a license for operation at the new nominal conditions, a series of tests had to be accomplished.

The R4-QP-101 maneuverability test was performed on March 3, 2015. The test was focusing on evaluation of the system responses for ± 10 % perturbances in the load. The data collected during test provided a good opportunity for verification of the full plant model, which is being developed for the RELAP5/Mod3.3 Patch04 computer code, with incorporation of the new component models. The present International Agreement Report introduces the test procedure and shows an overview on the key parameters that are utilized. There is a brief summary given on the applicability field of the computer code. Preparation of the input deck and the nodalization of the primary and secondary sides are touched upon. Strategies applied for achievement of steady-state conditions are addressed in the document. The steady-state results are presented in plotted format, demonstrating how the control system brought the entire unit to stable conditions. Quantification of simulation accuracy has proven that the stand-alone RELAP5 thermal-hydraulic model is capable of reproduction of the key features and events of the test. Sufficiently good agreement between the measured and simulated data resulted in a successful verification of the plant model. The Ringhals 4 model is suitable for analysis of other types of transients already in its current state of development. Nevertheless, further refinement in the input is planned as soon as new test data will be available.

12. KEY WORDS/DESCRIPTORS (List words or phrases that will assist researchers in locating the report.)

Ringhals 4 NPP
Power Uprate
Load Step
Relap5
SNAP
Westinghouse 3-loop Pressurized Water Reactor
Code Validation

Validation of RELAP5 Model of Ringhals 4 Against a Load Step Test at Uprated Power